FINAL REPORT

Hydraulic Tomography and High-Resolution Slug Testing to Determine Hydraulic Conductivity Distributions

SERDP Project ER-1367

FEBRUARY 2011

Carl D. McElwee
Brett R. Engard
Brian J. Wachter
Shane A. Lyle
John Healey
J.F. Devlin
University of Kansas Center for Research

SERDP
DOD ▪ EPA ▪ DOE

Report Documentation Page

Form Approved
OMB No. 0704-0188

1. REPORT DATE	2. REPORT TYPE	3. DATES COVERED
FEB 2011	**N/A**	**-**

4. TITLE AND SUBTITLE	5a. CONTRACT NUMBER
Hydraulic Tomography and High-Resolution Slug Testing to Determine Hydraulic Conductivity Distributions	5b. GRANT NUMBER
	5c. PROGRAM ELEMENT NUMBER
6. AUTHOR(S)	5d. PROJECT NUMBER
	5e. TASK NUMBER
	5f. WORK UNIT NUMBER
7. PERFORMING ORGANIZATION NAME(S) AND ADDRESS(ES) **University of Kansas Center for Research**	8. PERFORMING ORGANIZATION REPORT NUMBER
9. SPONSORING/MONITORING AGENCY NAME(S) AND ADDRESS(ES)	10. SPONSOR/MONITOR'S ACRONYM(S)
	11. SPONSOR/MONITOR'S REPORT NUMBER(S)

12. DISTRIBUTION/AVAILABILITY STATEMENT
Approved for public release, distribution unlimited

13. SUPPLEMENTARY NOTES
The original document contains color images.

14. ABSTRACT

15. SUBJECT TERMS

16. SECURITY CLASSIFICATION OF:			17. LIMITATION OF ABSTRACT	18. NUMBER OF PAGES	19a. NAME OF RESPONSIBLE PERSON
a. REPORT	b. ABSTRACT	c. THIS PAGE			
unclassified	**unclassified**	**unclassified**	**SAR**	**168**	

Standard Form 298 (Rev. 8-98)
Prescribed by ANSI Std Z39-18

Table of Contents

Background:

Considerable research has shown that the major control on the transport and fate of a pollutant as it moves through an aquifer is the spatial distribution of hydraulic conductivity. Although chemical and microbial processes play important roles, their influence cannot be understood without a detailed knowledge of the subsurface variations in hydraulic conductivity at a site. Many theories have been developed to quantify, in a generic sense, the influence of these variations using stochastic processes or fractal representations. It is increasingly apparent, however, that site-specific features of the hydraulic conductivity distribution (such as high conductivity zones) need to be quantified to reliably predict contaminant movement. Conventional hydraulic field techniques only provide information of a highly averaged nature or information restricted to the immediate vicinity of the test well. Therefore, development of new innovative methods to delineate the detailed hydraulic conductivity distribution at a given site should be a high priority. The research proposed here is directed at addressing this problem by developing techniques to map 3-D hydraulic conductivity distributions.

Objective:

Since spatial changes in hydraulic conductivity are a major factor governing the transport and fate of a pollutant as it moves through an aquifer, we focus on the development of new innovative methods to delineate these spatial changes. The objective of the research proposed here is to build on our previous work to develop and improve field techniques for better definition of the three-dimensional spatial distribution of hydraulic conductivity by using hydraulic tomography coupled with high-resolution slug testing.

Technology Approach:

We have worked for many years to quantify hydraulic conductivity fields in heterogeneous aquifers. One promising method we have worked on extensively is high-resolution slug testing. This method allows the delineation of the vertical distribution of hydraulic conductivity near an observation well. We propose to combine this method with another innovative method for investigating the hydraulic conductivity distribution between wells, called hydraulic tomography. We will use an oscillating signal and measure its phase and amplitude through space in order to estimate the hydraulic conductivity distribution of the material through which it has traveled. Our preliminary work shows that the phase and amplitude of the received signal can be measured over reasonable distances. The high-resolution slug testing results will be used as an initial condition and will provide conditioning for the tomographic inverse procedure, to help with any non-uniqueness problems. Slug test data are most accurate near the tested well and should probably not be extrapolated blindly between wells. Together, slug testing and hydraulic tomography should be more powerful than either one used alone and should give the best opportunity to characterize the hydraulic conductivity in-situ by a direct measure of water flow, as an alternative to indirect methods using geophysical techniques.

Introduction

A typical method used to determine fluid behavior in a geologic matrix near a well is a pumping test. Here a pump is installed into a well and groundwater is removed or injected while water levels in surrounding observation wells are monitored. Then the aquifer parameters can be estimated by monitoring changes in water levels at observation wells at some distance. These tests are typically large in scale (Schad and Teutsch, 1994). Another test is an interference test, which is a special pumping test where the pump discharge has a variable rate. Interference tests are conducted by variable production or injection of fluid (hydraulic head changes) at one well, and observing the changing pressure or hydraulic head with time and distance at other locations. These tests are valued to estimate flow characteristics *in situ,* but are measures of the aquifer material over large volumes also.

On the other hand, physical cores of aquifer material can be obtained by various drilling methods. These samples can then be tested in a laboratory (i.e., falling or constant head permeability tests) to estimate the hydraulic properties. One advantage to this method is that the sample can be visually inspected. Some disadvantages to this method are that the material is disturbed from its natural environment and the sample is a small representation of the total aquifer.

Another common technique for determining aquifer parameters is slug tests. A slug test initiates a head change in a well, then monitors the response of the aquifer material to estimate the hydraulic conductivity (K). Slug testing is usually only conducted in a single well. It is generally accepted that the radius of influence of a slug test is small and only provides a limited view of subsurface hydrogeologic properties near

the well. Traditionally, slug tests have been initiated with the addition into a well of a known volume of water or a physical slug. More recently, pneumatic methods have become popular (Zemansky and McElwee, 2005; Sellwood, 2001; McCall et al., 2000) for multilevel slug testing. Slug tests in low K formations can take much longer than in material with high permeability. To overcome this, the fluid column in a well can be pressurized and the pressure change with time can be used as an alternative (Bredehoeft and Papadopulos, 1980).

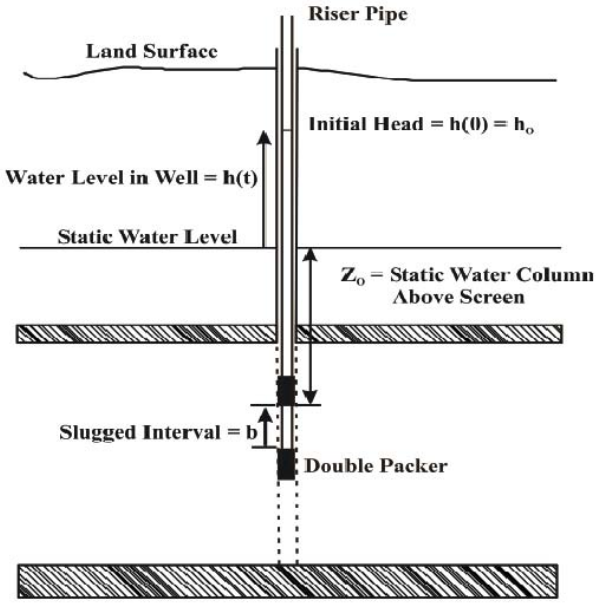

Figure 1. High resolution slug testing equipment deployed in a fully penetrating well.

Typical slug tests are conducted by exciting the entire length of the well screen. Whole well slug testing can provide information near the tested well but it is an average response over the total length of that well's screen. However, aquifers are naturally heterogeneous and whole well slug testing is unable to distinguish areas of high or low K. High resolution slug testing [(HRST), over short screen intervals (Figure 1)], provides a more detailed vertical profile of K near the tested well. In this research the HRST

interval is approximately 0.5 m; but, stressed intervals as small as 5 cm have been used (Healey et al., 2004). Currently there is no accepted method to bridge the gap between the larger lateral well-to-well averages from pumping or interference tests and detailed vertical estimates of K from HRST. Proposed here is a method to obtain estimates of aquifer parameters at larger radii of influence, while simultaneously maintaining a higher resolution.

Pulse testing is one method of determining fluid flow parameters that is often employed by the petroleum industry. Johnson et al. (1966) published results of experiments conducted in a sandstone reservoir near Chandler, OK. They found that the new pulse method was as effective as typical interference tests. The transient pressure signal is propagated by *in situ* fluid and is therefore a direct measure of reservoir diffusivity. Other advantages of the pulse method are the ability to distinguish the test from background noise because of its controlled frequency of oscillation and the reduction of down time relative to production. Since 1966, pulse testing has been used to delineate fractures (Barker, 1988; Brauchler, et al., 2001) and to predict water flood performance (Pierce, 1977).

Other pulse test examples include tidal, seismic, and oil field methods. The changes in groundwater levels as a result of tidal fluctuations have been well studied (Ferris, 1951; Hantush, 1960; Jiao and Tang, 1999). The sinusoidal tidal fluctuations that propagate inland through an aquifer are related to aquifer storativity and transmissivity. Solutions to water level fluctuations induced by seismic waves were presented by Cooper et al. (1965). The pressure head fluctuations controlling water levels are a result of the vertical motion of the aquifer but are dominated by dilation of aquifer porosity. An

interference test of alternating oil production and shut-in time was conducted to determine the interconnectivity of wells in a production field (Johnson et al., 1966). Here the source well is assumed to be a line source in an infinite homogeneous reservoir. The time lag and the received amplitude were used to estimate the average well-to-well transmissivity and storage properties of the reservoir. These oil field methods were theoretically adapted to hydrogeologic characterization by Black and Kipp (1981). Analytical solutions of a fracture responding to a single pulse interference test, a slug of water, was modeled and tested by Novakowski (1989). Straddle packers isolated the fracture and were used to apply the slug of water by being deflated. The duration of these tests was on average 30 min. The sequential pumping or removal of water was used to collect head responses between wells (Yeh and Liu, 2000). In these experiments multiple ray paths were analyzed as a hydraulic tomography experiment. Such experiments show promise in their ability to distinguish lateral and vertical 2-D variations in heterogeneity by changes in the signal over the travel path.

The research presented in this report uses continuous, controlled, sinusoidal pressure signals [the continuous pulse test (CPT)] as a means to estimate vertical profiles of well-to-well averaged hydraulic diffusivity. In this research, the primary method of stimulation of the alluvial aquifer was achieved by pneumatic methods or by mechanical pumping methods. In the pneumatic method the column of air within a well was pressurized via an air compressor. A signal generator or computer controlled switch was used to open and close valves at the well-head allowing air to enter or exit the well. The signal generator or computer controlled signal produced an adjustable frequency excitation voltage, which controlled the periodicity of the continuous pulse-testing signal.

Theoretically, a square wave pressure test is the simplest to conduct because of the instantaneous pressure changes (Lee, 1982). Due to the input air pressure, the water column in a well will be depressed creating flow through the well screen. This pulse of hydraulic pressure is transferred to the aquifer system based on the diffusivity of the material. As the air column within the well is allowed to return to atmospheric pressure, water rushes back into the well from the aquifer. The mechanical pumping method used a surface reservoir of water and a pump to inject water into the aquifer. The pressurized water was allowed to flow into the aquifer in a periodic sinusoidal fashion with the help of a computer controlled valve. These fluctuations are periodic and similar to tidal fluctuations acting upon a costal aquifer system. The governing equations for an aquifer responding to tidal fluctuations were adapted to Cartesian, cylindrical, and spherical coordinate systems describing groundwater flow with sinusoidal boundary conditions, in order to describe the data used in this report.

The period, the phase, and the amplitude of the produced wave can then be measured simultaneously at the source well and at observation wells. Through dispersion, the aquifer material will decrease the fidelity of the input signal, retard the propagation, and attenuate the propagating wave front, resulting in a phase lag or shift, and a decrease in the amplitude. The amplitude ratio [received amplitude A_r divided by the initial amplitude A_0] and the phase difference [reference phase ϕ_0 minus the received phase ϕ_r] can then be used to calculate the hydraulic diffusivity (Lee, 1982).

Zero Offset Profile (ZOP, source and receiver at same elevation) data and Multiple Offset Gather (MOG, source location fixed; receiver elevation varied) data were collected at the University of Kansas' Geohydrologic Experimental and Monitoring Site

(GEMS), a well-studied shallow semi-confined alluvial aquifer system in the Kansas River floodplain. Line sources equal to the total screen length and point sources isolated by custom bladder packers were used in these experiments. Field data indicate that sinusoidal signals can propagate reasonable distances, and may provide estimates of the well-to-well diffusivity. Vertical profiles of hydraulic conductivity (K), measured with high-resolution slug testing (HRST), were collected for correlation with the CPT data.

The GEMS area is located in Douglas County, northeast Kansas, along the northern margin of the Kansas River floodplain (Figure. 2). GEMS is in a Pennsylvanian bedrock valley filled with Wisconsinan-age glaciofluvial terrace sediments (O'Conner, 1960; Schulmeister, 2000). The upper 11 m of sediments are mostly silts and clays and the lower 12 m of sediments at GEMS is a fining upward sequence of pebbles, coarse sand, and fine sand, underlain by the Tonganoxie Sandstone member (Jiang, 1991). Within the sequences of sandy material are lenses of low permeability fine-grained sediments. These clay lenses occur at various elevations and can be up to 1 m thick (Schulmeister, 2000; Healey et al., 2004). As an aquifer, the Kansas River alluvium is a prolific deposit of unconsolidated sands and gravels. This high yielding semi-confined aquifer meets the needs of agricultural, industrial, and community interests.

Many studies have been conducted at GEMS and many well nests have been completed to various depths with various screen lengths. Porosity, grain size, and K were estimated by laboratory experiments performed on physical samples of the aquifer material (Jiang, 1991). A single-well injection tracer test was used to estimate a K distribution by monitoring the transport of an electrolytic solution (Huettl, 1992). The K distribution in an area of GEMS was also estimated by conducting an induced-gradient

tracer test through a multilevel groundwater sampling well field (Bohling, 1999). Direct push bulk electrical conductivity (EC) profiling (Figure 3) and direct push pneumatic slug tests were also done adjacent to the tracer experiment well field (Sellwood, 2001).

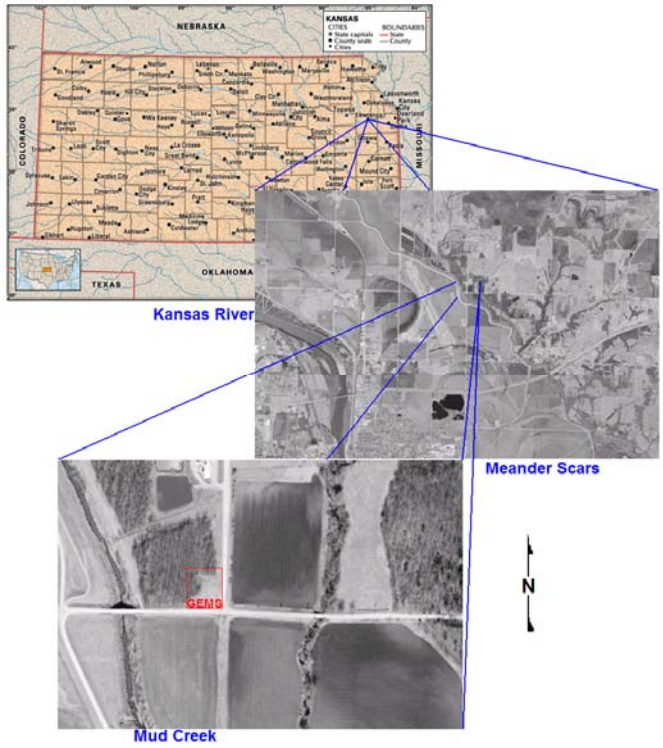

Figure 2. GEMS location map and aerial photographs.

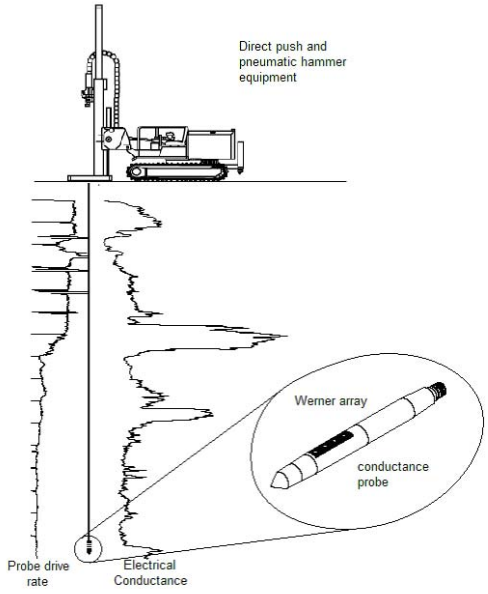

Figure 3. Direct push drilling unit, Electrical Conductance probe, and example profile.

Most recently, HRST K estimates were collected in numerous wells that were fully screened through the aquifer material (Ross, 2004; Ross and McElwee, 2007). These independent studies and the research presented here produced estimates of K that can be collected into a database. After compiling these data, vertical and lateral variations of the K distribution are evident. Typically at GEMS, K increases with depth in the sands and gravels, and low K material can be associated with high EC measurements, usually associated with the overlying silt and clay sediments. In most areas at GEMS, "layers" or zones of high K material are apparent in the sand and gravel aquifer.

Theory

Fluid flow in saturated aquifers behaves much like heat flow and can be described by similar equations. Excess pore pressures, matrix permeability, compressibility, and storativity all influence the fluctuations of groundwater levels in response to applied

stresses. The excess fluid pressure P_e, above hydrostatic pressure P_s, is related to the total stress on the aquifer σ, and changes the stress $\Delta\sigma$ by

(1) $$\sigma + \Delta\sigma = \sigma_e + (P_s + P_e)$$

The above equation allocates the additional stress to either the aquifer matrix itself (σ_e) or to excess hydraulic pressure, P_e. By changing the hydraulic pressure or hydraulic head, the water levels in an aquifer also change accordingly. The total hydraulic head (h) hydraulic potential measured in a well is a combination of the elevation head z, and the hydraulic pressure head, P

(2) $$h = z + P/\rho g$$

such that

(3) $$P = P_s + P_e$$

Since the elevation is static, the only dynamic portion of h is due to pressure changes as shown in the following equation

(4) $$\frac{\partial h}{\partial t} = \frac{1}{\rho g}\frac{\partial P}{\partial t}$$

where ρ is the fluid density and g is the acceleration of gravity. Substituting equation (3) into equation (2) the total head measured in a well can also be expressed as

(5) $$h = z + (P_s/\rho_w g + P_e/\rho_w g)$$

Darcy's law states that the discharge Q of a fluid through a porous media depends on the hydraulic gradient (the change in head with distance) $\frac{\partial h}{\partial L}$, and the cross sectional area A. Darcy's Law is

(6) $$Q = -KA\frac{\partial h}{\partial L} \ .$$

Darcy's proportionality constant K, now called hydraulic conductivity, is a measure of how easily a fluid flows through an aquifer. By combining equation (5) with equation (6) the one-dimensional horizontal flow in the x direction q_x is

(7) $$q_x = -K_x\left(\frac{\partial h}{\partial x}\right) = -K_x\left(\frac{\partial}{\partial x}\right)\left[z + \left(\frac{P_s}{\rho g} + \frac{P_e}{\rho g}\right)\right]$$

Assuming that z and P_s are constant, the flow due to excess pressure is

(8) $$q_x = -\frac{K_x}{\rho g}\left(\frac{\partial P_e}{\partial x}\right)$$

Diffusivity is the ratio

(9) $$D = T/S = K/S_s.$$

D is a measure of the ability of an aquifer to transmit changes in the hydraulic head. The following conservation equations, written either in terms of P_e or h, demonstrate the relationship between K, S_s, and D

(10) $$K_x\frac{\partial^2 P_e}{\partial x^2} = S_s\frac{\partial P_e}{\partial t} \quad \rightarrow \quad D\frac{\partial^2 P_e}{\partial x^2} = \frac{\partial P_e}{\partial t}$$

and

(11) $$K_x\frac{\partial^2 h}{\partial x^2} = S_s\frac{\partial h}{\partial t} \quad \rightarrow \quad D\frac{\partial^2 h}{\partial x^2} = \frac{\partial h}{\partial t}$$

The above equations can be generalized to three dimensions. The goal of this research is to utilize the response of hydrogeologic material to cyclic pressure signals to estimate the D or K distribution in an aquifer.

Groundwater fluctuations near coastal regions have been studied and elementary equations have been developed to associate regional groundwater levels with tidal

fluctuations (Hantush, 1960). The basic mathematical description of a one-dimensional transient pressure head signal with sinusoidal boundary conditions [sin(2πft)] is

(12) $$h(r,t) = h_o e^{d} \sin(\Phi_0 - \Phi_r).$$

The head at some distance and time h(r,t) is the initial amplitude h_o, some decay term e^d, multiplied by the sine of the source reference phase (Φ_o=2πft) minus the phase shift, Φ_r. The amplitude decay and the phase shift depend on the ability of the aquifer to transmit the sinusoidal signal. Namely, it is the hydraulic diffusivity (D or K/Ss) of the aquifer that influences the hydraulic head measured at some distance and time from the source of a pressure head fluctuation. Three equations for the head response to the propagation of a sinusoidal boundary condition (causing excess fluid pressure) within a homogeneous isotropic formation have been adapted from equation (12). Equation (12) has been extended to various coordinate systems, presented below.

Linear Cartesian System

(13) $$h(x,t) = h_o e^{-\sqrt{\frac{\pi f S_s}{K}}x} \sin\left(2\pi ft - \sqrt{\frac{\pi f S_s}{K}}x\right)$$

Cylindrical Radial System

(14) $$h(r,t) = h_o \frac{e^{-\sqrt{\frac{\pi f S_s}{K}}r}}{\sqrt{r}} \sin\left(2\pi ft - \sqrt{\frac{\pi f S_s}{K}}r\right)$$

Spherical Radial System

(15) $$h(r,t) = h_o \frac{e^{-\sqrt{\frac{\pi f S_s}{K}}r}}{r} \sin\left(2\pi ft - \sqrt{\frac{\pi f S_s}{K}}r\right)$$

Where t is time, x or r is the distance from the source, f is the frequency, h_o is the initial amplitude of the pressure head fluctuation at the source, S_s is the specific storage, and K is the hydraulic conductivity. Specific storage is the volume of fluid added or released per unit volume of aquifer per unit thickness, from compression or relaxation of the aquifer skeleton and pores due to changes in stress. Equation (13) is exact (Hantush, 1960); however, equations (14) and (15) are good approximations away from the origin. This issue will be confirmed by numerical modeling later. The coordinate equations (13, 14, and 15) can be thought of as two parts: the amplitude [AMP] on the right hand side

(16) $$AMP = h_o \frac{e^{-\sqrt{\frac{\pi f S_s}{K}} r}}{r^*}$$

where r^* is the appropriate denominator in equations (13, 14, and 15), and the sinusoidal source phase Φ_o,

(17) $$\Phi_o = (2\pi f t) \ .$$

The difference in phase Φ_r between two locations is expressed by the term

(18) $$\Phi_r = -\sqrt{\frac{\pi f S_s}{K}} r = d$$

which is equal to the exponential decay term (d) in equations (12, 13, 14, and 15). Both the amplitude decay and the degree of phase shift depend on the ratio of hydraulic conductivity to specific storage, which is the hydraulic diffusivity (D). Estimates of K may be inferred from equation (18) to compare with other methods if S_s is assumed.

The preceding equations can be used to predict phase and amplitude versus distance for homogeneous systems, where K and S_s are constant. However, for heterogeneous systems where no analytical solutions are available, one must resort to

numerical solutions. We postulate that relatively simple formulas presented above can be used to analyze the data for heterogeneous cases by using a distance weighted average for the K. The premise is that the following replacement in the above equations might work.

(19) $$\sqrt{\frac{\pi f S_s}{K}}r \quad \Rightarrow \quad \sum_{i=1}^{I}\sqrt{\frac{\pi f S_s}{K_i}}(r_i - r_{i-1})$$

The index (I) indicates the present location of r; so, the summation continues up to the present location of r and terminates at that point.

As indicated above, one must resort to numerical methods to calculate the phase and amplitude relations with respect to distance for heterogeneous cases where K and Ss change with distance. We have developed numerical models for calculating the amplitude and phase in the presence of heterogeneity for Cartesian, cylindrical, and spherical coordinate systems. This research will in later sections show that the simple replacement proposed by equation (19), along with equations (13) through (15), can be used to simplify the inversion for K in certain cases.

Equations (14) and (15) represent the two experimental approaches utilized in this research. The cylindrical radial equation (14) describes the behavior of the excitation of a relatively long and small radius section of screen that behaves as a line source. Fully penetrating wells are often constructed at GEMS. Any test where the total screen length is excited is termed a whole well test. The spherical radial equation (15) is a representation of the point source geometry, where the excited length of well screen is relatively short. To achieve this, either a partially penetrating well with a relatively short screen length or a straddle packer apparatus must be used. A straddle packer is a double

inflatable packer arrangement, which isolates a centralized interval. It is advantageous if the packer apparatus can be deployed down typical 2 inch (5.08 cm) observation wells; so, considerable effort has been expended to design such packers for this research.

Previous studies have shown that a line source allows for higher energy input, higher amplitudes, and increased signal propagation (Black and Kipp, 1981). A line source can create multiple ray paths to the receiver, decreasing the resolution and only approximating gross K distributions. High K material can also preferentially propagate excess pore pressures generated by a line source, which will induce a vertical gradient and cross-flow within the aquifer. Depending on the 3-D heterogeneity distribution, this cross-flow will alter the receiver signal, similar to a weighted average, again decreasing the resolution. Even high amplitude line source signals decay rapidly in the subsurface. Most of the decay is due to the exponential term in equations (14) and (15). In addition, the radial distance between source and receiver wells will cause further decay (the cylindrical or line source will additionally decay by the inverse square root of r [equation (14)] and the spherical or point source will decay by the inverse of r [equation (15)]). These additional amplitude decay effects are due to wavefront spreading loss. However, the point source arrangement may increase the resolution of the K distribution profile because of fewer ray path possibilities.

The common component of the amplitude decay and the phase shift is $\sqrt{\frac{\pi f S_s}{K}} r$;

therefore, it is possible to compare the phase data to the amplitude data (after correcting for spreading loss). Using aforementioned assumptions, estimates of K can be obtained through algebraic manipulation. However, this method does not give a specific value for K, but rather an average ratio of S_s/K for the signal travel path from source well to

receiver well. Simple theory presented here indicates that the phase and the corrected amplitude ratio should vary linearly with $\sqrt{\frac{S_s}{K}}$ and distance (r) from the source well. Therefore, average parameters between well pairs may be estimated. Further, if multiple source and receiver offsets (relative to their elevations) are used, multiple diagonal ray paths may be recorded (Multiple Offset Gathers, MOGs). This type of testing is called hydraulic tomography (Yeh and Liu, 2000; Bohling et al., 2002; Bohling et al., 2003), and can give more detailed information about hydraulic properties between wells. In the first phase of this project we concentrated on horizontal rays where the source and receiver are at the same elevation (Zero Offset Profiles, ZOP). A ZOP survey is the simplest tomographical survey to conduct and process, but can only give information on average horizontal aquifer parameters. During follow up phases of this project we started collecting diagonal ray path data (MOGs). These data show the effects of heterogeneity in K and offer the best opportunity to measure the hydraulic conductivity distribution. Therefore, we expended considerable effort trying to find the optimum method of processing these field data.

Field Methodology

Recent studies at GEMS have utilized custom-built straddle packers (McElwee and Butler, 1995; Zemansky and McElwee, 2005; Ross and McElwee, 2007), and pneumatic slug testing technique techniques (McElwee and Zemansky, 2005; Sellwood, 2001; Ross and McElwee, 2007). In this work custom made packers are used to isolate a zone for testing. This testing may either be high resolution slug testing (HRST) or cross-hole measurement of relative amplitudes and phases for hydraulic tomography .

HRST Techniques

The aquifer material at GEMS exhibits linear and non-linear responses to slug testing (Figure 4). The response of the aquifer material to the slug can be dampened such that water levels in a well return to static head conditions with time in a smooth non-oscillatory curve. However, the aquifer can be underdamped and water levels will oscillate, decaying with time, until pre-test conditions are reached (Van Der Kamp, 1976). Theoretical advances, presented by McElwee and Zenner (1998) and McElwee (2001, 2002), have made analysis of nonlinear behavior practical and meaningful. The aforementioned slug tests are localized tests; but, continuous layers of geologic material between tested well pairs should correlate with HRST data from each well in the well pair.

Slug testing of an aquifer is an important tool for determining aquifer heterogeneity near a well. This type of test will average the hydraulic properties over a limited volume of aquifer. The volume of aquifer tested depends on the length of screen in the aquifer at the tested well. A vertical profile of hydraulic conductivity distributions can be determined using high-resolution slug testing in wells (Zemansky and McElwee, 2005; Ross and McElwee, 2007), or even with small diameter direct push equipment (Sellwood, 2001; Butler et al., 2002a,b; McCall et al., 2000). High-resolution slug testing enables hydrogeologists to examine vertical variations in K at a much finer scale relative to whole well slug testing.

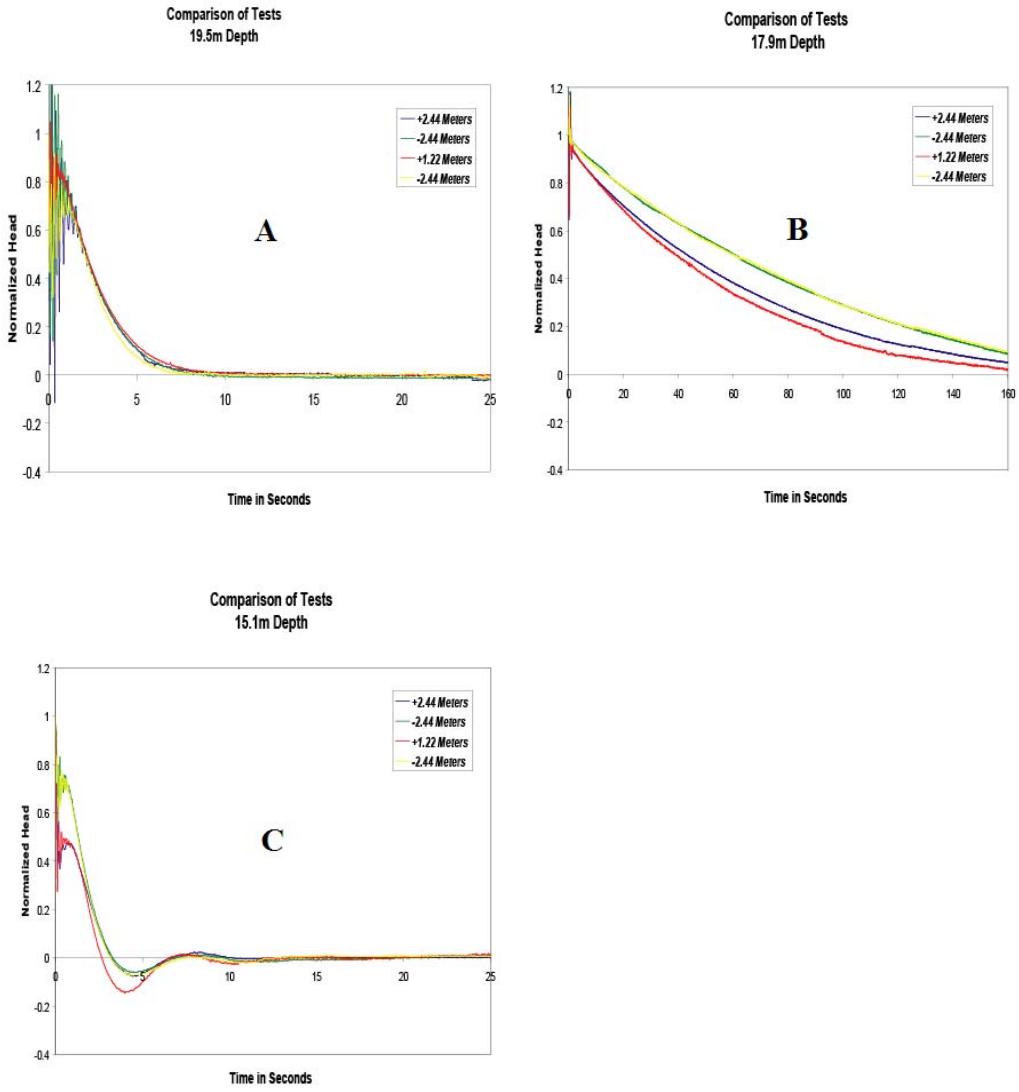

Figure 4. Three examples of slug tests performed at GEMS. Graph A displays no head dependence and behaves linearly. Graph B shows a dependence on the initial slug height and direction. Graph C is oscillatory and has some nonlinear characteristics.

The preferred method for initiating a multi-level slug test is to use pneumatics (Prosser, 1981; Zurbuchen et al., 2002; Zemansky and McElwee, 2005; Ross and McElwee, 2007). The advantages of using pneumatics are that nothing is added to or produced from the aquifer and less equipment is needed, which is best for contaminated sites. The program NLSLUG (McElwee, 2000, 2001) based on the model presented by

McElwee and Zenner (1998), was used to aid in the interpretation of oscillatory and non-oscillatory hydraulic head responses obtained from slug testing.

CPT Techniques

The Continuous Pulse Test (CPT) is an exploratory method for extending slug test results between well pairs by propagating a sinusoidal signal. As mentioned earlier, two different methods were used to produce a sinusoidal signal: pneumatic means and mechanical pumping. The distance between wells in pairs tested and analyzed with the CPT method in this research have ranged from 3 to 11.5 m. The instrumentation's ability to discern signal from noise may be a limiting factor at greater distances. As with most geophysical techniques, the equipment set up time can consume considerable time in the field. The CPT vertical profile method usually takes longer to perform (depending on the interval spacing) than the typical high resolution slug test vertical profile for a given well.

In the pneumatic method an air compressor is used to supply the driving force behind the CPT method and it is connected to an apparatus attached to the top of the casing at the well (Figure 5).

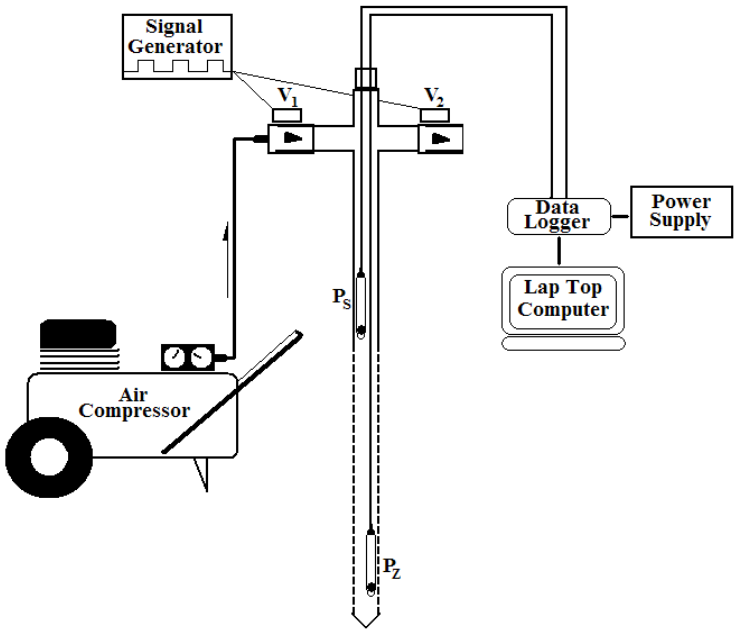

Figure 5a. The pneumatic CPT equipment set up for a line source configuration. A signal generator opens and closes valves (V_1 and V_2) to control the flow of air supplied by the air compressor. The pressure transducers record the amplitude and phase at depth P_z and a reference location P_s. This setup can be easily modified for a point source configuration by using a double packer to isolate the stressed interval.

A signal generator or computer controlled signal is used to power servo-controlled valves on the apparatus, which allows air pressure to be increased in the well or to be released to the atmosphere. Increasing pressure depresses the water column, releasing the air pressure allows the water column to rebound. A single pulse of pressure is a slug test, while stacking them one after another, will create a CPT. The frequency and amplitude of the CPT data should be adjusted to give optimal results (Engard et al., 2005; Engard, 2006). Figure 5b shows the pneumatic pressure manifold with the servo-controlled values, which was used at the top of the source wells.

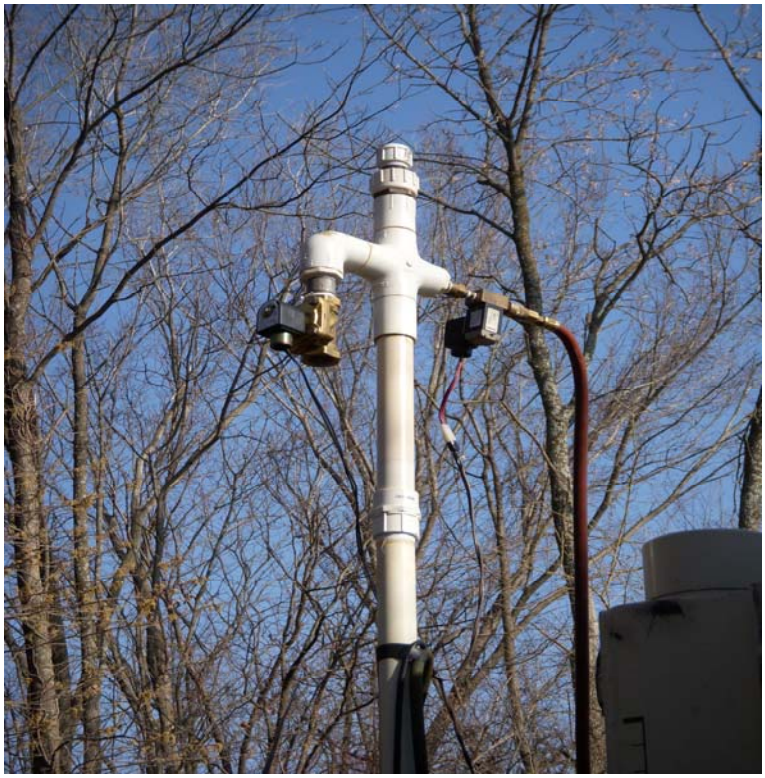

Figure 5b. Pneumatic pressure manifold with servo-controlled valves.

In the mechanical pumping method the air is replaced by water from a surface reservoir and supplied to the aquifer by a pump through a computer controlled valve, operated in such a way that the pressure response at the injection location approximates a sine wave. This field setup is shown in Figure 5c. In this setup the upper pressure transducer shown in Figure 5a is not used. The net result is again a pressure signal injected into the aquifer and measured by the lower pressure transducer. Since we are continually injecting water in this method, there is a trend of increasing pressure that must be removed by data processing before the phase and amplitude are determined. In an ideal setup the period of this mechanical pumping period would be variable. However, in this project we were only able to find hardware off the shelf that would allow a pumping period of 30 seconds. In future research, it would be preferable to

design and build a system that would allow smaller pumping periods, for reasons that will be discussed later.

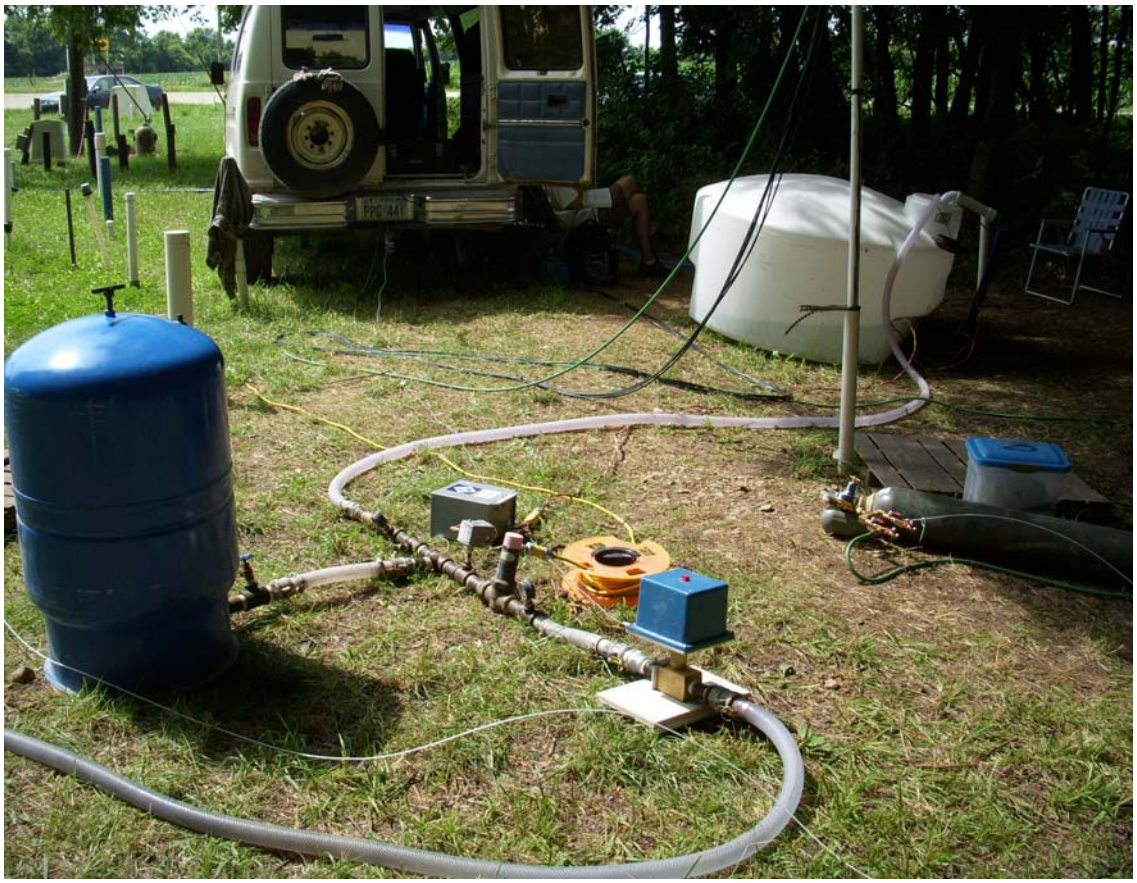

Figure 5c. Pumped hydraulic injection apparatus for the CPT.

Surveys were done in the form of zero offset profiles (ZOP) and multiple offset gathers (MOG). For a ZOP the packed-off source excitation interval with a transducer and the packed-off receiver interval with a transducers are kept at the same level, as they are moved through the common screened interval of the source and receiver wells. For a MOG, a packed-off source excitation interval with a transducer is kept at a fixed depth in the source well while another packed-off receiver interval with a transducer is moved

throughout the screened interval of the receiver well. For this study, measurements were usually taken in 0.30 m (one ft) intervals (sometimes 1.0 m or 3 ft intervals were used). After measurements were collected between one source location and all the receiver locations, the source was moved by 0.30 m and measurements were again collected at all the receiver locations. The process was repeated until rays had traveled from every location in the source well to every location in the receiver well (Figure 6). The collective examination of these multiple ray paths forms the tomographic study.

Initially, a single-channel receiver was used in data collection. However, a multi-level receiver with five pressure transducers was later constructed to expedite data collection. Pressure ports were located approximately 1 m apart isolated on either side by packers measuring approximately 0.6 m in length. The main advantage of this apparatus is that it allows efficient collection of multiple MOGs, which are needed for tomographic surveys.

The MOG data taken from a well pair should produce a parabolic phase shift curve due to the path lengths of the rays. Path lengths are greater for more distant offsets (Figure 6). Larger phase and amplitude changes occur at these larger offsets. If the source is in the middle of the well, the greatest distance and therefore greatest change in amplitude and phase should occur when the receiver is at the top or bottom. The shortest distance is when the source and receiver are at the same depth. The general shape should be a parabola with distortions due to heterogeneity. When the source is at the top, the shortest distance is to the receiver location at the same depth and the greatest distance is to the receiver location at the bottom of the well. The curve should therefore have a half-parabola shape when the source is at the top of the well. The same is true when the

source is at the bottom of the well. Examples of these parabolic shapes are shown in Figures 6.

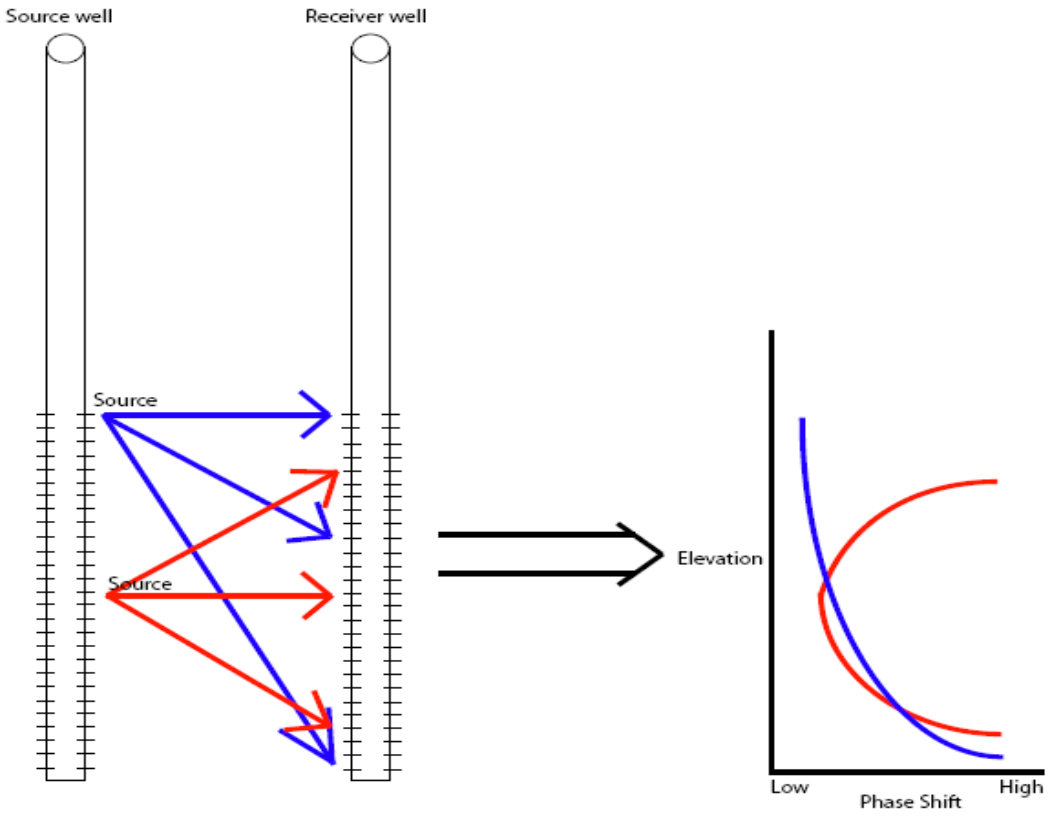

Figure 6. MOG setup for the tomographic study.

Pressure transducers were used to monitor pressure head fluctuations in both the source well and at the observation wells. The data were collected from the pressure transducers by a data-logger and stored on a field computer for later analysis. Data were typically recorded at a 20 Hz sampling rate, which provided sufficient temporal resolution. The field computer and data logger allowed real-time monitoring of the CPT records.

Vertical Sensor Array

Throughout the project we have continued to improve the design of the vertical sensor array. Moving the receiver location to many discrete locations along the receiver well screen is very time consuming. To speed this process, we designed a vertical sensor array with five pressure transducers and six packers. Each transducer is isolated by packers above and below, to allow measurements to be made on a 0.3 m (1 ft) section of the receiver well screen. The transducers are located every 0.91 m (3 ft) along the array, with 0.6 m (2 ft) length packers between. The array may be moved up in 0.3 m (1 ft) increments two times to allow uniform coverage of the first section of the screen at 0.3 m (1 ft) increments. Nearly complete coverage of the 11 m screen can be achieved by pulling the vertical sensor array 3.9 m (13 ft) and repeating the sequence described above. In this way recording six records with the vertical sensor array is equivalent to 30 records with the single receiver setup. This increases the speed of data collection. Pictures of the first generation vertical sensor array are shown below in Figure 7a.

According to the project plan, we were to adapt the sinusoidal source to be used with a Geoprobe unit. Initially, the Geoprobe unit is used to advance a drill string to the bottom of the aquifer. At that point, the drive tip is replaced with a source unit capable of generating a sinusoidal signal and then retracted in stages to occupy each desired source location. During data collection with the source on the end of the Geoprobe unit we used two vertical sensor arrays, since it was expensive to have the Geoprobe on site. We took this opportunity to improve the design of the vertical sensor array and to construct another one. This improved design is shown in Figure 7b. The basic dimensions are the

same; however, the port design and method of connection of the packers was changed to allow easier deployment and retrieval.

Figure 7a. First generation vertical sensor array.

Figure 7b. Second generation vertical sensor array.

New Wells Installed

In late October 2007, three wells were added to GEMS. The wells were chosen to provide better coverage of the area under study by hydraulic tomography. The wells were installed using the direct push method with a Geoprobe unit from the Kansas Geological Survey. The wells initially installed for this project were HT-1, HT-2, and HT-3. The new wells are HT-4, HT-5, and HT-6. All of these wells and others previously used for hydraulic tomography work are shown below in Figure 8. After installation and development, the wells were surveyed to establish the elevation of the top of each casing. The Geoprobe source well location is also shown. Various radii between wells were measured for future analysis of the cross-well data. All of this information about the various wells that were candidates for tomographic study is shown in Table 1.

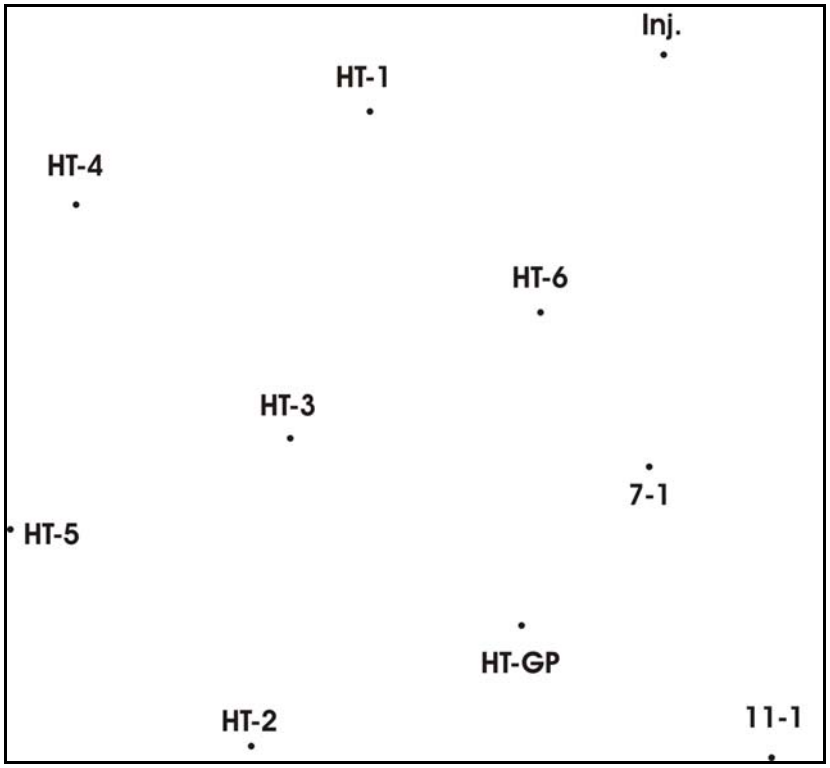

Figure 8. Relative well locations at GEMS (north is up). This shows the locations of the new wells installed in Oct. 2007 and the Geoprobe source location, in addition to older wells previously used in this study.

Table 1. Well Information

Location	Elevation ft	Elevation m	Depth ft	Depth m	Screen ft	Screen m
Stake	827.556	252.239	-----	-----	-----	-----
HT-1	830.005	252.986	72.3	22.04	35.0	10.67
HT-2	829.66	252.880	72.4	22.07	35.0	10.67
HT-3	829.705	252.894	~70.	~21.3	35.0	10.67
HT-4	830.129	253.023	72.2	22.01	35.0	10.67
HT-5	829.651	252.878	71.9	21.92	35.0	10.67
HT-6	830.272	253.067	~72.	~21.9	35.0	10.67
7-1	828.342	252.479	68.85	20.99	30.0	9.14
11-1	828.358	252.484	69.40	21.16	45.0	13.72
Inj. Well	829.794	252.921	71.09	21.67	34.0	10.36
HT-GP ref.	828.82	252.62				

Well to Well Radial Distances, r

Well	Well	Radius (m)	Radius (ft)
HT-3 to	HT-1	4.77	15.65
HT-3 to	HT-2	4.36	14.31
HT-3 to	HT-4	4.46	14.62
HT-3 to	HT-5	4.21	13.81
HT-3 to	HT-6	3.99	13.10
HT-3 to	HT-GP	4.25	13.94
HT-2 to	HT-GP	4.23	13.88
HT-6 to	7-1	2.70	8.85
HT-6 to	11-1	7.19	23.58
HT-6 to	Inj. Well	4.04	13.26
Inj. Well to	HT-1	4.28	14.05
Inj. Well to	HT-4	8.67	28.45
Inj. Well to	HT-5	11.55	37.89
Inj. Well to	HT-2	11.49	37.70
Inj. Well to	HT-3	7.66	25.15
7-1 to	HT-2	6.94	22.79
7-1 to	HT-5	9.18	30.10
7-1 to	HT-3	5.13	16.84
7-1 to	HT-4	9.00	29.53
7-1 to	HT-1	6.46	21.20
HT-6 to	HT-1	3.79	12.42
HT-1 to	HT-4	4.40	14.44
HT-4 to	HT-5	4.63	15.21
HT-5 to	HT-2	4.57	15.00
HT-2 to	HT-6	7.40	24.28

Data Processing, Modeling, and Inversion

Data Processing

Data processing for the ZOP data was done with FitAmpPhaseV8, a program written in Visual Basic by Carl McElwee. The program fits sine waves to the transducer data taken in the field and generates plots of the amplitude ratio and phase shift (x-axis) between the source and receiver transducers. All values are plotted against location (y-axis). The program analyzes data for a single source location at a time. For each MOG, the amplitude ratio and phase shift between the two (upper and lower) source transducers should plot as a vertical line, as there is no change in material within the source well itself. The amplitude ratio and phase shift between the (lower) source and receiver transducers should both plot as nearly parabolas or half-parabolas. If the source location is near the middle of the well, the shape will be a full parabola, and the shape will only be half a parabola if the source is near either the top or bottom of the well. The shape should be nearly parabolic assuming no change in aquifer material (or measurement error), so any deviations from the overall parabola must be due to changes in K (or some experimental error).

Data processing for the MOG data was done with FitAmpPhaseV10HT (early 3-4 sec. data) or FitAmpPhaseV12HT (later 30 sec. and 3 sec. data). These versions of the program analyze all five receiver transducers at once. Aside from accounting for multiple receiver transducers, the programs are based on the same algorithms as FitAmpPhaseV8. Some improvements or changes were made along the way, giving rise to version numbers. Version 10 had to fit the period as a parameter, because the early data used a frequency generator for manual period selection (which was never quite the

same). Version 12 deals with data whose period is computer controlled and consistent from record to record, and also removes any trend of increasing pressure due to the continual injection for the mechanical pumping system. Plots are generated for the receiver location versus both amplitude and phase shift. The raw data and the fitted sine wave for a single receiver location are shown below in Figure 9 for some example data.

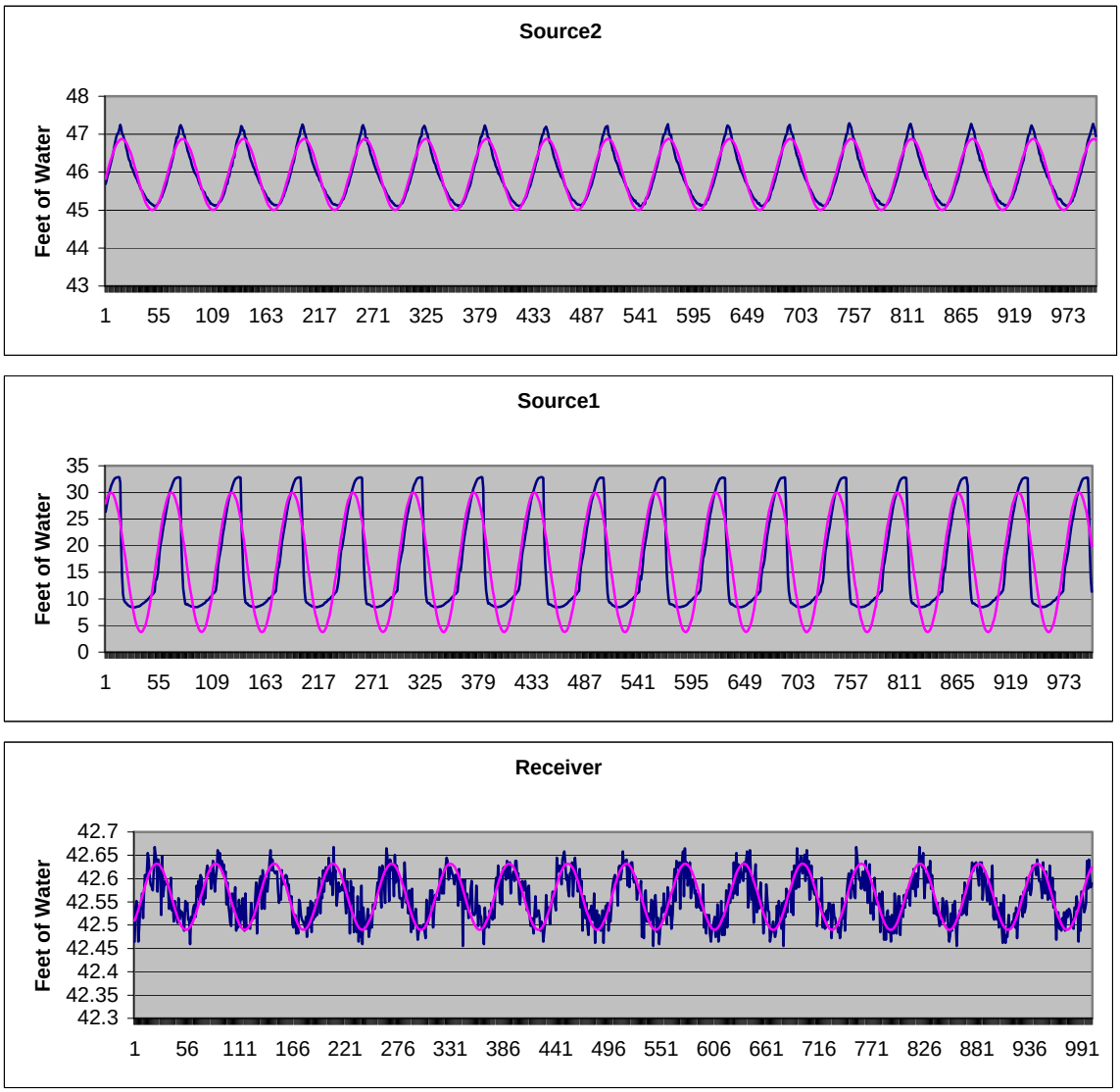

Figure 9: The data for one particular receiver location in the FitAmpPhaseV10HT program. Three plots are shown: one plot for each of the two source transducers and one plot for a receiver transducer. The raw data are shown in blue while the fitted sine wave is shown in pink.

High resolution slug test (HRST) data were processed using the program NLSLUG (McElwee, 2000), developed by Carl McElwee using Fortran and run from Microsoft Excel. Water and air pressure transducers are used to record the initial height of the slug test. For each record, a time break is chosen to begin measuring time, and static values at long times are determined for a base line. Multiple initial heads are used. If the results are independent of initial head and behave linearly, all records lie on top of each other. Usually the records do not completely overlie one another, so there can be problems with both directionality, i.e. positive or negative initial head, and repeatability. Mobile fine sediments could explain both problems (McElwee and Zemansky, 2005). Slug testing can cause fine sediments to move, and these sediments may move more easily into the well than away from the well, creating an annulus containing more fine material at some radius. HRST data for the wells in this study were processed by Brett Engard and Pema Deki (Appendix B). The HRST results can be used to constrain the inversion to ensure that the interwell K values remain in the range observed in HRST results.

Straight Ray Modeling With Spatially Weighted K Values

Typical hydraulic tomography inversions use nonlinear least squares fitting, a numerical model, and iterations to get the best fit, a process that can take much time and computing power. An approximation for the numerical model has been used in this research using straight, spatially weighted ray paths. The path length in each zone of differing K is multiplied by a coefficient involving K to get the phase. This is a direct

implementation of equation (19), and, the accuracy of this approximation must be checked by comparison to a numerical model (which will be done in a later section).

Ray path data were generated by HydraulicTomAnal(V19 and V21, slight differences in version numbers), developed by Carl McElwee in Microsoft Excel. The field area was divided into a grid system with approximately evenly spaced divisions in the horizontal and vertical directions. Each box within the grid is referred to as an element. The model was divided into a series of nodes, elements, and grid spaces (Figure 10).

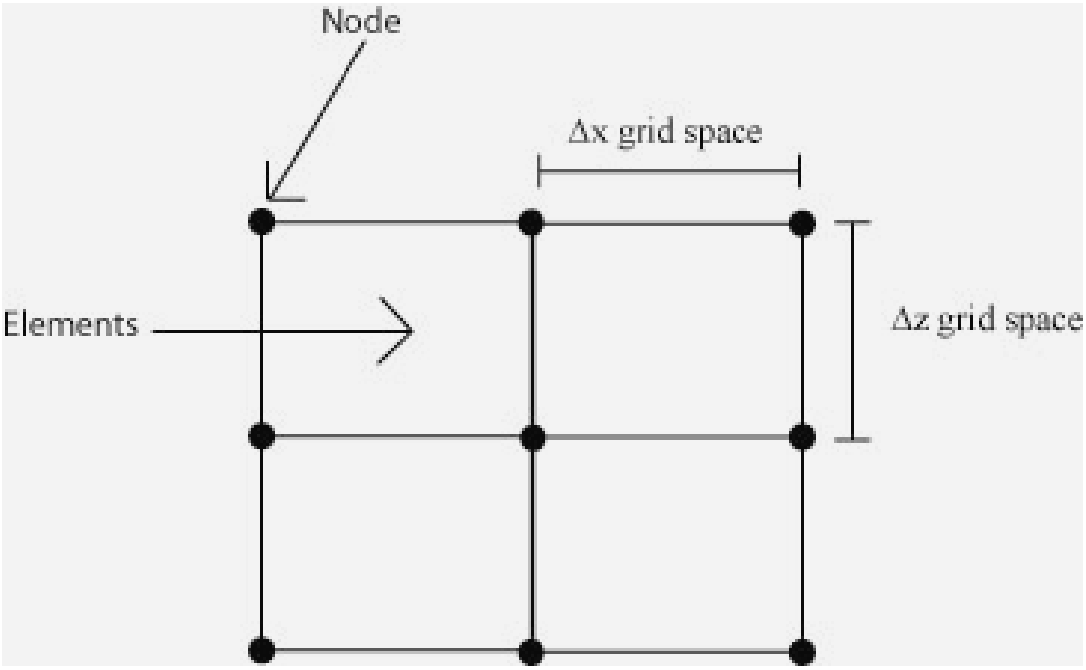

Figure 10: Depiction of a node, an element, and a grid space.

Nodes are any of the individual points throughout the grid. The vertical or horizontal spaces between two nodes, Δx and Δz, are known as grid spacings. An element is the rectangular area enclosed by four adjacent node points.

The values of K may be given either by nodes or elements. If K is given by nodes the K value is linearly interpolated between nodes. If K is given by elements then K is constant everywhere within that element. The program allows zones of constant K by grouping elements or nodes together (depending on how K is specified), which share a common value of K. The program computes the distance of each ray path through every element based on the Pythagorean Theorem. The phase shift for each element is given by an implementation of equation (19), multiplying the path length by the appropriate value of K. Path lengths through each element or zone and phase shift values for each total ray path are then available as output for use in an inversion program.

Data Inversion for K Values

Once we have obtained data, either from the field or by running a numerical model, we have a time series representing the source at some location and a receiver at another location. These time series may be analyzed to find the phase and relative amplitude at the receiver by the method outlined above. We may have a few (ZOP) or many (MOG) ray paths to analyze. In the case of synthetic numerical data we know the input K values and can test the inversion process to see how well these values are returned. In the case of real field data we do not know the correct values. In any case, we must assume some model structure for the data in order to perform the inverse. This will involve assuming the number of nodes, elements, and zones of constant K to use. It is well known in the inverse literature that the inversion may be non-unique due to a number of factors, including model structure and measurement error. In a later section

the stability and uniqueness of various models will be investigated. In this section we merely describe the inversion program that will be used.

The output of the program HydraulicTomAnal(V19 or V21) contains path lengths through each K zone and total phase shift for each straight ray in the data set. These data may be transferred to the LeastSquareSVDV13 or V15 (slight program differences in version numbers) program, developed by Carl McElwee in Microsoft Excel. The SVD, or Singular Value Decomposition, program performs a least squares fitting inversion using zone path lengths and total phase shift values for all ray paths, to obtain K values for each zone by using a set of linear equations (Aster et al., 2005). Equations used in the program do not require iterations with a numerical model because they are linear due to the straight ray approximation used here. The SVD method divides G (matrix of zone ray path lengths), an *m* (number of ray paths and equations) by *n* (number of zones and unknowns) matrix into the following equation:

$$G = UWV^T \qquad (20)$$

where U is an *m* by *m* orthogonal matrix, W is an *m* by *n* matrix with nonnegative diagonal elements known as singular values, V is an *n* by *n* orthogonal matrix, and the T superscript indicates that V is a transpose matrix. Standard deviations of the fitted parameters (K) are calculated based on the goodness of fit. The program has the added feature of reducing to deterministic inversion if the number of equations (ray paths) and unknowns (K values) are equal, provided the matrices are non-singular. This is the program we will use to theoretically evaluate model stability and uniqueness and to perform inversion of the field data to obtain K distributions.

The inversion program (LeastSquareSVDV13 or V15) has options which can be selected. If synthetic data are being inversed, then the program can be run in Monte Carlo mode with a specified per cent of random error added to the data, and, a large number of inversions may be analyzed statistically. The program allows an initial estimate of the K values to be made and a penalty constraint to be applied as the inferred values deviate from the initial estimate. This is a valuable tool to constrain any non-uniqueness tendencies, if one has independent data regarding K. In our case we have some K values from HRST which can be used as constraints.

Finite Difference Numerical Modeling

As indicated above, one must resort to numerical methods to calculate the phase and amplitude relations with respect to distance for heterogeneous cases where K and Ss are changing with distance. We have adapted a numerical model written by Carl McElwee during his years of teaching groundwater modeling at the University of Kansas. This model allows calculation of the pressure response at an arbitrary receiver location in response to an oscillatory input at any given finite location on the well screen in the presence of heterogeneity for Cartesian and radial coordinate systems.

GSIT2DTVHeter is a computer program in VBA (Visual Basic for Applications) written within the Excel spreadsheet environment to evaluate the Cartesian or radial equation for a two-dimensional system of coordinates.

$$\nabla \cdot (K \nabla h) = S_s \frac{\partial \mathrm{h}}{\partial \mathrm{t}} - \frac{Q}{\Delta V} \ , \quad 0 \le x \text{ or } r \le MaxX \, , \ 0 \le z \le MaxZ$$

The above equation has been written for groundwater flow. Hydraulic head (Length) is given by h, the sources or sinks of water (Q) for the system (Length^3/Time) represents

water added to (positive) or subtracted from (negative) the system per unit volume (ΔV), K is the hydraulic conductivity (Length/Time), and S_s is the specific storage (1/Length). The physical parameters Kx (hydraulic conductivity in x direction), Kz (hydraulic conductivity in z direction), Ss (specific storage), and m (aquifer thickness) may be specified for every node, simulating heterogeneity. MaxX and MaxZ are the lengths in the x and z directions of the region for solution. Boundary conditions on the four sides can be either head specified or derivative specified. For the radial case an alternate is to specify the pump rate of the well at the left-hand boundary (assumed well screen location); in this case, the boundary condition on the well screen can vary from node point to node point. This feature allows us to put a sinusoidally varying pumping rate at one or more nodes and then specify a barrier boundary condition (simulating the presence of a packer) for the other well screen nodes.

The use of GSIT2DTVHeter allows us to generate synthetic field records for various source and receiver locations, simulating ZOP and MOG field records. These simulated field records may be processed thorough the FitAmpPhase program to obtain the relative amplitude and phase shift at the receiver and then processed further by the HydraulicTomAnal and LeastSquareSVDV programs as discussed above in order to test the validity of the straight, spatially weighted ray path approximation.

Investigation of Straight Ray Approximation

As presented earlier in this report it is postulated that perhaps a spatially weighted average K value [equation (19)] could be substituted into the homogeneous analytical solution [equations (13) through (15)] as an approximation to the heterogeneous case.

Since no analytical solutions exist for arbitrary heterogeneous systems, we must resort to numerical modeling to check this approximation. Modeling studies were performed to compare results from the spatially weighted ray-tracing method with those from a numerical model for Cartesian and cylindrical coordinates. The goal is to see if the simple replacement proposed above can simplify the inversion for K.

Using the output of the numerical models, we used an early version of the FitAmpPhase program to calculate the phase and amplitude as a function of distance for heterogeneous models for the Cartesian and cylindrical coordinate systems (no variation in the vertical direction). Using equation (19) as an approximation we can calculate the K values expected from these values of phase. We looked at systems consisting of blocks of material with differing K and for systems where K varied systematically, such as in a linear trend. As can be seen from the data presented in Table 2, the agreement between the numerical data and the theory using a spatially weighted average to solve for K is excellent, except near boundaries and near the origin. The calculated values for K were determined by considering the phases from the numerical models. The results for K using the amplitude data are similar but have a little more error near the origin. We believe this technique will work for the spherical coordinate system also (allowing variation in the vertical direction) and is the subject of a following section. This simplification in solving for K should make the tomographic inversion considerably simpler than if a full numerical model was needed to solve for K.

Table 2. Comparison of approximate results for hydraulic conductivity compared with true numerical model values.

Cartesian coordinates:

Two zones for K

x	0	5	10	15	20	25	30	35	40
Amplitude	1	0.333887	0.111552	0.03766	0.010765	0.0046	0.002118	0.000974	0.000449
Phase	0	-0.17316	-0.34662	-0.51784	-0.68759	-0.81992	-0.94258	-1.0656	-1.18951
Cal. K		0.002985	0.002968	0.003198	0.002403	0.005955	0.005943	0.005891	0.005786
True K		0.003	0.003	0.003	0.003	0.006	0.006	0.006	0.006

Linearly varying K

x	0	5	10	15	20	25	30	35	40
Amplitude	1	0.33608	0.126081	0.051371	0.022336	0.010236	0.004895	0.002428	0.001256
Phase	0	-0.16353	-0.3115	-0.44764	-0.5744	-0.69342	-0.806	-0.91361	-1.01703
Cal. K		0.003653	0.004393	0.005133	0.005875	0.006625	0.007354	0.00797	0.008727
True K		0.0036	0.00435	0.0051	0.00585	0.0066	0.00735	0.0081	0.00885

Cylindrical coordinates:

Two zones for K

r	0.0833	1.0231	5.1071	10.0331	15.2399	20.3548	25.4931	30.9181	35.1619	39.9883
Amplitude	1.0000	0.3834	0.0805	0.0200	0.0053	0.0013	0.0005	0.0002	0.0001	0.0000
Phase	0.0000	-0.0494	-0.2012	-0.3753	-0.5565	-0.7248	-0.8690	-1.0028	-1.1080	-1.2289
Cal. K		0.0013	0.0026	0.0029	0.0030	0.0033	0.0045	0.0059	0.0058	0.0057
True K		0.0030	0.0030	0.0030	0.0030	0.0030	0.0060	0.0060	0.0060	0.0060

Linearly varying K

r	0.0833	1.0231	5.1071	10.0331	15.2399	20.3548	25.4931	30.9181	35.1619	39.9883
Amplitude	1.0000	0.3696	0.0766	0.0211	0.0068	0.0025	0.0010	0.0004	0.0002	0.0001
Phase	0.0000	-0.0466	-0.1861	-0.3334	-0.4757	-0.6052	-0.7271	-0.8484	-0.9394	-1.0395
Cal. K		0.0026	0.0035	0.0044	0.0052	0.0060	0.0068	0.0074	0.0081	
True K		0.0031	0.0038	0.0045	0.0053	0.0060	0.0068	0.0076	0.0083	

As shown above, the homogeneous equations can be used to predict K based on the measurable amplitude decay and phase shift. However, the values obtained for the horizontal rays must be interpreted as spatially weighted averages over the horizontal distance between wells. Equations (14) and (15) represent the two experimental approaches utilized in this research. The cylindrical radial equation (14) describes the behavior of the excitation of a relatively long and small radius section of screen and is

considered to behave like a line source. Fully penetrating wells are often constructed at GEMS. Any test where the total screen length is excited is termed a whole well test. The spherical radial equation (15) is a representation of the point source geometry, where the excited length of well screen is relatively short. To achieve this, either a partially penetrating well with a relatively short screen length or a straddle packer apparatus must be used.

Finally, we investigate the validity of the spatially weighted straight ray approximation where vertical variation can occur in K and rays are allowed to be diagonal in addition to horizontal (spherical geometry case). Again, modeling studies were preformed to compare results from the spatially weighted ray tracing method with those from a numerical model. The numerical model and straight ray method were both used to simulate the phase shift of 108 rays between a theoretical well pair with three CPT source locations, each with 36 corresponding receiver locations. Modeling was completed for both the 3-sec and 30-sec CPTs to compare the difference between the two source methods. The aquifer between the well pair was simulated by a 3-element, 8-node, model which corresponds to the screen interval [10.68 m (35 ft)] and radial distance [5.85 m (19.20 ft)] between the theoretical well pair. The upper, middle and lower elements are, respectively, 4.88 m (16 ft), 0.92 m (3 ft), and 4.88 m (16 ft) thick. The upper, middle and lower elements have K values of 0.0009 m/sec (0.003 ft/sec), 0.0018 m/sec (0.006 ft/sec), and 0.0009 m/sec (0.003 ft/sec), respectively (Fig. 11). A representative Ss value of 0.00018 was also assumed for the verification modeling. Although these values were arbitrarily chosen, they fall within the range of values observed at GEMS and are consistent with Wachter's (McElwee et al., 2007; Wachter,

2008; Wachter et al., 2008) earlier verification of the heterogeneity extension using a 4-sec pneumatic CPT. The numerical phase data from this model comprise a theoretically perfect CPT data set and phase data from the straight ray model should closely approximate it. However, the numerical model does use a barrier boundary on the top and bottom rather than an infinite domain, so some boundary effects are expected. In any case, good agreement between the two methods is a line of evidence supporting the heterogeneous extension [equation (19)] adapted for this research.

Wachter's 4-sec CPT numerical validation of the heterogeneity extension was reproduced with the latest version(s) of the Visual Basic data processing programs so his verification could be compared to the numerical verification of the 30-sec CPT data used in the later stages of this research. Numerical modeling simulated three MOG data sets from source locations at 0.305-0.610 m (1-2 ft), 5.486-5.791 m (18-19 ft), and 10.668-10.973 m (35-36 ft), which correspond to the lower, middle, and upper intervals of the aquifer model (Fig. 11 – 13). The numerical model had 36 rows to simulate each of the 36 theoretical receiver locations in a MOG. To simulate a file of head data from the CPT source and receiver transducers, numerical phase data was parsed from the numerical model rows at radial distances which correspond to the center of the source and receiver well locations (e.g., 0.25 m [0.833 ft]) and 5.85 m [19.20 ft]) and were saved to a text file. FitAmpPhase used the text files to calculate the numerical phase shift for each of the MOGs. HydraulicTomAnal was used to create an element matrix of the aquifer and apply the straight ray approximation method through the matrix to generate the straight-ray phase shift data for all three MOGs. The element matrix was imported into

LeastSquaresSVD and both numerical and straight-ray phase shift data for the three MOGs were inverted through the element matrix to calculate diffusivity and solve for K.

The current version of the SVD inversion program also has the ability to perform Monte Carlo simulations using random error, rather than running individual simulations. Monte Carlo simulations were run with both 5% and 10% random noise for 1000 simulations. The 5% random noise approximates the expected variation in the field due to instrument imprecision and ambient noise and the 10% random noise simulates the expected worse-case scenario of signal inference. Verification of the heterogeneity extension and comparison of the 4 and 30-sec CPT sources are further discussed below.

The numerical phase shift from the 4 sec sources were compiled and compared to their corresponding straight-ray approximation to evaluate the relative goodness of fit between the simulated field data and its model approximation (Fig. 11 – 13). Because the phase originates from synthetic data, the two curves should fit relatively close. The 4-sec CPT phase shift values from the spatially weighted ray method and the numerical model for the upper, middle, and lower source locations were in good agreement with each other except for some slight boundary effects (Fig. 11 – 13). There was some deviation of the straight ray phase shift at the middle source location through the thinner, middle layer (Fig. 12). Straight rays projected through this element more directly measure the K without the averaging across the middle layer from the numerical model due to wavelength considerations and result in the higher K values (i.e., low phase) seen in this layer of the graph. Overall, the data fit is good indicating resolution of about 1 m (3 ft) layers with a 4-sec period, reconfirming Wachter's (McElwee et al., 2007; Wachter, 2008; Wachter et al., 2008) assessment of the resolution.

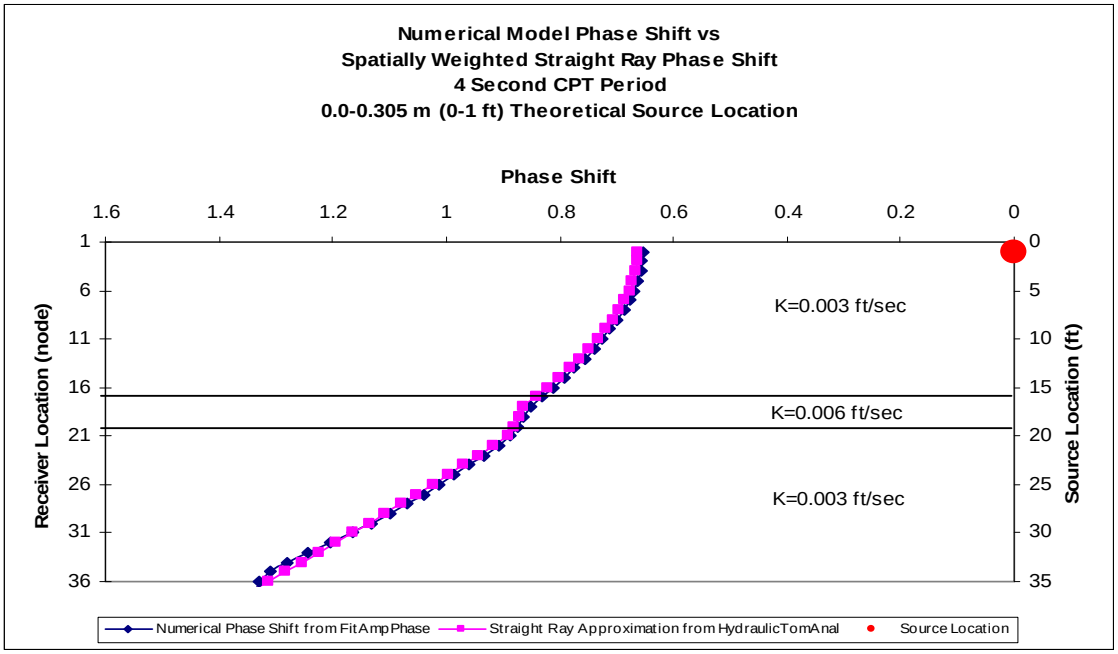

Figure 11 – A comparison of 4 second CPT period phase shift values from a numerical model and the spatially weighted ray path method at the 0.0-0.305 m (0-1 ft) source location.

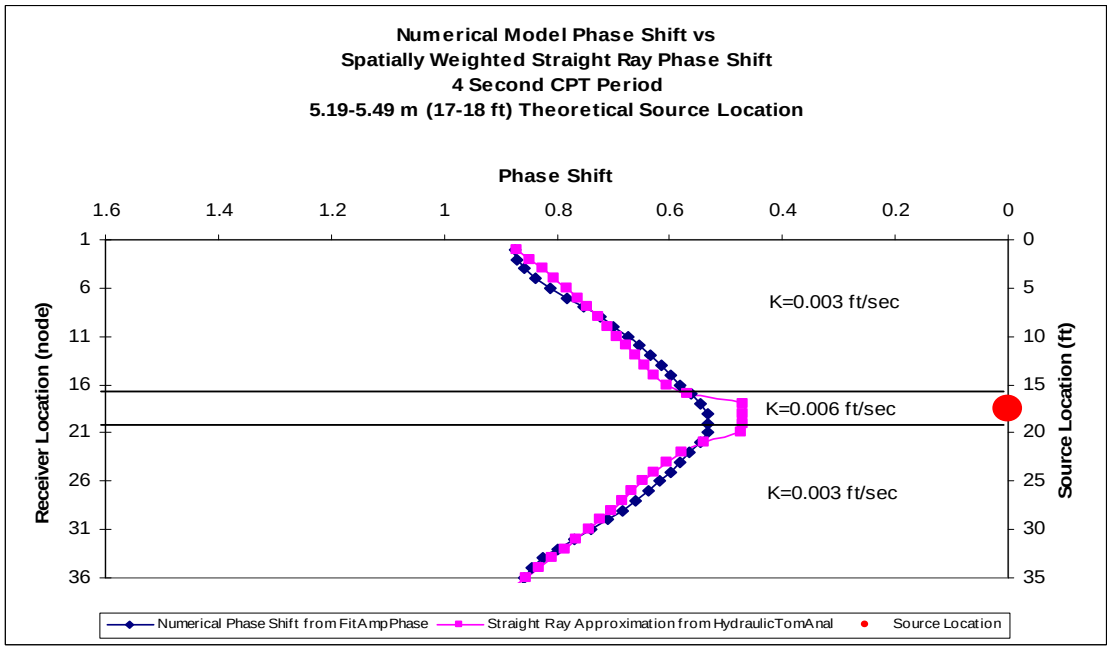

Figure 12 – A comparison of 4 second CPT period phase shift values from a numerical model and the spatially weighted ray path method at the 5.19-5.49 m (17-18 ft) source location.

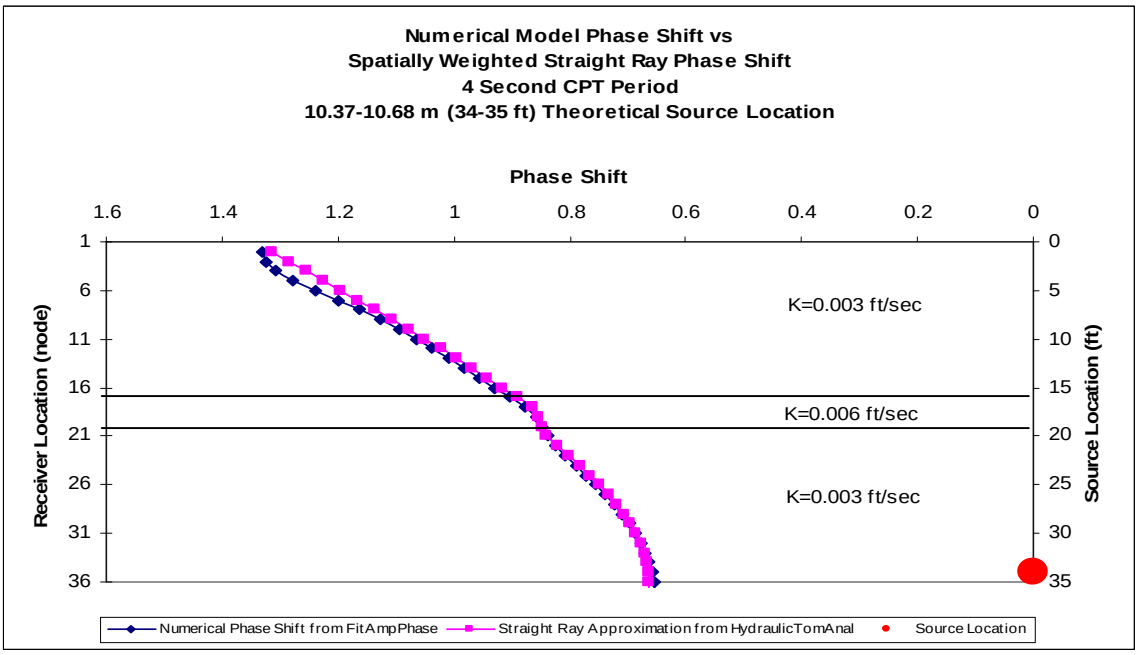

Figure 13 – A comparison of 4 second CPT period phase shift values from a numerical model and the spatially weighted ray path method at the 10.37-10.68 m (34-35 ft) source location.

The 30-second CPT phase shift values from the spatially weighted ray method and the numerical model at the upper, middle, and lower source locations were in reasonable agreement although the data resolution or overlap of the two curves was not as precise as the 4-second MOG data sets. The resolution of a longer period signal is expected to be less due to the longer wavelength of the propagating signal (therefore averaging over a larger volume) and results such as this are a piece of evidence to support that theory. In general, the data curves are similar and the slight boundary effects are still present (Fig. 14 - 16). Again, there was some deviation of the straight ray phase shift through the thinner, middle layer (Fig. 15). Also, the two phase shift curves were offset slightly at this CPT location. Figures 14 and 16 show nearly mirror symmetrical plots which can lead to non-unique data and inversion problems. Non-unique data were encountered in some of the simple, early developmental models which used only a few

symmetrical rays for each source and suggest that non-unique data can arise from ray path simulation through theoretical models. These plots suggest that some constraint may be required during inversion and is further discussed below.

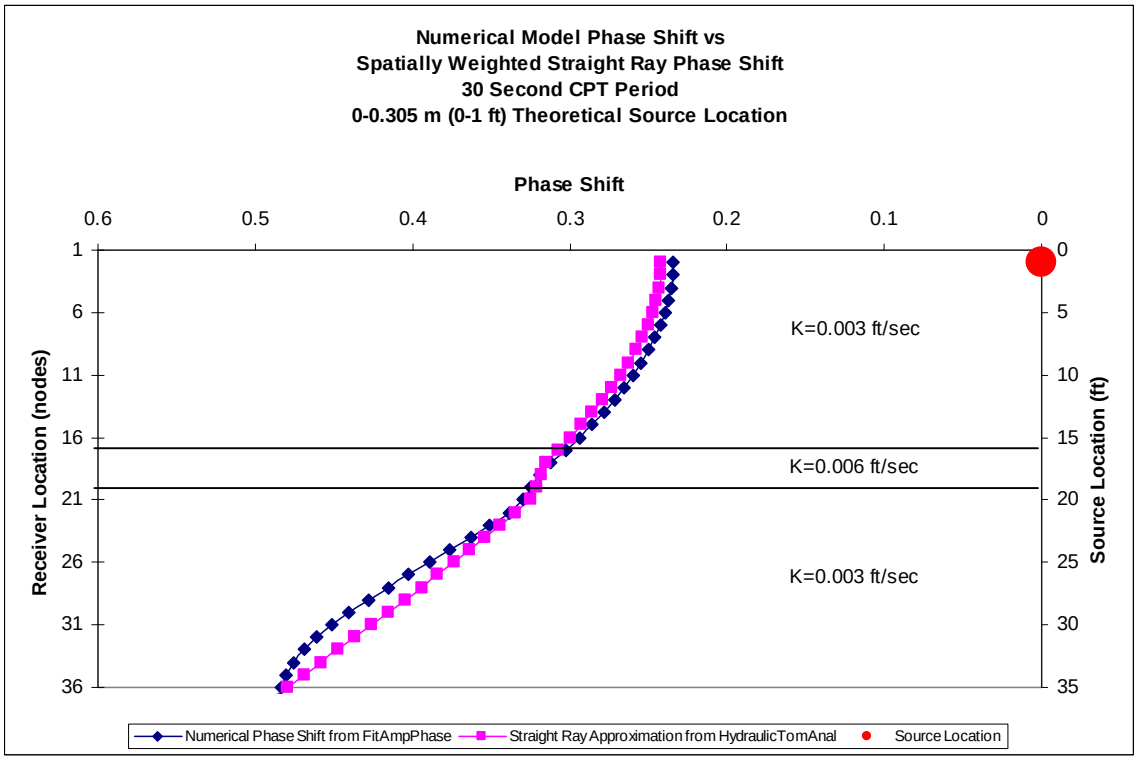

Figure 14 – A comparison of 30-sec CPT period phase shift values from a numerical model and the spatially weighted ray path method at the 0-0.305 m (0-1 ft) source location.

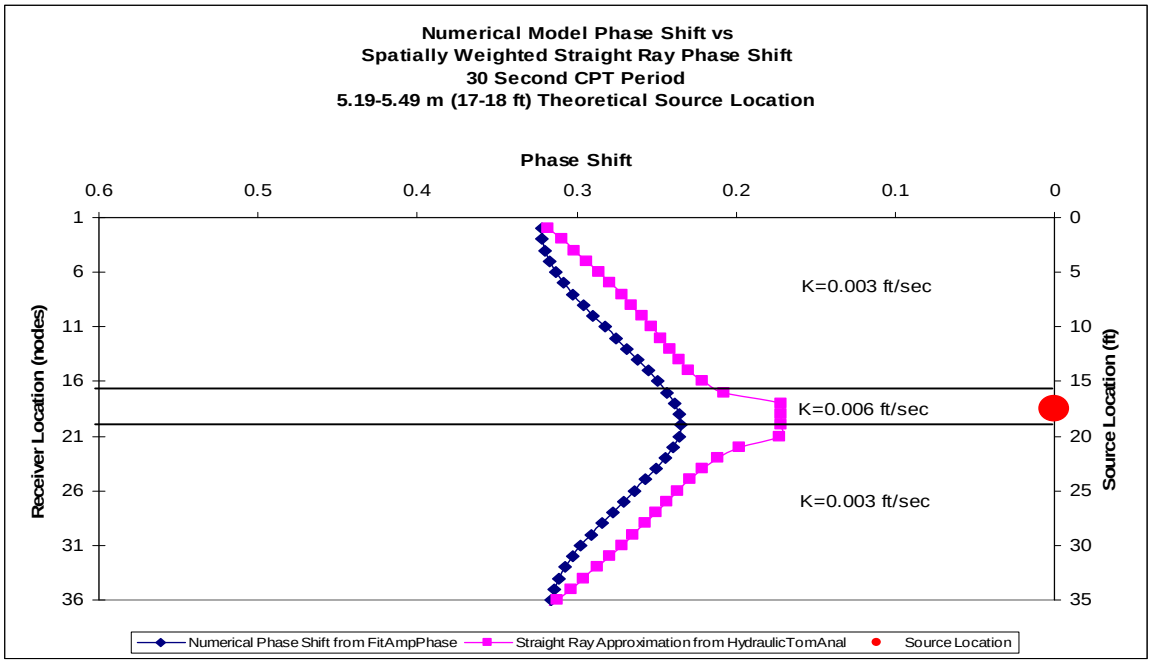

Figure 15 – A comparison of 30-sec CPT period phase shift values from a numerical model and the spatially weighted ray path method at the 5.19-5.49 m (17-18 ft) source location.

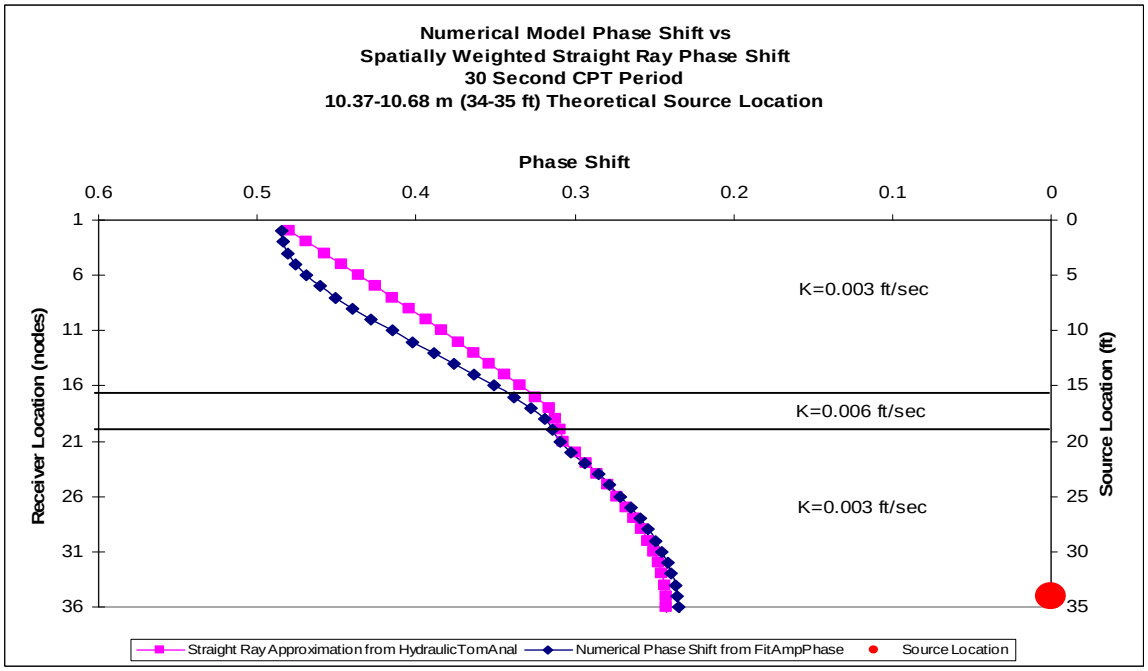

Figure 16 – A comparison of 30-sec CPT period phase shift values from a numerical model and the spatially weighted ray path method at the 10.37-10.68 m (34-35 ft) source location.

After the goodness of fit between the straight ray and numerical phase shift data were evaluated (Figs. 11-16), the straight ray phase shift data (Table 3), along with the numerical phase shift data (Table 4) were inverted through the element matrix by SVD analysis, a method of least squares fitting and inversion. As expected, direct inversion of the straight ray model data reproduced the input model K values for each of the layers with practically no error (Table 3). The percent standard deviation on the K values for each of the elements were essentially zero, implying the inversion was almost perfect for a data set with no noise. Random error of 5% and 10% was applied by Monte Carlo simulation to replicate a normal and worst-case scenario of ambient noise. The 2.5% - 5.2% range indicates the inherent error associated with levels of random noise in the middle layer and a 4-sec CPT period (Table 3). In contrast, the 6.9% - 14.5% range is the inherent error associated with the levels of random noise in the middle layer and a 30-sec period and indicates that the period difference tends to amplify the effect of random error.

Table 3 – SVD analysis of spatially weighted straight ray approximation phase shift through a three-element, eight-node, 10.68 m (35 ft) thick model used to verify the heterogeneous extension.

Spatially Weighted Straight Ray SVD Analysis			
4-Sec CPT Period			
Monte Carlo – No Error			
Element	K (ft/sec)	Stdr Dev K	% Stdr Dev K
1	0.003	3.616E-19	0.00
2	0.006	3.137E-18	0.00
3	0.003	3.870E-19	0.00
Monte Carlo - 5% Error			
Element	K (ft/sec)	Stdr Dev K	% Stdr Dev K
1	0.003	1.849E-05	0.62
2	0.005999	1.515E-04	2.52
3	0.003	1.899E-05	0.63
Monte Carlo – 10% Error			
Element	K (ft/sec)	Stdr Dev K	% Stdr Dev K
1	0.002999	3.482E-05	1.16
2	0.006018	3.098E-04	5.15
3	0.003001	3.702E-05	1.23

Spatially Weighted Straight Ray SVD Analysis			
30-Sec CPT Period			
Monte Carlo - No Error			
Element	K (ft/sec)	Stdr Dev K	% Stdr Dev K
1	0.003	8.636E-19	0.00
2	0.006	7.492E-18	0.00
3	0.003	9.242E-19	0.00
Monte Carlo - 5% Error			
Element	K (ft/sec)	Stdr Dev K	% Stdr Dev K
1	0.003	5.063E-05	1.69
2	0.006012	4.159E-04	6.92
3	0.003001	5.205E-05	1.73
Monte Carlo - 10% Error			
Element	K (ft/sec)	Stdr Dev K	% Stdr Dev K
1	0.003	9.542E-05	3.18
2	0.006109	8.869E-04	14.52
3	0.003005	1.017E-04	3.38

Inversion of the 4-sec period numerical phase shift data through the element matrix was also reasonable and the percent standard deviation on the K values for the middle elements was 3.1% (Table 4), in the absence of random noise. The error associated with the straight ray method is about 14.1 % error in the recovery of the 0.006 ft/sec K by the straight ray method (i.e., 0.006 vs. 0.005s ft/sec). These error percents indicate that the spatially weighted straight ray model and 4-sec CPT period can resolve layers of about 1 m (3 ft) in thickness with about 16-19% total error.

Inversion of the 30-sec period numerical phase shift data through the element matrix had 3.6% percent standard deviation on the K values for the middle element (Table 4), in the absence of random noise. This inversion was constrained slightly; the offset curves (Fig. 15) and nearly mirror symmetric plots in the upper and lower elements (Fig. 14 and Fig. 16) tend to suggest non-uniqueness data issues were arising during inversion. The SVD analysis was slightly weighted with a constrained least squares factor of 0.25, which gives a small weight to the initial estimates of K to overcome non-unique data and shouldn't unnecessarily restrain the analysis. The error associated with the straight ray method is about 25% error in the recovery of the 0.006 ft/sec K by the straight ray method (i.e., 0.006 vs. 0.0045 ft/sec). These error percents indicate that the spatially weighted straight ray model and 30-sec CPT period can resolve layers of about 1 m (3 ft) in thickness with about 27-29% total error.

Table 4 – SVD analysis of spatially numerical phase shift through a three-element, eight-node, 10.68 m (35 ft) thick model used to verify the heterogeneous extension.

Numerical/Straight Ray Model SVD Analysis			
4 Sec CPT Period			
Monte Carlo No Error			
Element	K (ft/sec)	Stdr Dev K	% Stdr Dev K
1	0.003032	2.365E-05	0.78
2	0.005155	1.608E-04	3.12
3	0.002986	2.474E-05	0.83
Monte Carlo 5% Error			
Element	K (ft/sec)	Stdr Dev K	% Stdr Dev K
1	0.003032	1.875E-05	0.62
2	0.005154	1.206E-04	2.34
3	0.002986	1.885E-05	0.63
Monte Carlo 10% Error			
Element	K (ft/sec)	Stdr Dev K	% Stdr Dev K
1	0.003031	3.545E-05	1.17
2	0.005169	2.464E-04	4.77
3	0.002987	3.675E-05	1.23

Numerical/Straight Ray Model SVD Analysis			
30 Sec CPT Period			
Monte Carlo No Error - CLS 0.25			
Element	K (ft/sec)	Stdr Dev K	% Stdr Dev K
1	0.002869	4.125E-05	1.44
2	0.004514	1.644E-04	3.64
3	0.002847	4.256E-05	1.49
Monte Carlo 5% Error - CLS 0.25			
Element	K (ft/sec)	Stdr Dev K	% Stdr Dev K
1	0.002869	3.830E-05	1.33
2	0.004513	9.347E-05	2.07
3	0.002848	3.703E-05	1.30
Monte Carlo 10% Error - CLS 0.25			
Element	K (ft/sec)	Stdr Dev K	% Stdr Dev K
1	0.00287	7.678E-05	2.67
2	0.004515	1.869E-04	4.14
3	0.002849	7.419E-05	2.60

Horizontal Ray Paths – ZOP Profiles

Introduction

The first phase of this project was to use horizontal rays only and thus collect ZOP profiles where the source and receiver were at the same elevations in the source and receiver wells. The source signal was generated by the pneumatic method, as described earlier, using a manually tuned frequency generator giving a period of between 3-4 seconds. The signal frequency was manually adjusted to give a signal that best represented a sinusoidal form. It was found that it was necessary to stay near the natural frequency of the well for best results. Two kinds of profiles for the receiver well were collected. In whole well tests the entire column of the source well was oscillated and only the receiver well location was packed off. Both the source and receiver intervals were isolated by straddle packers for the point source well profiles. Early research results

in this project showed that it was necessary to pack off the receiver interval to obtain the best aquifer response. Both the stressed interval of the source well and the isolated receiver interval in the receiver well were about 0.5 m in length. The locations below top of casing (BTOC) were referenced to the center of the stressed or received interval. Each location center was approximately 0.3 m from the next, so that one location overlapped with the adjacent locations. The overlapping intervals acted much like a centered moving average, where the vertical changes in aquifer heterogeneity were averaged over the 0.5 m interval, but were assigned to the center point. At this stage we were developing processing techniques and much of the work was done by hand in multiple steps. The details of data processing are given in Engard et al. (2005) and Engard (2006). Later this would be automated in the FitAmpPhase program, which would speed things up considerably.

One is able to approximate the diffusivity from the final corrected amplitude derived exponential decay term d and the phase shift Φ_r, equation (18). In theory, we have two independent measures of K, one from amplitude and one from phase measurements. However, we have found the amplitude estimates to be difficult to make because we do not know precisely the effective radius to use, see Engard et al. (2005) and Engard (2006) for details. For this reason, we will only present here results of K for phase measurements. The frequency was calculated from the field data from the reciprocal of the fitted source well period for each CPT. After referring to the literature an initial value of 0.00001 was used for S_s (Fetter, 2001; Domenico and Schwartz, 1998). Using a constant value for S_s is unrealistic but is necessary, because even with today's technology, it is difficult to measure S_s *in situ*. A final estimate of S_s was made by

requiring consistency between the vertical K profiles obtained by HRST methods and CPT methods. The radial distance r can easily be measured in the field or from survey data. With some algebraic manipulation estimates of K can be made from the CPT experimentally measured phase and amplitude data. Based on the numerical results presented earlier, the CPT derived values of K should be interpreted as distance weighted averages of K over the path between the source and receiver wells. HRST K values that differ significantly from the CPT K values are evidence of inter-well heterogeneity.

Results From High Resolution Slug Testing and Continuous Pulse Testing

For this project, high-resolution slug test (HRST) techniques (discussed earlier) were applied to newly installed wells HT-1, HT-2, and HT-3 after they were properly developed. HRST data from other wells (Ross, 2004) also was used for comparison to continuous pulse tests CPTs. A dual packer arrangement with a 0.5 m interval open to the formation was used for pneumatic slug testing (Ross, 2004; Zemansky and McElwee, 2005; Ross and McElwee, 2007).

The research presented here uses continuous, controlled, sinusoidal pressure signals as a means to estimate vertical profiles of well-to-well hydraulic diffusivity. The received signal is measured at various depths in observation wells at various distances and locations. The length of the vertical profiles measured by the CPT methods are limited by the amount of open screen common to the well pair in question and by the length of the bottom packer on the source and receiver double packer apparatus. Typically, the CPT profile was about 8 m in length.

In total, 7 line source (whole well tests, the entire column was oscillated) well pairs were tested with the pneumatic CPT method at GEMS. The shortest well separation distance, 4.36 m, was between well HT-2 and well HT-3. The longest separation distance, 11.5 m, recorded was between well 00-3 and well 7-1. These results are presented in figures 17- 23. The averages of the HRST values at each depth for the source and receiver wells are plotted along with the highest and lowest values shown by error bars. This curve is labeled HRST. The other curve labeled CPT presents the results of analyzing the CPT data for K. The two curves generally agree fairly well, with the exception of figure 18. It appears that the general features of the HRST curve are captured by the CPT curve, but it seems smoother. This is probably because of the long line source geometry giving poorer resolution. It is unknown at this time why the CPT curve in figure 18 is so flat; perhaps it is due to some experimental or processing problem we have not discovered. In general it is difficult to analyze the whole well tests, since the source area is so large and multiple paths of energy lead from the source to the point receiver. In later work we decided not to use whole well tests due to the difficulty in analyzing them.

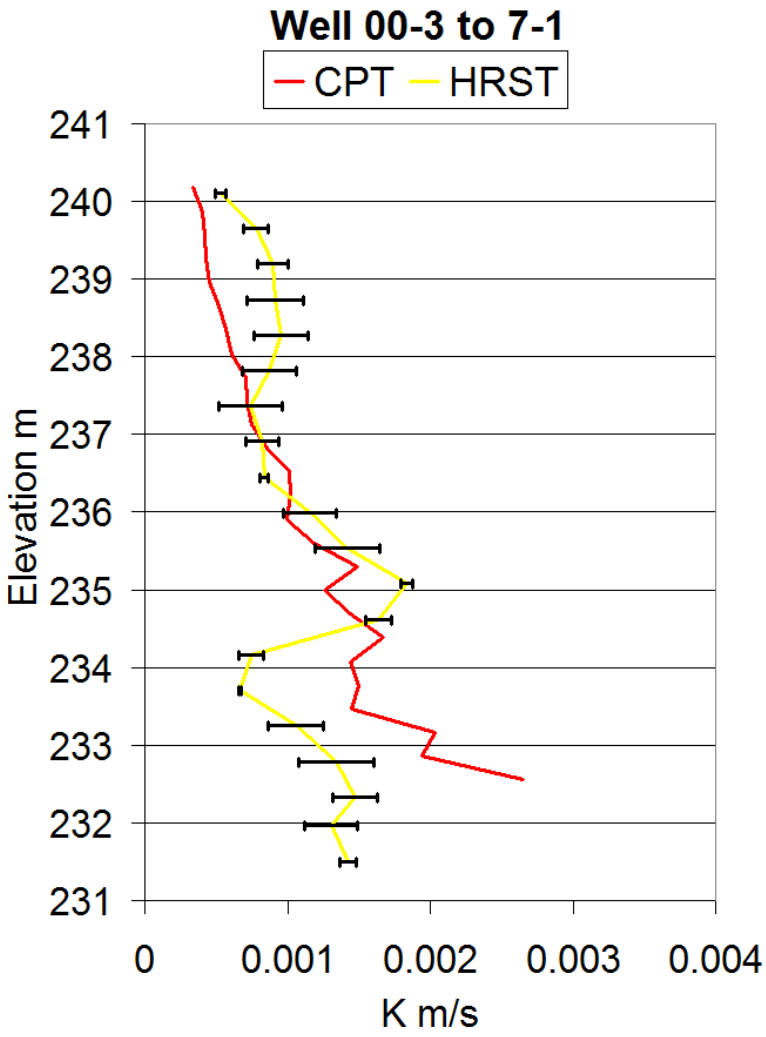

Figure 17. Comparisons of the composite HRST values from each well and the average estimated K profile from a line source pneumatic CPT between wells 00-3 to 7-1.

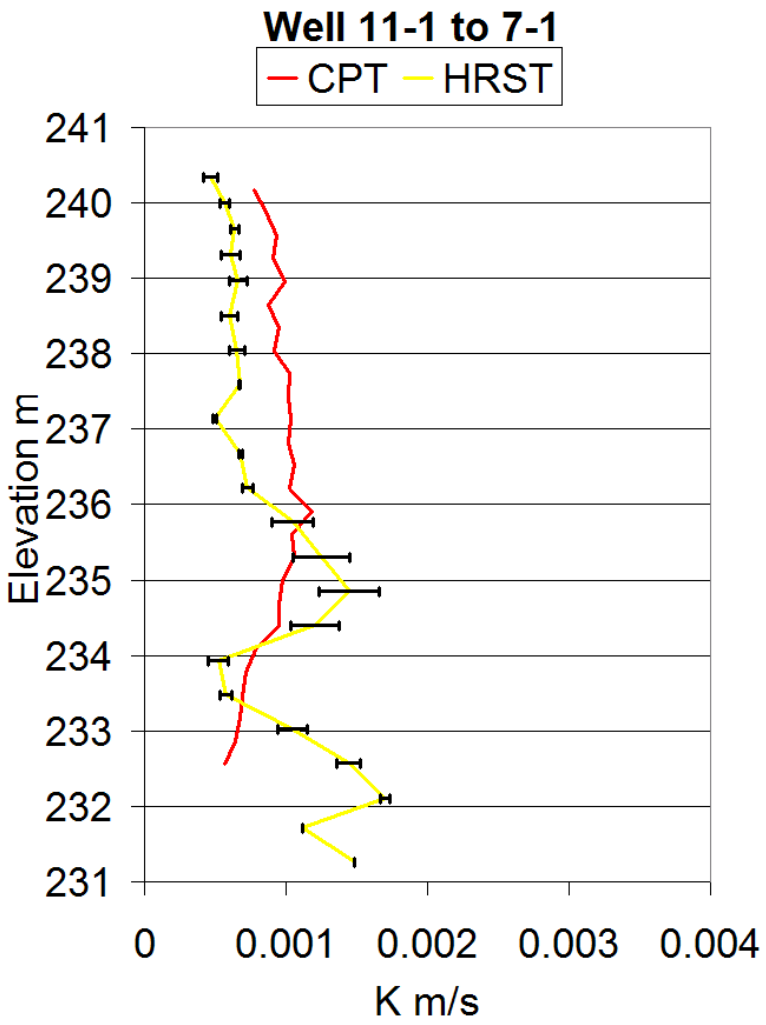

Figure 18. Comparisons of the composite HRST values from each well and the average estimated K profile from a line source pneumatic CPT between wells 00-3 to 7-1.

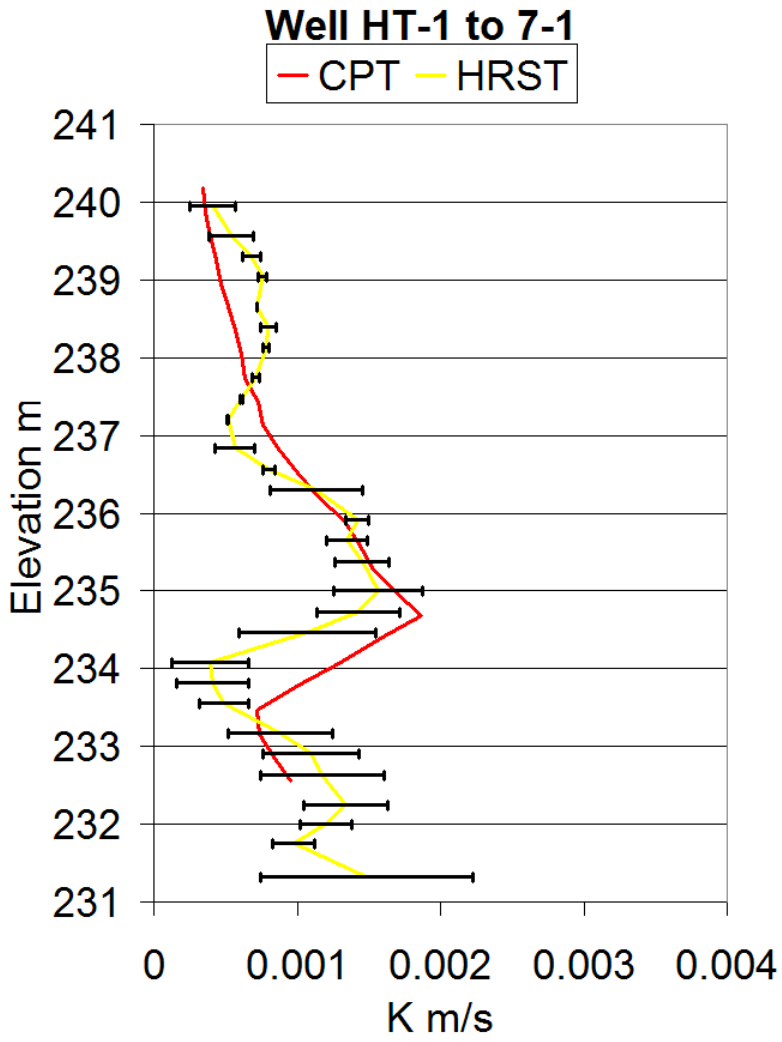

Figure 19. Comparisons of the composite HRST values from each well and the average estimated K profile from a line source pneumatic CPT between wells HT-1 to 7-1.

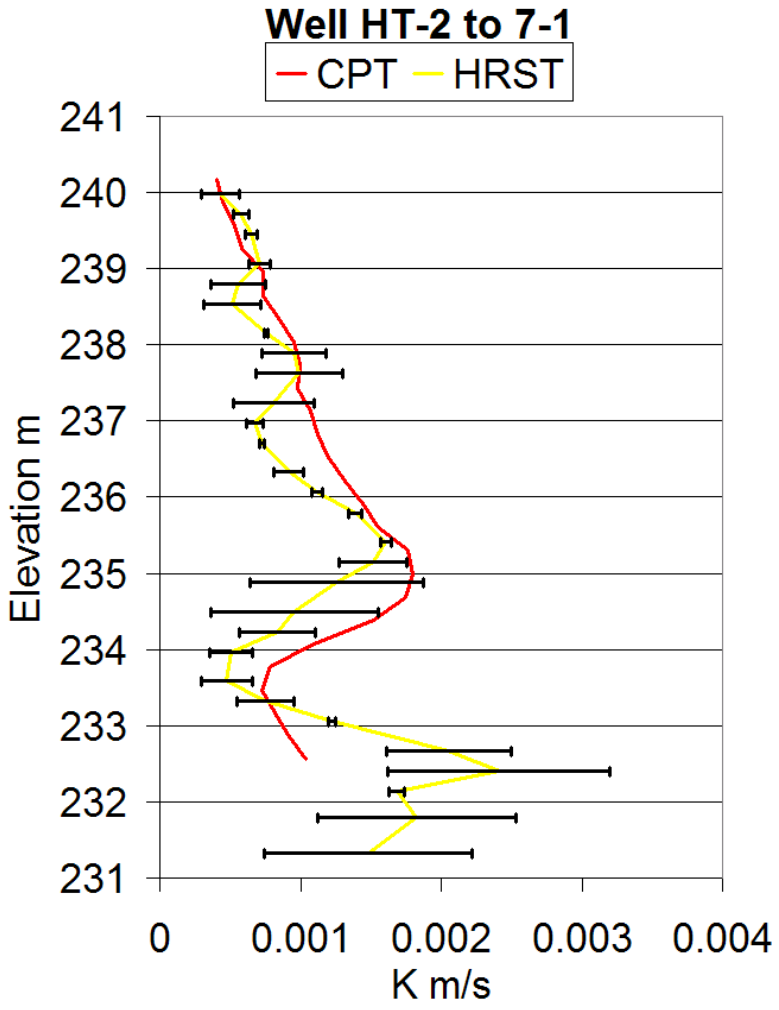

Figure 20. Comparisons of the composite HRST values from each well and the average estimated K profile from a line source pneumatic CPT between wells HT-2 to 7-1.

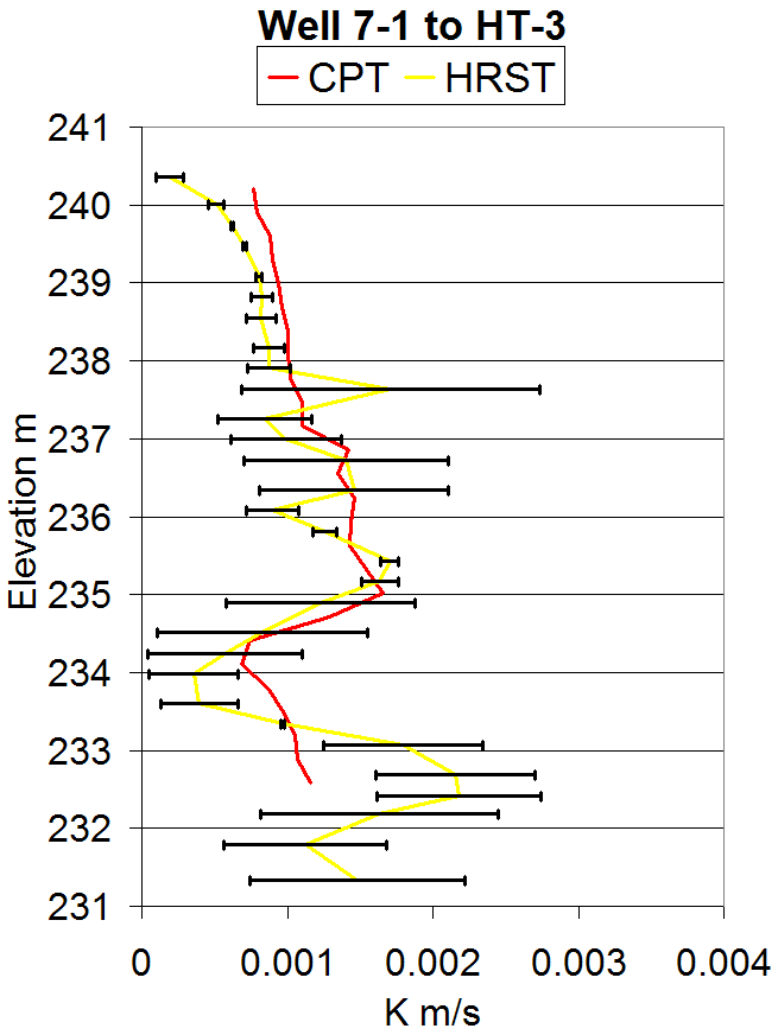

Figure 21. Comparisons of the composite HRST values from each well and the average estimated K profile from a line source pneumatic CPT between wells 7-1 to HT-3.

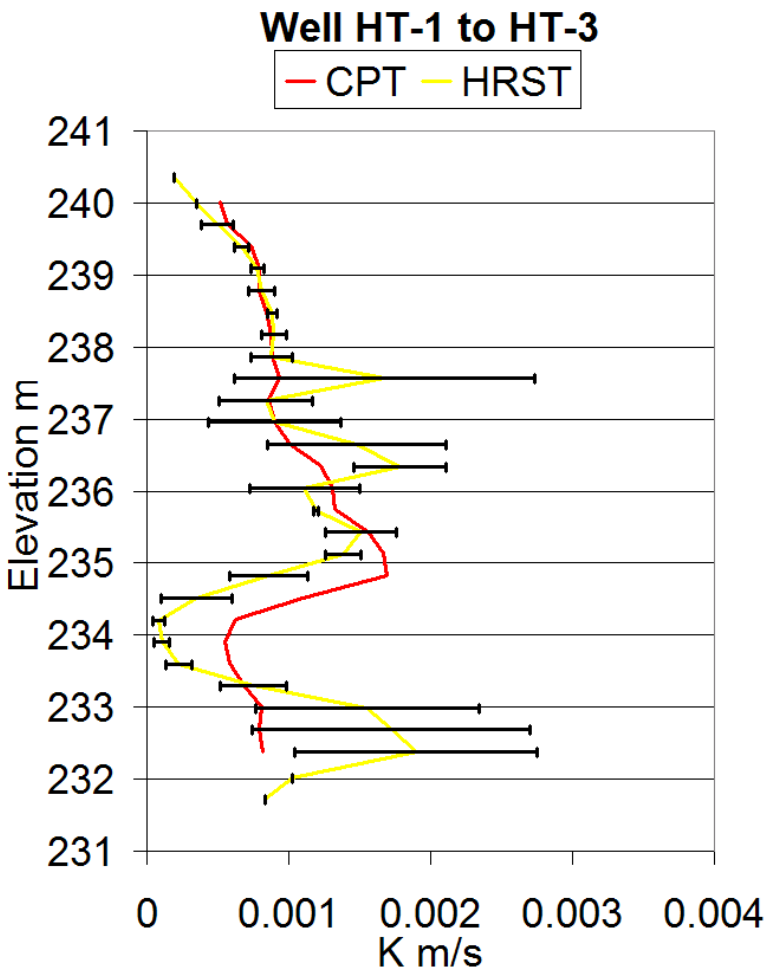

Figure 22. Comparisons of the composite HRST values from each well and the average estimated K profile from a line source pneumatic CPT between wells HT-1 to HT-3.

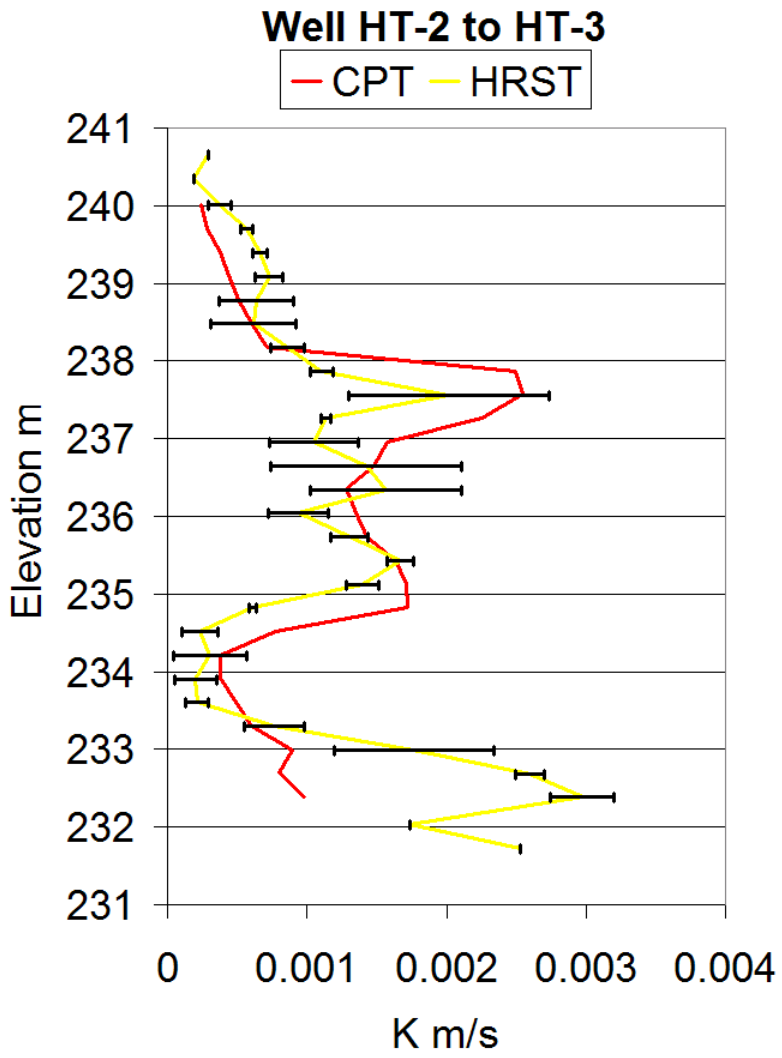

Figure 23. Comparisons of the composite HRST values from each well and the average estimated K profile from a line source pneumatic CPT between wells HT-2 to HT-3.

Five point source profiles (both source and receiver packed off) were completed at GEMS with the pneumatic CPT method. Also, one point source profile was completed with an early crude version of the mechanical pumping or injection CPT method (an improved version of the mechanical pumping system will be the subject of later sections of this report). The shortest well separation distance of 4.36 m was between well HT-2 and well HT-3. The longest separation distance, 6.91 m, was recorded between well HT-2 and well 7-1. These results are presented in figures 24- 28 for the pneumatic profiles and in figure 29 for the injection profile. The presentation style is the same as for figures 17-23 with the HRST curves being the same as before. The CPT curves are now for the point source CPT method and seem to have more detail and are more closely correlated to the HRST data. It appears that the point source CPT tests are giving better K resolution, as we might expect. Comparison of the pneumatic method of figure 24 and the injection method of figure 29 for the same well pair shows that the results are similar, but some differences do occur.

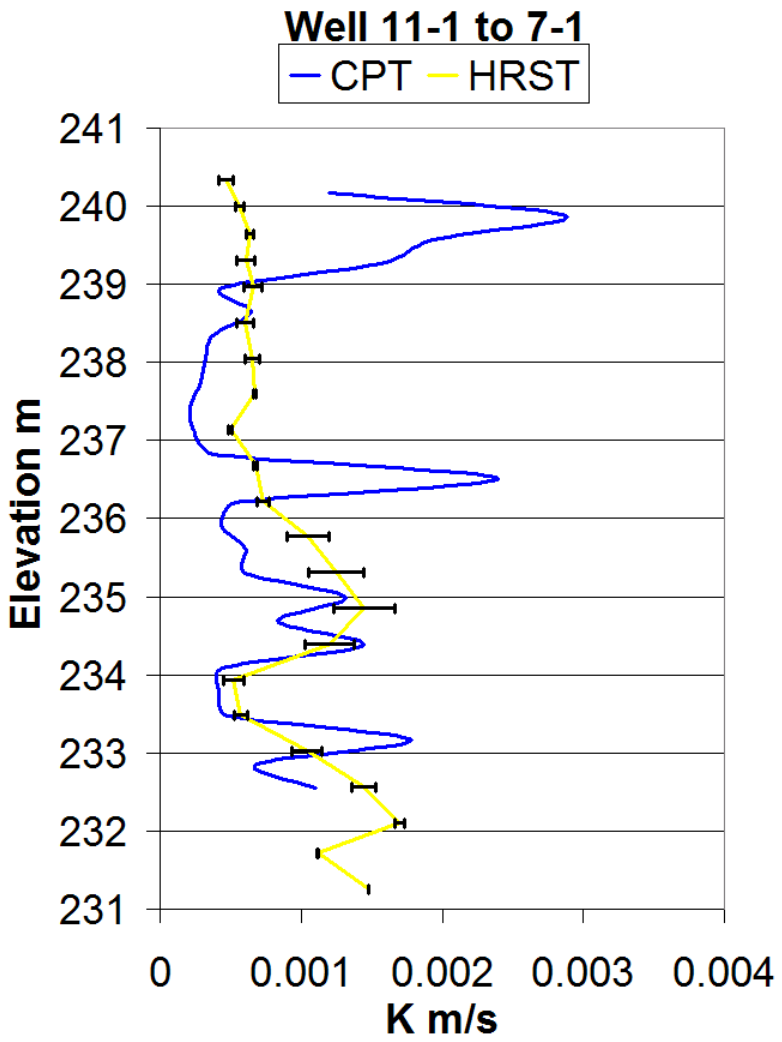

Figure 24. Comparisons of the composite HRST values from each well and the average estimated K profile from a point source pneumatic CPT between wells 11-1 to 7-1.

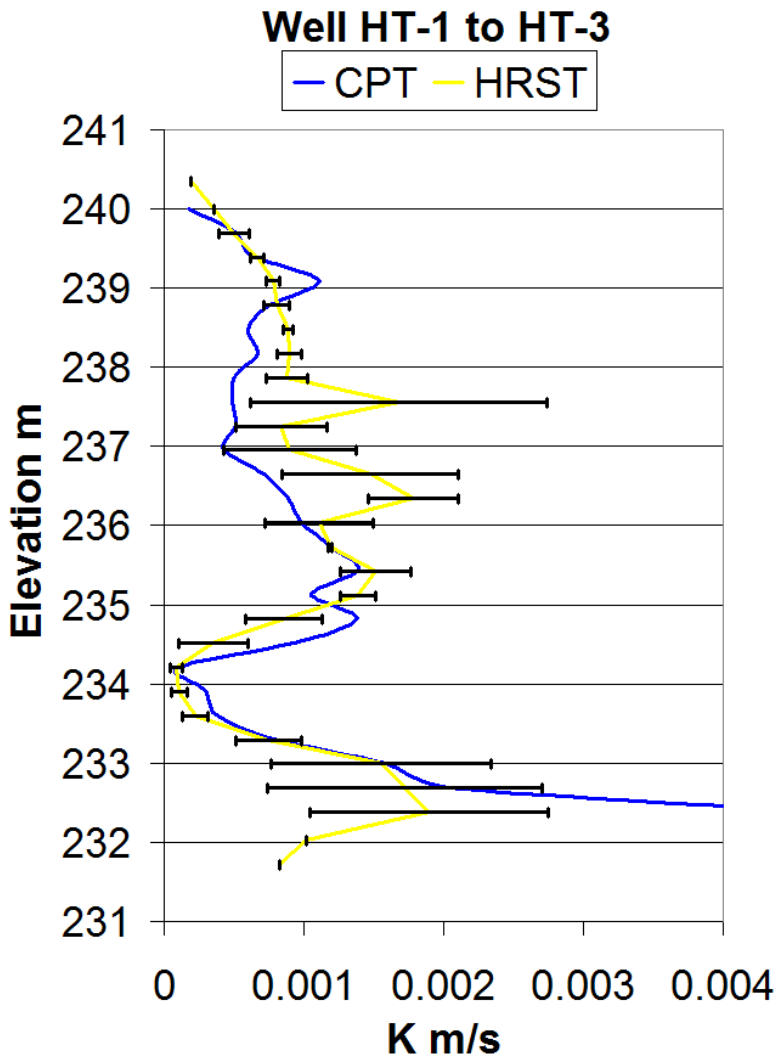

Figure 25. Comparisons of the composite HRST values from each well and the average estimated K profile from a point source pneumatic CPT between wells HT-1 to HT-3.

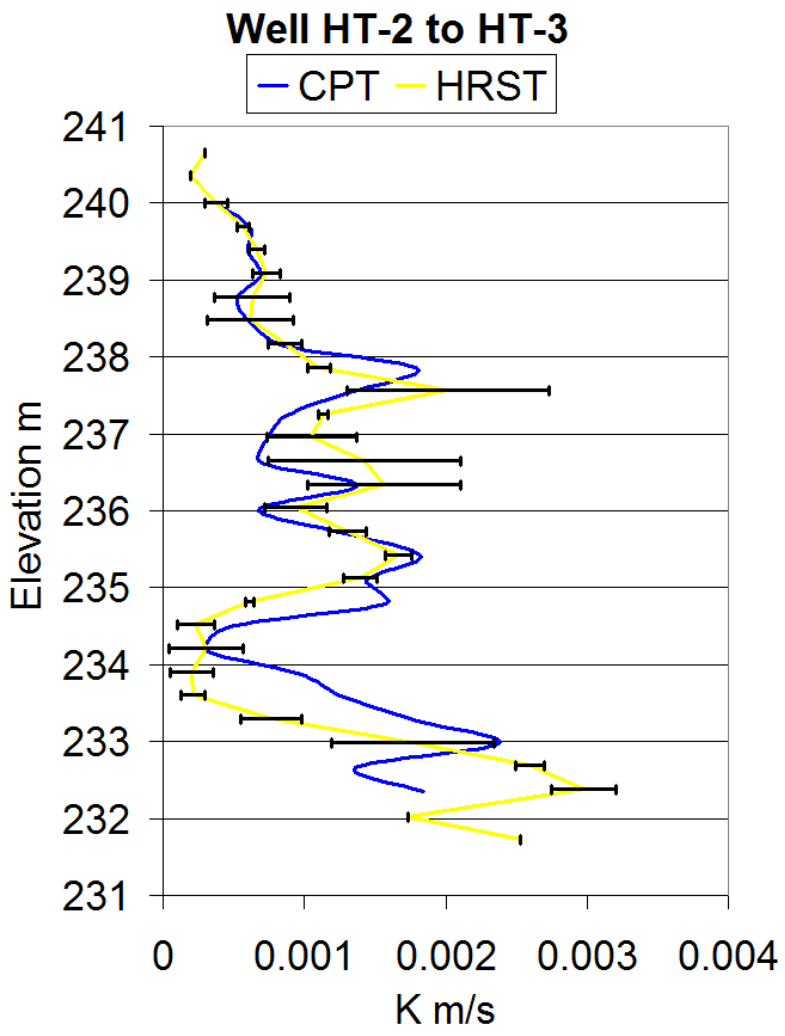

Figure 26. Comparisons of the composite HRST values from each well and the average estimated K profile from a point source pneumatic CPT between wells HT-2 to HT-3.

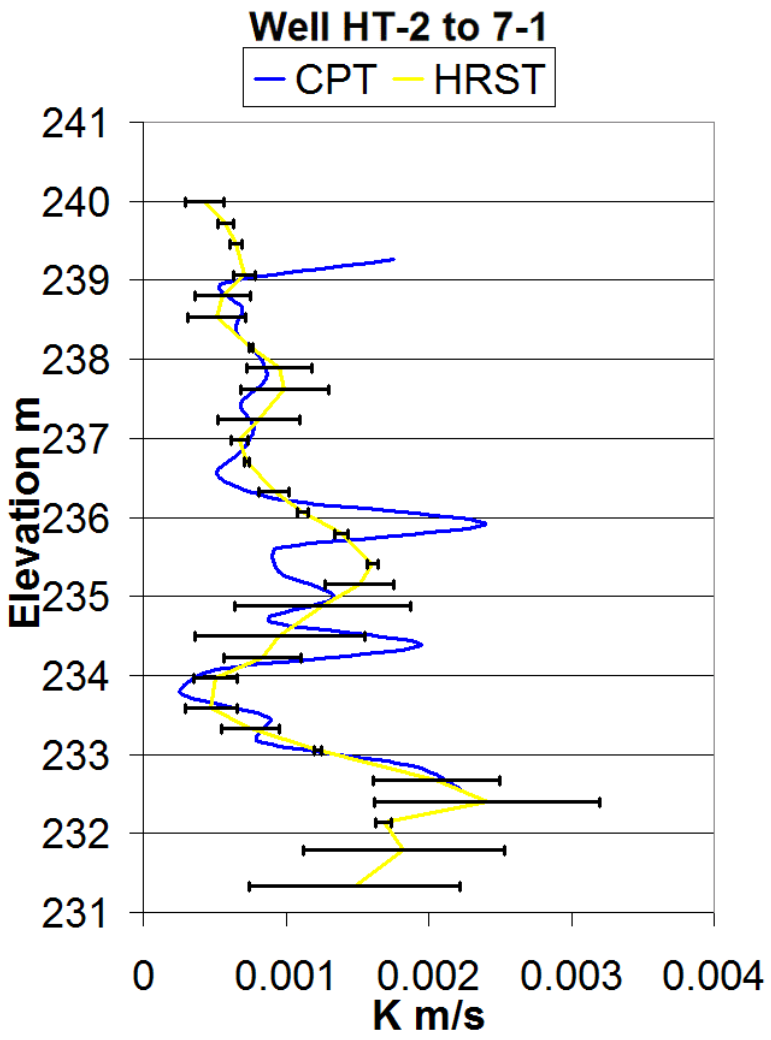

Figure 27. Comparisons of the composite HRST values from each well and the average estimated K profile from a point source pneumatic CPT between wells HT-2 to 7-1.

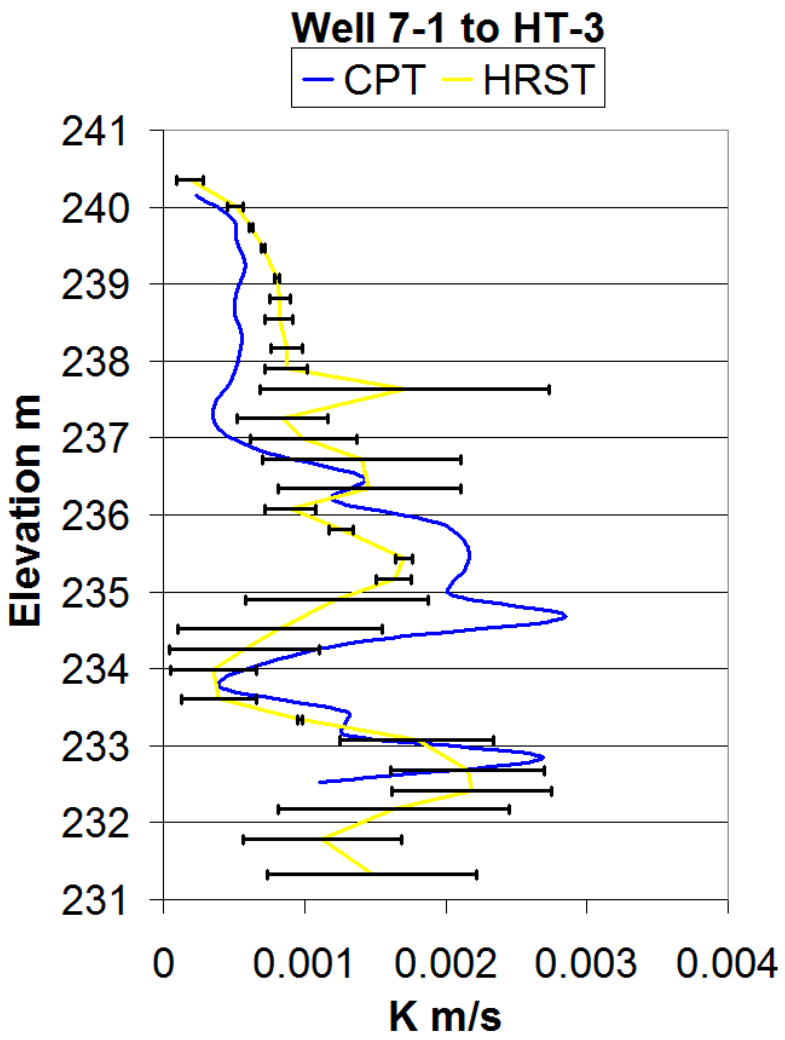

Figure 28. Comparisons of the composite HRST values from each well and the average estimated K profile from a point source pneumatic CPT between wells 7-1 to HT-3.

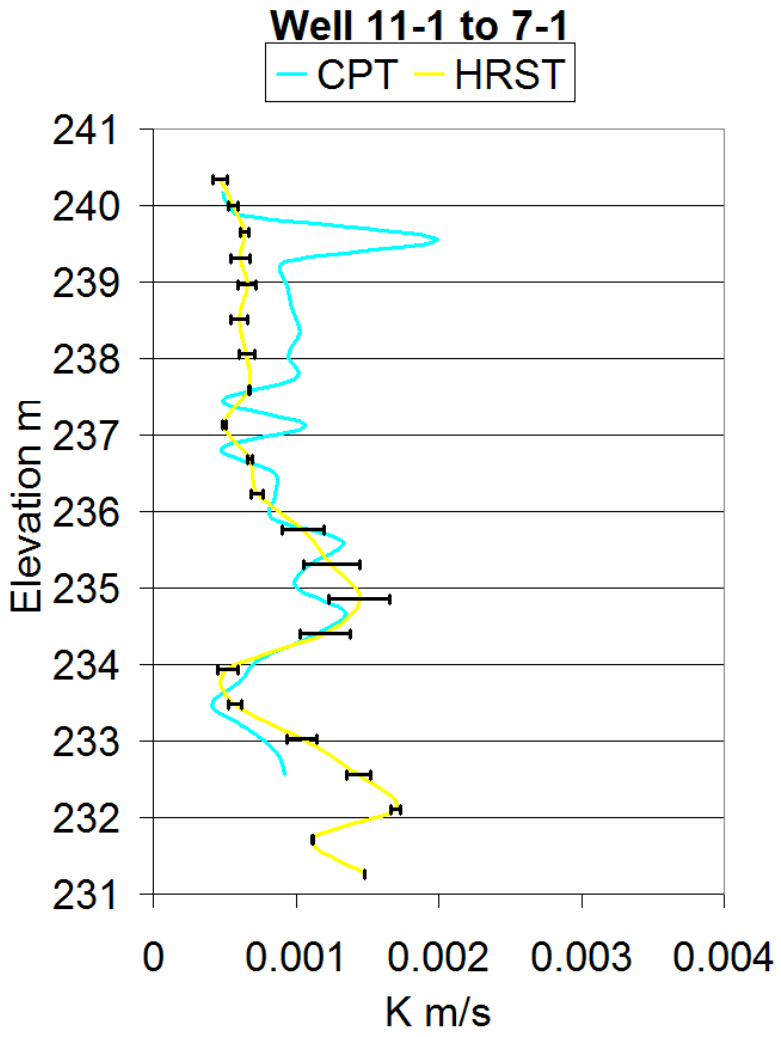

Figure 29. Comparisons of the composite HRST values from each well and the average estimated K profile from a point source injection CPT between wells 11-1 to 7-13.

It is evident that the CPT profiles mimic the general trends in the HRST K profiles measured at the respective wells. Overall, the CPT data appear to average the K profiles of the well pair in question. However, there are important differences. The heterogeneities of the geologic material between the well pair are probably the cause of this difference; and the difference can not be fully explained without using more advanced models and numerical solutions. The point source data appear to increase the

resolution of the data, distinguishing variations in K that are not present in the HRST and line source data.

Calculation of "Anomalous K Values"

The previously discussed comparison of the straight ray approximation to numerical results indicates that using a spatially weighted average for K should be appropriate. This allows the interpretation of the hydraulic conductivity (K) data that have been collected for high-resolution slug tests at wells and the inter-well spatially averaged K that has been determined by the continuous pulse testing horizontal ray path data. Unfortunately, there is no unique way to do the spatial weighting with the horizontal ray path data, since we only have one ray path crossing each segment of the aquifer. When we are able to collect diagonal ray path data, we will have multiple rays that cross each given segment of the aquifer and it will be possible to estimate the spatial averaging to some scale limited by the density of ray paths. However, in the present case (horizontal ray path data) one must assume some spatial averaging scheme to interpret what the inter-well average K is telling us about the variation of K between wells. It is well known that slug tests only give a K value that is representative near the well. Therefore, we should give less weight to the slug test values and more weight to the inter-well average K determined from the horizontal ray-path data. Arbitrarily, let us assume that the weight for each of the two slug test values is 1/6 and the weight for the inter-well average K is 2/3 = 4/6. These weighting coefficients add up to 1, as any weighting scheme should. This assumption will allow us to calculate a new value of K between the source and receiver wells that may be different from the slug test K values or the inter-

well average K determined from the horizontal ray path data. In what follows we will call this calculated value of K between the source and receiver wells the "anomalous K value" (Engard et al., 2006) because it can be different from any of the experimentally determined K values. Ideally, if the K values changed in a linear fashion from the source well to the receiver well, the inter-well average K determined from the horizontal ray path data should fall between the values of K determined by slug tests at each well. However, we have observed that this often is not the case, which means that the K values are not varying linearly between wells. The above outlined scheme allows us to calculate an "anomalous K value" that shows how K may in fact be varying between wells.

This procedure has been applied to three of the source-receiver well pairs from which we have collected data. The calculations for the Well pairs HT-1 to HT-3, HT-2 to HT-3, and 7-1 to HT-3 are show in figures 30, 31, and 32 respectively. What we observe is that the inter-well average K (CPT K value in the figures, shown in dark blue) is many times outside the interval defined by the two slug test values of K shown in pink and yellow. This means that the K value is not varying linearly between wells and an anomalous value outside that range may be calculated. The anomalous values are shown in light blue-green. When the anomalous curve is significantly outside the slug test K interval, we have an indication that the K value between wells is significantly different from that observed at the source and receiver wells. The values of the anomalous K are calculated using the weighting scheme detailed earlier. It should be reiterated that the choice of weighting scheme is arbitrary at this point and is not unique. However, the calculations presented here should be useful in identifying areas of "anomalous K" between the source and receiver wells.

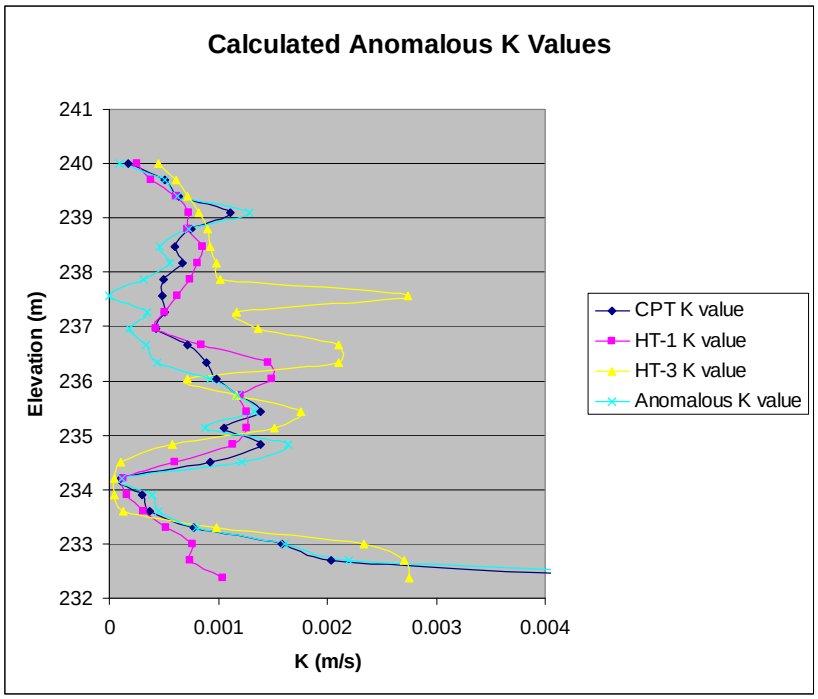

Figure 30. Experimentally determined K values from high resolution slug tests and horizontal ray path data along with "anomalous K values" calculated from the weighting scheme, for well pair HT-1 and HT-3.

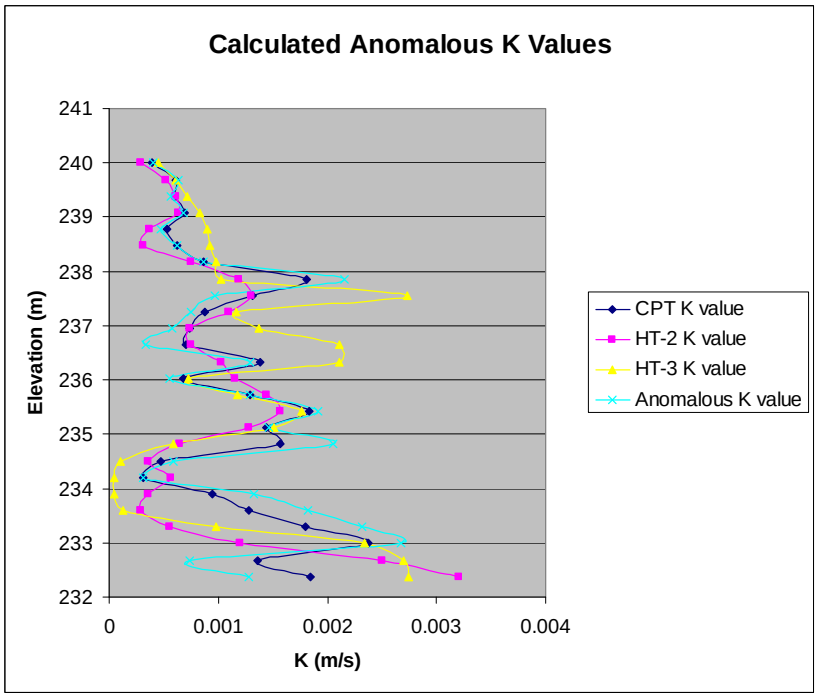

Figure 31. Experimentally determined K values from high resolution slug tests and horizontal ray path data along with "anomalous K values" calculated from the weighting scheme, for well pair HT-2 and HT-3.

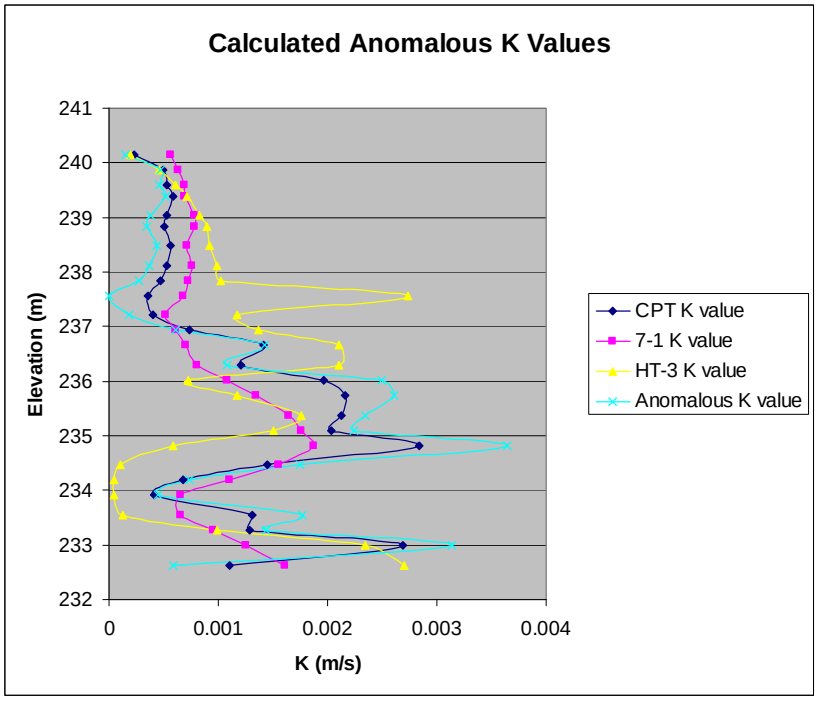

Figure 32. Experimentally determined K values from high resolution slug tests and horizontal ray path data along with "anomalous K values" calculated from the weighting scheme, for well pair 7-1 and HT-3.

Reproducibility and Reciprocity

We have investigated the reproducibility of the data and the reciprocity of source and receiver wells (Engard et al., 2006). In well pair HT-1 and HT-3 we have taken data at two different times and with the source and receiver locations reversed. The results are shown in Figure 33 for the measured phase which is the basic data used to calculate K. It is seen that the signals are reproducible within experimental error over an extended time interval between data collection and with the source and receiver reversed. Similarly, for well pair HT-2 and HT-3 we have taken data at four different times and once with the source and receiver reversed. These data sets are shown in Figure 34. The general shape and features of the phase shift curve are reproduced and the various data sets agree within

experimental accuracy. Therefore, we conclude that the data are reproducible and that they are nearly independent of source and receiver position, within experimental error.

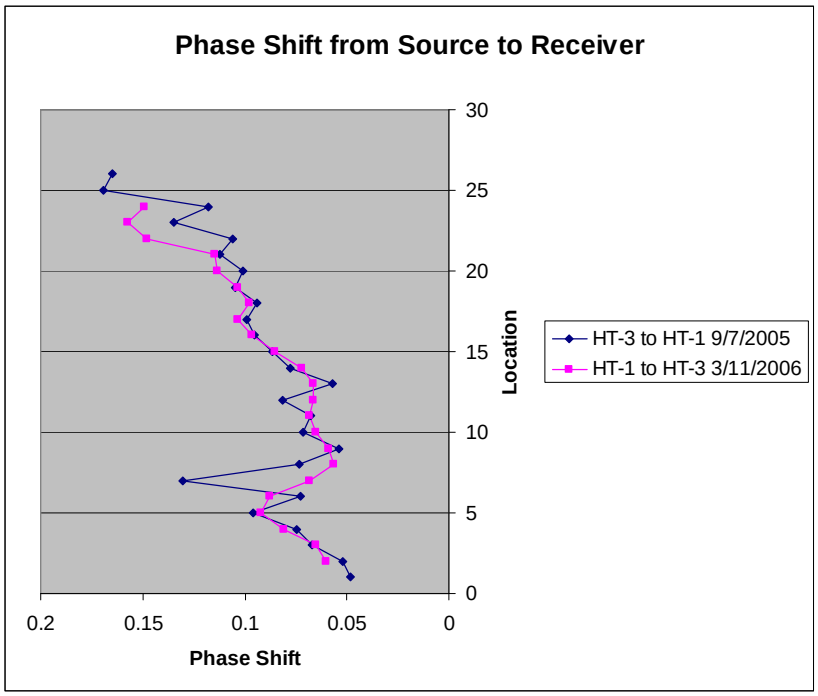

Figure 33. Phase data for well pair HT-1 and HT-3 at two different times with the source and receiver reversed.

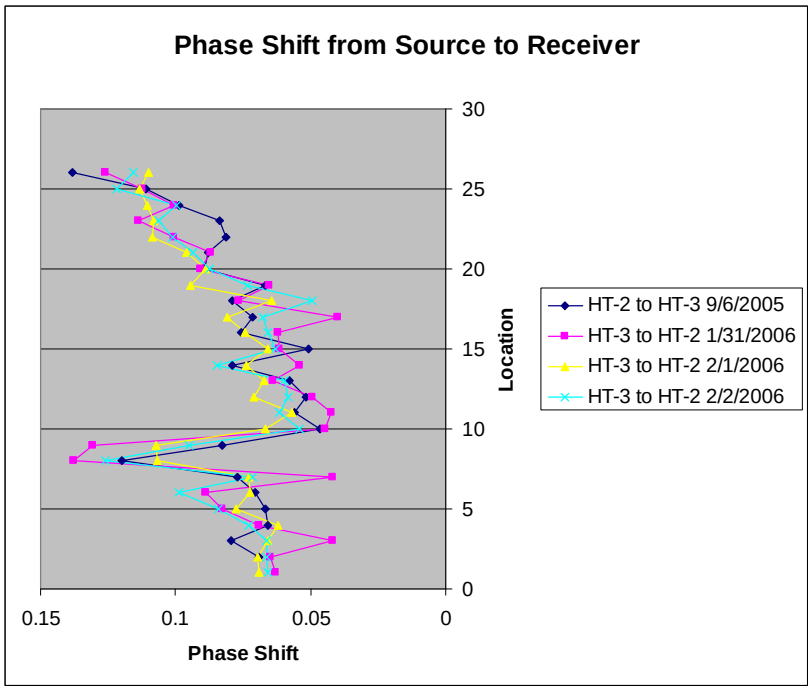

Figure 34. Phase data for well pair HT-2 and HT-3 at four different times with the source and receiver reversed on one data set.

Diagonal Ray Paths –3-4 Sec. Pneumatic MOG Data

Introduction

In the second phase of this research we started collecting MOG data with diagonal ray path using the pneumatic method described earlier. It is only with MOG data that a true tomography can be utilized, since it is necessary to have multiple rays at different angles passing through the area of interest. The period of the oscillations was determined by a manually set frequency generator, so the period was not absolutely constant between records, but was in the 3-4 sec. range. At processing time all the records were corrected to a standard period. Figure 8 shows all the hydraulic tomography (HT) wells installed as part of this project. HT-3 sits at the center of the array with other wells surrounding it.

All pairs of the hydraulic tomography wells using HT-3 as a common center were tested using the pneumatic method. This allows a series of slices through the aquifer, which when taken as a whole allows a 3-D view of the hydraulic conductivity distribution as determined by this research. The following sections summarize the model selection for inversion and the results for constrained inversion of the data. For a more complete description of the details see McElwee et al., 2007; Wachter, 2008; Wachter et al., 2008.

Sensitivity of Various Models to Inversion for K Values

It is well known that the stability and uniqueness of an inverse problem depends both on the data collected (quantity and quality) and the structure of the selected model for inversion. The number of parameters to be estimated and the size and shape of the zone they occupy are critical to the inversion. For these reasons a number of runs were made with synthetic and real data to try and determine a reasonable model structure for our inversion (Wachter, 2008).

Theoretical values of phase and amplitude for more complex models were run through data processing programs before applying the programs to field data. The synthetic data sets could be generated with no error or a given level of random noise. The current version of the SVD inverse program has the ability to perform Monte Carlo simulations in the presence of random error. The Monte Carlo simulations were run with both +/- 1% and +/- 5% noise for 1000 simulations. A variety of models with differing numbers of nodes in the x and z directions, numbers of elements, and numbers of zones were investigated. All initial models used 100 ray paths, consisting of 10 source locations and 10 receiver locations, and S_s values of 0.00018 or .00001. K values were

arbitrarily chosen to start at 0.000914 m/s (0.003 ft/s) at shallow depths and gradually increased with depth to 0.00213 m/s (0.007 ft/s). Although the K values were arbitrarily chosen for the modeling phase, they fall within the range observed at the site (0.000305 m/s to 0.00305 m/s) from HRST and other methods.

The HydTomAnal program calculates the length of each ray path through a particular element or near a given node. The total amount of ray path length through each element or associated with each node can be calculated by adding the lengths from each individual ray path of the 100 rays used. The ray path sums give a measure of the sensitivity of a given model to the K value in an element or near a node. The ray path density was highest in the center of the region, so there was less resolution at the top and bottom of the modeled area. The problem can be avoided by having spatially variable element sizes across the model. The latest versions of the processing programs offer the ability to specify K by zones, which are formed by one or more nodes or elements and must be input manually. The purpose of the zones is to provide variable resolution across the model, with finer zones towards the center and coarser zones at the edges of the grid where fewer rays are crossing.

The amount of error produced by a given set of input parameters was balanced with the amount of resolution provided by that particular model. Increasing the number of zones increases the resolution, but only at the cost of increased error. A mode with 50 elements and 16 zones resulted in the least amount of error of the models studied here, but some models with more zones also produced acceptable amounts of error. A good balance of error and resolution when S_s equaled 0.00001 was achieved with this 16 zone, 50 element model (6 nodes in x direction). The average error was 7.79% in the presence

of 1% noise. This 16 zone 50 element model with six nodes in the x direction will be used in all following discussions.

The grid layout for the chosen 16 zone 50 element model is shown in Figure 35. In Figure 35, each of the 50 elements is numbered, with element 1 at the bottom of the source well and element 50 at the top of the receiver well. The greatest resolution is provided in the middle of the grid while the top and bottom have the least resolution. As discussed above the total ray path length associated with each element or zone is a measure of the model sensitivity to the value of K in that element or zone. The sum of ray path lengths going through each zone of the chosen model for the suite of rays used was also calculated and is presented below in Figure 36. They were calculated using field geometry and the actual number of rays collected in the field for each well pair.

46	47	48	49	50
41	42	43	44	45
36	37	38	39	40
31	32	33	34	35
26	27	28	29	30
21	22	23	24	25
16	17	18	19	20
11	12	13	14	15
6	7	8	9	10
1	2	3	4	5

Figure 35: The grid shows the division of elements into 16 zones.

In each well pair, the center of the model prior to zoning had the highest sum of ray path lengths because the most ray paths passed through those areas. Other elements were combined together to produce zones with sums comparable to the value in the

center. Zone sums may differ by a factor of two but should not vary by as much as an order of magnitude for a well behaved model. Zone sums in a given zone are fairly similar between well pairs with approximately the same number of ray paths. Variation occurs from one well pair to another partially due to differing radii but largely due to the changing number of ray paths.

(a). HT-3 to HT-2 (750 rays)

823.77		
1228.00		
630.15	405.42	537.70
667.15	548.02	523.73
664.30	546.10	526.06
616.21	404.27	545.03
1213.79		
820.19		

(b). HT-3 to HT-1 (780 rays)

1154.96		
1434.27		
691.30	472.55	597.74
707.20	612.89	585.77
704.63	580.72	591.74
651.07	416.50	605.51
1278.80		
807.51		

(c). HT-4 to HT-3 (100 rays)

139.51		
166.25		
75.58	52.77	75.72
75.27	72.18	75.30
75.07	73.41	75.05
75.94	54.72	75.81
170.54		
152.43		

(d). HT-5 to HT-3 (190 rays)

143.02		
211.02		
150.46	71.51	75.04
148.99	124.07	102.38
140.86	144.98	160.69
136.40	123.90	199.25
403.52		
362.43		

(e). HT-6 to HT-3 (300 rays)

361.10		
454.76		
209.34	143.64	214.51
211.15	202.04	212.24
211.16	210.42	209.94
216.29	158.90	211.12
487.74		
456.77		

Figure 36: The sums of ray paths in each zone for well pairs HT-3 to HT-2 (a), HT-3 to HT-3 (b), HT-4 to HT-3 (c), HT-5 to HT-3 (d), and HT-6 to HT-3 (e).

SVD Processing

After choosing a zoning model, field data were run through the inversion program to determine K values. As stated in the Modeling section, the model chosen for this scenario was a 16 zone model where K was determined by elements and there were six nodes in the X direction. The data set from well HT-3 to well HT-2 was first examined because it seemed to be the best of the initial data sets. The HRST K values determined in previous tests were input as constant K nodes to help fix the other K values within a reasonable range. HRST results were processed by Brett Engard (2006) for wells HT-1, HT-2, and HT-3, and by Pema Deki (2008) for wells HT-4, HT-5, and HT-6 (Appendix B).

Contour plots were made of K values plotted against elevation and the radial distance between wells using a program called QuikGrid, a public domain program. The program contours between points written in an x,y,z format, in this case corresponding to radius, elevation, and K. The contour interval chosen is 0.0002 m/s. The HRST values were chosen for the K values at each well in the plot. Interwell K values were determined by the SVD analysis, a method using least squares. In the contour plots of K, the source well is on the left side and the receiver well is on the right side.

Initially the field data were processed using an unconstrained SVD procedure. The results were unstable with regions of K occurring that were known to be unreasonable. The SVD inverse program performs perfectly on model data without noise, so it must be much more sensitive to noise than originally thought. To compensate for the sensitivity to noise, a seven point filter was used on the data. In addition, noise reduction was attempted by editing larger offset rays, where noise was expected to be

greater. Little improvement was observed due to filtering and ray path editing. Apparently, the inverse procedure needed some additional conditioning to become stable. As an alternative processing scheme, an SVD least squares fit was employed constrained by the HRST data, which is detailed in the following section.

Constrained SVD Results

Inverse problems are commonly constrained with data known from other sources or methods; in this case, HRST results were used to constrain the inversion for K values. Initial guesses of K in each zone were obtained through a linear interpolation of HRST values at the same Z elevations. The sum of squared errors (SSE) was calculated by comparing the phase values measured in the field to the phase values calculated using SVD. A weighting factor is used in the latest version of the SVD program to determine to what extent the HRST results constrain the inversion. A weighting factor of zero is equivalent to the unconstrained SVD analysis, and increasing values for the weighting factor result in increasing weight given to the HRST results and therefore less deviation from HRST values. For this study, a factor of 1.0 was used, resulting in about equal weight of the HRST data and the tomographic data. The K value in a zone is only changed if it is still in the approximate range of values seen from HRST. The results were calculated using two values for S_s, 10^{-5} (Table 5) and 1.5×10^{-5} (Table 6).

Table 5: K values (m/s) obtained after iterating using the constrained SVD analysis ($S_c = 10^{-5}$).

Zone	HT-3toHT-1 50elem 780 rays	HT-3toHT-2 40elem 750 rays	HT-3toHT-2 50elem 750 rays	HT-3toHT-2 50elem 270 rays	HT-3toHT-2 50elem 170 rays	HT-3toHT-2 50elem 90 rays	HT-4toHT-3 50elem 100 rays	HT-5toHT-3 50elem 190 rays	HT-6toHT-3 50elem 300 rays
1	0.004404	0.0074862	0.0058252	0.0051154	0.0051625	0.0049338	0.0060699	0.005425	0.0107446
2	0.0011044	0.0007794	0.0012579	0.0011813	0.0015434	0.0012734	0.0014829	0.0009898	0.001248
3	0.0003231	0.001476	0.0006166	0.0005975	0.0007826	0.0006126	0.003498	0.0027994	0.0037067
4	0.0004029	0.0012684	0.0010956	0.0010228	0.0010677	0.0010214	0.0024315	0.0020906	0.004816
5	0.0003207	0.00413	0.0012579	0.001162	0.0013765	0.0011777	0.0015143	0.0007947	0.0033531
6	0.0067165	0.001326	0.002753	0.0028131	0.0024481	0.0025694	0.0033182	0.005046	0.0158121
7	0.0018712	0.002018	0.0017516	0.0016532	0.0017923	0.001771	0.0065138	0.000976	0.0023381
8	0.0020057	0.0064817	0.0052522	0.0041009	0.004814	0.0036683	0.0079078	0.003463	0.0061995
9	0.0017238	0.0054021	0.0016193	0.0017939	0.0014134	0.0016523	0.0053158	0.0013502	0.0031366
10	0.0010119	0.0013811	0.0010374	0.0009865	0.0010515	0.0009151	0.007074	0.0005979	0.0012969
11	0.0019704	0.0022031	0.0035885	0.002996	0.0027921	0.0033401	0.0074449	0.00148	0.004094
12	0.0011519	0.0037096	0.0022713	0.0022118	0.0015644	0.0019312	0.0047499	0.0007769	0.001627
13	0.0012693	0.0026868	0.0031371	0.0032096	0.0032301	0.0027179	0.0040592	0.0019252	0.003049
14	0.0009069	0.0023642	0.0030193	0.0027131	0.0034024	0.0031891	0.0051039	0.0016292	0.0030399
15	0.0006855	0.0015154	0.0015675	0.0014628	0.0012573	0.0013588	0.005706	0.0004734	0.0007758
16	0.0004172	0.0014292	0.001563	0.0014545	0.001413	0.0013843	0.0040793	0.0005685	0.0004313

Table 6: K values (m/s) obtained after iterating using the constrained SVD analysis ($S_s = 1.5 \times 10^{-5}$).

Zone	HT-3toHT-1 50elem 780 rays	HT-3toHT-2 40elem 750 rays	HT-3toHT-2 50elem 750 rays	HT-3toHT-2 50elem 270 rays	HT-3toHT-2 50elem 170 rays	HT-3toHT-2 50elem 90 rays	HT-4toHT-3 50elem 100 rays	HT-5toHT-3 50elem 190 rays	HT-6toHT-3 50elem 300 rays
1	0.0059224	0.0110622	0.0083746	0.0074443	0.0078103	0.0073452	0.0098291	0.0081054	0.0165329
2	0.0018614	0.0010535	0.0019261	0.0018041	0.0023823	0.0019379	0.0019216	0.0014876	0.0016687
3	0.0003661	0.0020754	0.0007449	0.0007199	0.000909	0.0007349	0.004419	0.0037312	0.0049737
4	0.0004441	0.0017475	0.0013065	0.001226	0.001314	0.0012316	0.0028086	0.0026506	0.005839
5	0.0003943	0.0046685	0.0016376	0.0015258	0.0018896	0.0015556	0.0017495	0.0010506	0.0042925
6	0.0117715	0.0019606	0.0042273	0.0042145	0.0036413	0.0038003	0.0041749	0.0069156	0.0225553
7	0.0029366	0.0028427	0.0026044	0.0024617	0.0026194	0.0026404	0.0091596	0.0014505	0.0034871
8	0.0030084	0.0068331	0.0073598	0.0057864	0.0067727	0.0051398	0.0112893	0.0051215	0.0084238
9	0.0024074	0.0063557	0.0021918	0.0023827	0.00192	0.0022097	0.0070657	0.0017724	0.0037579
10	0.0014646	0.0020357	0.0014203	0.0013562	0.0014085	0.0012542	0.0098941	0.0008195	0.0018103
11	0.0028141	0.0030217	0.0045188	0.003851	0.0033914	0.0042758	0.0103932	0.0018801	0.0056214
12	0.0016502	0.0039212	0.0032263	0.0031156	0.0022854	0.0027373	0.0060878	0.0011181	0.0021965
13	0.0016482	0.004098	0.0040081	0.004086	0.0039623	0.0034614	0.0047432	0.0024411	0.0039505
14	0.0012285	0.0033796	0.0042178	0.0038217	0.0043313	0.0044617	0.006579	0.0021453	0.004361
15	0.0010405	0.0021742	0.0023255	0.00217	0.0018061	0.0019993	0.008918	0.0007141	0.0011548
16	0.0006021	0.001872	0.0021013	0.0019843	0.001795	0.0018571	0.0052272	0.0007761	0.0006102

Contour plots were made of K values plotted against elevation and the radial distance between wells for the data constrained by the HRST results. The HRST values are used at the left and right ends of the plot, with the source on the left and the receiver on the right. Interwell K values in the following plots were all determined by the constrained SVD analysis. The phase is a ratio between S_s and K, so changes in S_s will also result in changes in K. This introduces a potential source of error because, due to the difficulty of measuring S_s in situ, a value was obtained from the literature rather than from field measurements. To investigate the effect of S_s, the constrained SVD analysis was conducted on all of the data using S_s values of both 10^{-5} (Figures 37-44) and 1.5 x 10^{-5} (Figures 45-52). A value of 1.5 x 10^{-5} in general results in smoother transitions between zones. The negative aspect of choosing the higher S_s value is that well pair HT-6 to HT-3, which already had higher than expected K values with the lower S_s (Figure 44), continues to increase above the expected range (Figure 52).

Based on other work at the site, and in particular HRST, K values at the site are known to range from approximately 0.0003 m/s up to 0.003 m/s. The K values in figures 37 and 45 are all within this range. The trend also matches that seen in HRST results, with low K material near the top, a high K region in the middle, another high K region beginning at the bottom of the plot, and a low K zone between the two high K regions. The data set from HT-3 to HT-2 was used to verify that the program was working correctly before extending the analysis to other well pairs. Figure 45, using a value of 1.5 x 10^{-5} for S_s, shows a smoother transition between points than Figure 37, which is physically a more likely scenario.

Plots were also made of the HT-3 to HT-2 data set using less than 750 rays to determine if fewer rays can provide the same results. The number of rays in each example was based on the ray path geometry of the other well pairs. The 270 ray path example used all receiver data for each source used but only every third source location, just like well pair HT-6 to HT-3. Similarly, the 170 ray path example followed the same pattern as well pair HT-5 to HT-3 and the 90 ray path example followed the pattern of well pair HT-4 to HT-3. The three following figures (Figures 38-40) show the same trend seen in Figure 37, but the magnitudes of the K values decrease as the number of ray paths decreases. The 270 ray path scenario (Figure 38) is closest to the 750 ray path scenario. The bottom zone is about the same in the 750 and 270 ray path cases, but the K values in the bottom zone are noticeably smaller in the two cases with less ray paths. The plots using the higher S_s value (Figures 46-48) also show the same trends, but the transitions between zones are smoother.

The data set presented in Figure 41 is not as accurate as the other data sets. The amount of error between calculated and observed phases was greater than that in other well pairs. Problems with this data set are likely caused by the nitrogen leaks at the time of data collection. The equipment was repaired after this data set was completed. In spite of the problems, the plot shows the same general zones of high and low K seen elsewhere. Figure 49, using the larger S_s value, depicts the same zones of high and low K. The processing program is probably not causing the problems because it has been constrained and other well pairs do not have as many problems. So, drawing definite conclusions about this well pair would likely require recollecting the data with the current repaired equipment.

Both of the original well pairs verified the use of the constrained processing program by showing the trends observed in HRST results, so the data from fall 2007 were examined for the three newest wells. The vertical intervals were varied in the source and receiver wells for some of the wells pairs; this offered the opportunity to determine if data were being collected at adequate spatial intervals for appropriate resolution. The data in figures 42 and 50 show the overall trend observed between HT-3 and HT-2 and between HT-3 and HT-1. Once again, the plots demonstrate the expected trends of high and low K zones. The high K zone near the top of the plot is not seen elsewhere in that portion of the aquifer, but the values are at least within the overall range determined by other methods. This could potentially be caused by a combination of previously discussed problems of resolution in the top of the sampling area in combination with the low number of ray paths used for this particular well pair (100, compared to 750 for HT-3 to HT-2).

The results between well HT-5 and well HT-3 are presented in Figures 43 and 51. The difference between the two figures is that the transitions between K values are smoother in the plot using the higher value for S_s. Some of the values at the bottom of the plot are slightly above the general expected range, but still within reason. K values have been shown to slightly exceed 0.003 m/s in some of the HRST data toward the bottom of the wells. The same trend of low K material at the top, a moderately high K zone in the middle, and high K material at the bottom is again observed in this well pair. As with the plot from well HT-4 to well HT-3, the relatively large region of very low K values at the top could be due to the lower number of ray paths for this well pair.

The contour plots from well HT-6 to HT-3 (Figures 44 and 52) show the same trend seen in tomography experiments between all the other well pairs, as well as in HRST results. The zone of very high K in the middle left side of the plot exceeds the range of expected values for the site. The location of the zone could be due to the survey design for this well pair, namely, the source locations were sampled at a coarser interval than that used for the receiver locations. This well pair is the only one examined in this study for which increasing S_s resulted in K values farther above the expected range. Despite the problem of larger than expected K values, the transitions between zones are again smoother using 1.5×10^{-5} instead of 10^{-5} for S_s.

The number of ray paths collected for a well pair correlated well with the reasonableness of the K values. The well pair with the best results, HT-3 to HT-2 (750 rays), was characterized by the most rays of any of the well pairs, with the exception of the well pair with equipment problems. The well pairs of HT-4 to HT-3 and HT-5 to HT-3 had 100 rays and 190 rays, respectively, and some of the higher elevation zones were somewhat lower than expected for the site. The results suggest that 190 ray paths are not enough for accurate results. Time constraints may not always allow for 750 ray paths, but there does seem to be a strong correlation with the accuracy of the processing results and the number of ray paths. The work with editing ray paths for the data set from HT-3 to HT-2 also lends support for collecting as many ray paths as time permits. The resolution of K values decreased as more rays were edited out. Although it takes less time to collect 300 ray paths than to collect 750 ray paths, the additional rays will provide some increase in accuracy.

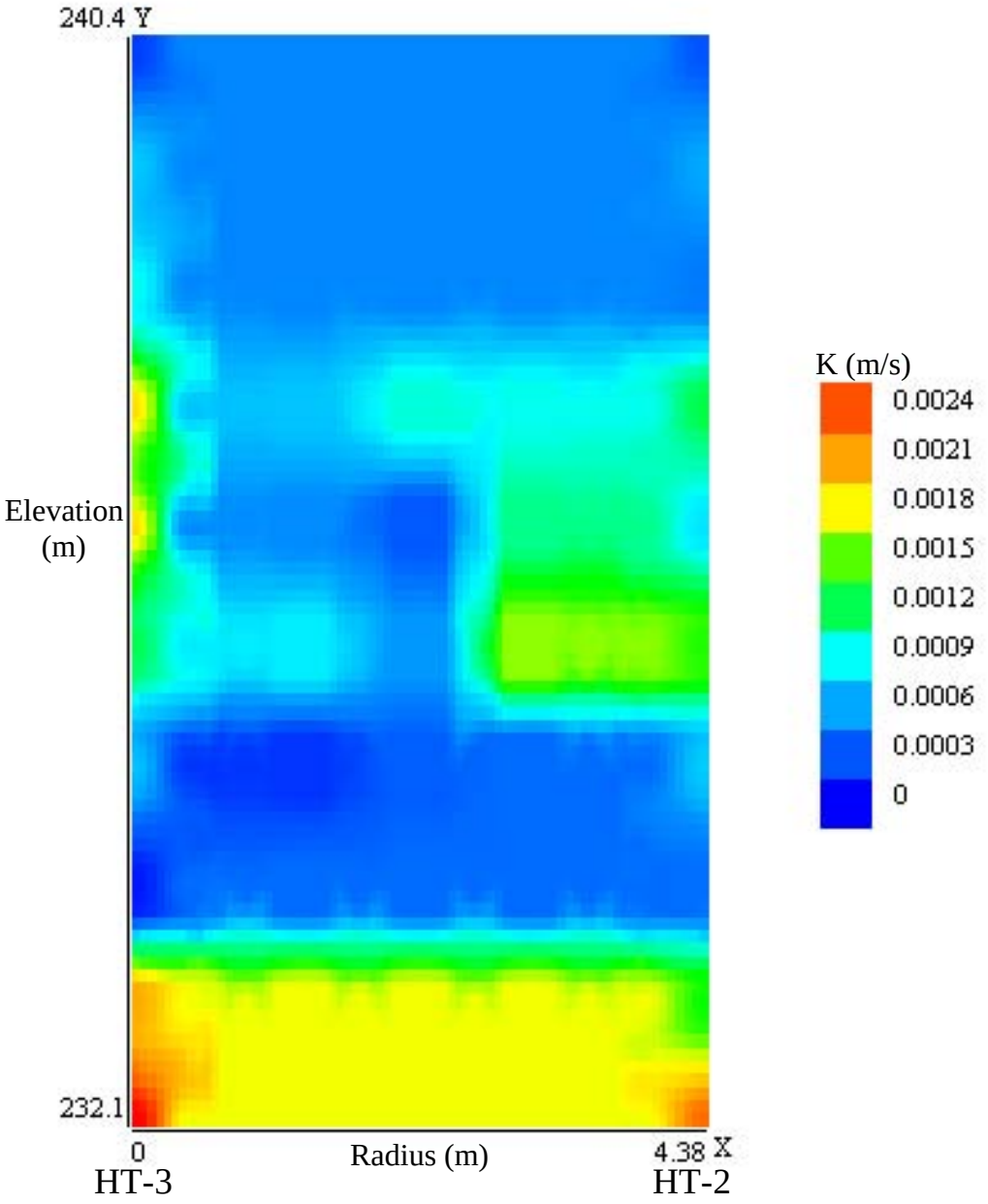

Figure 37: Interwell K values from constrained SVD analysis with HT-3 as the source well and HT-2 as the receiver well (750 rays, $S_s = 10^{-5}$).

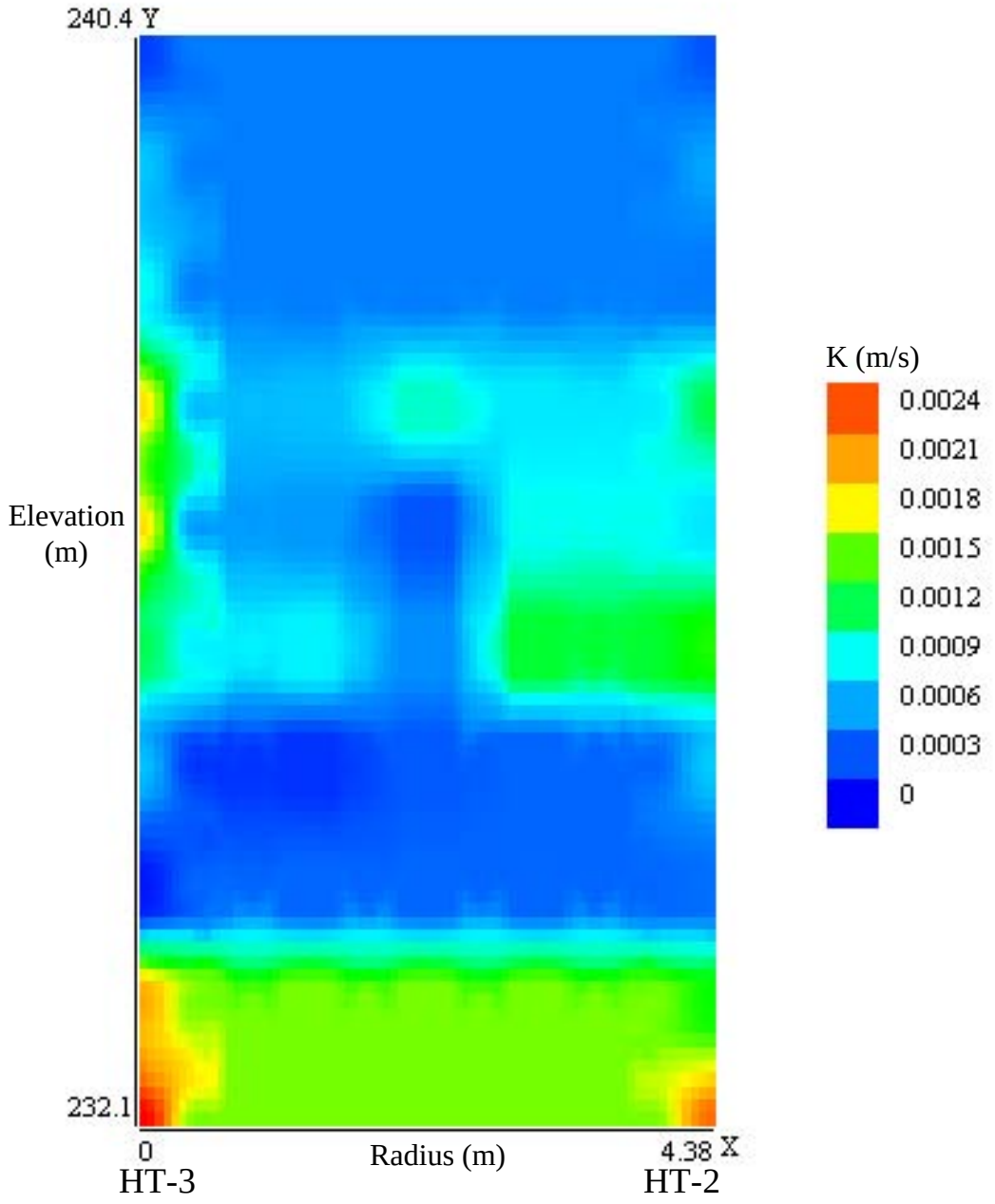

Figure 38: Interwell K values from constrained SVD analysis with HT-3 as the source well and HT-2 as the receiver well (270 rays, $S_s = 10^{-5}$).

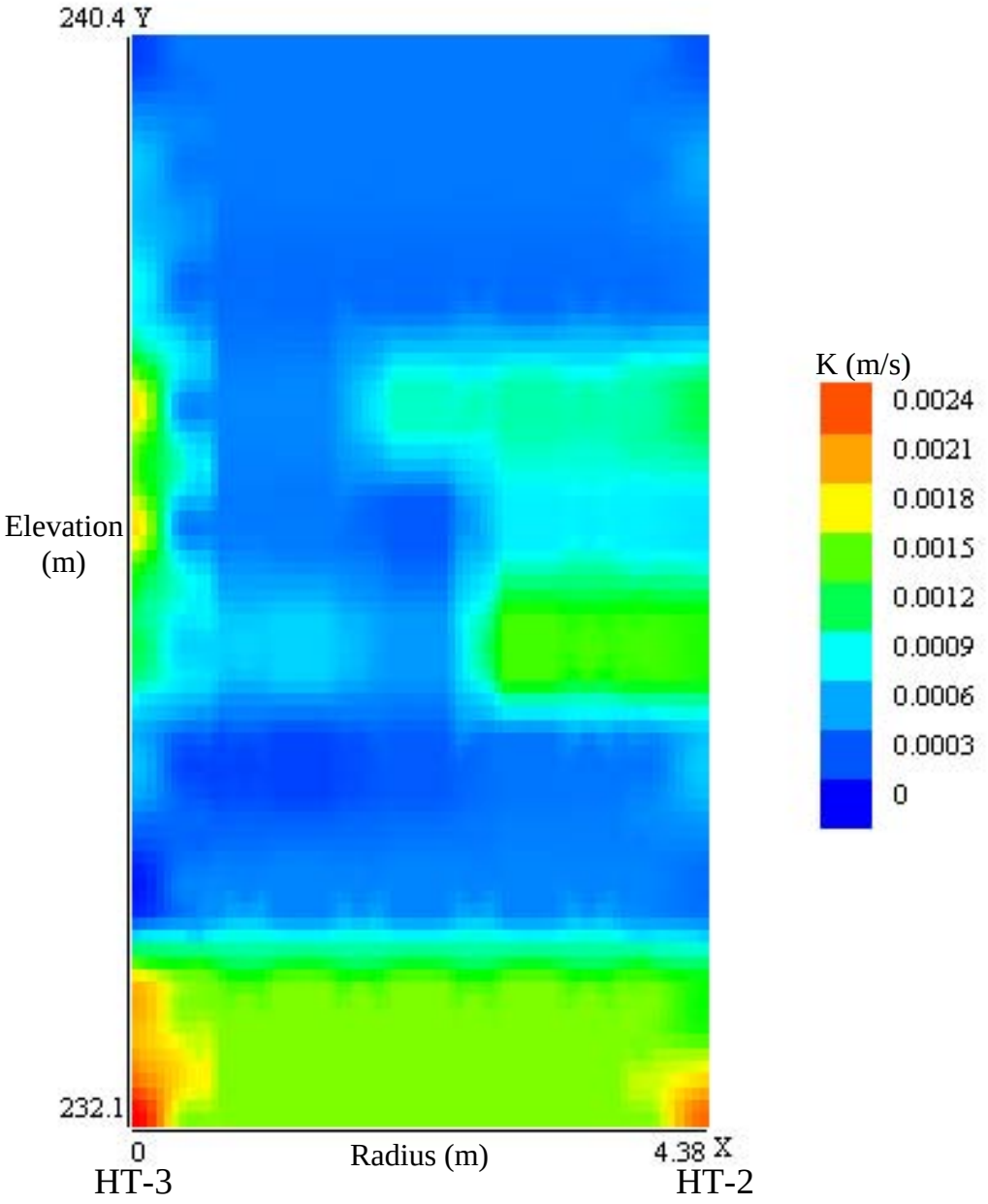

Figure 39: Interwell K values from constrained SVD analysis with HT-3 as the source well and HT-2 as the receiver well (170 rays, $S_s = 10^{-5}$).

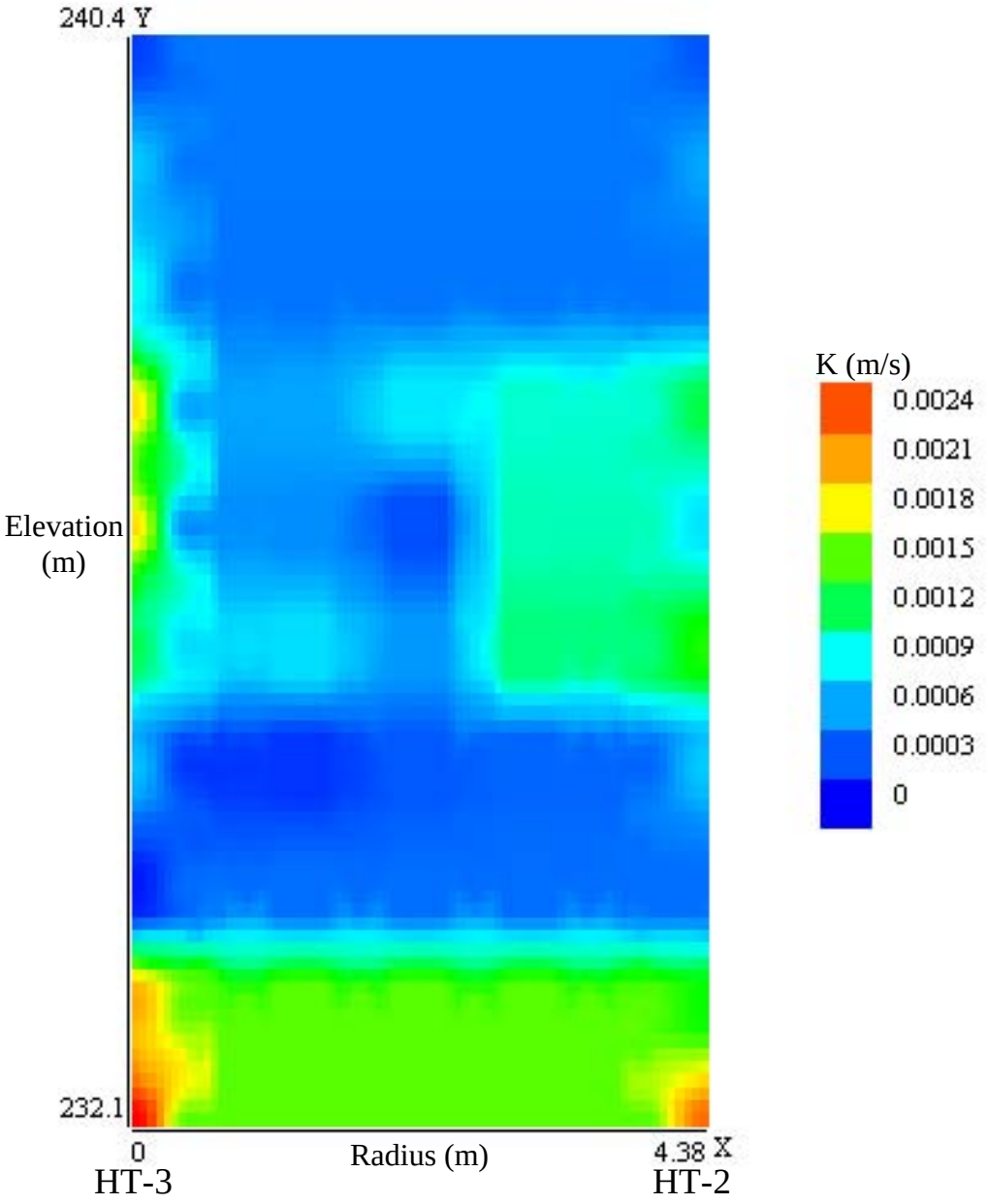

Figure 40: Interwell K values from constrained SVD analysis with HT-3 as the source well and HT-2 as the receiver well (90 rays, $S_s = 10^{-5}$).

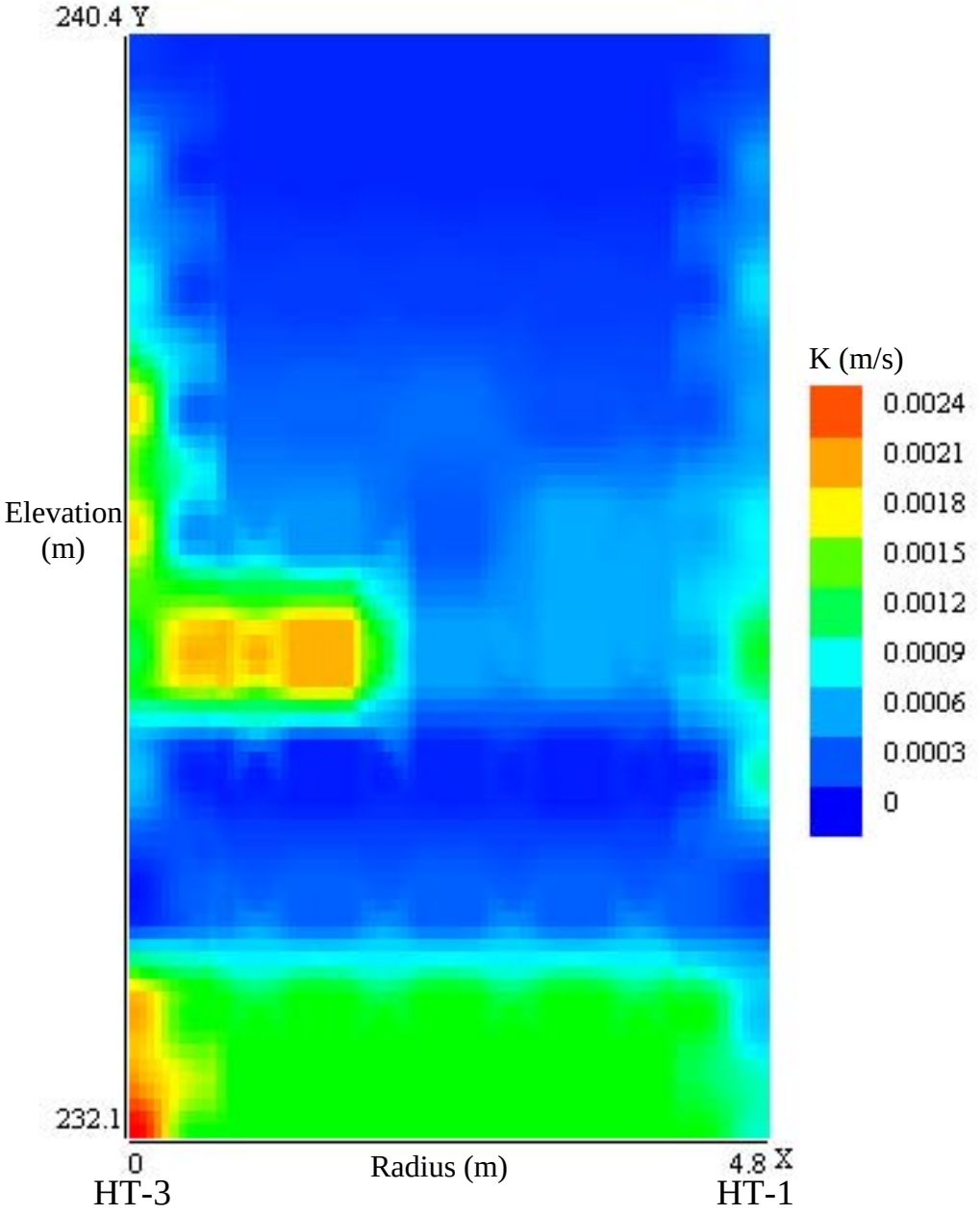

Figure 41: Interwell K values from constrained SVD analysis with HT-3 as the source well and HT-1 as the receiver well ($S_s = 10^{-5}$).

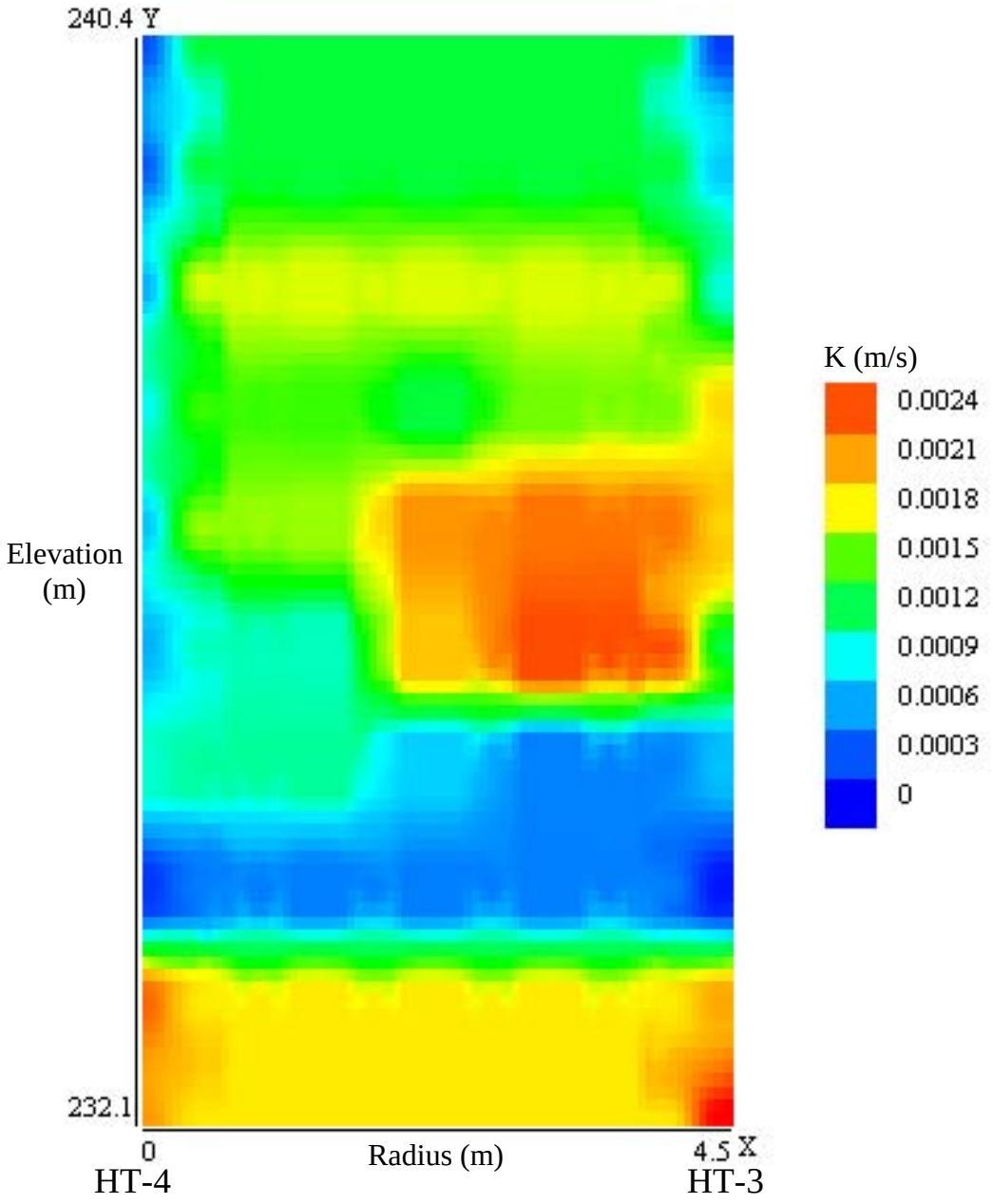

Figure 42: Interwell K values from constrained SVD analysis with HT-4 as the source well and HT-3 as the receiver well ($S_s = 10^{-5}$).

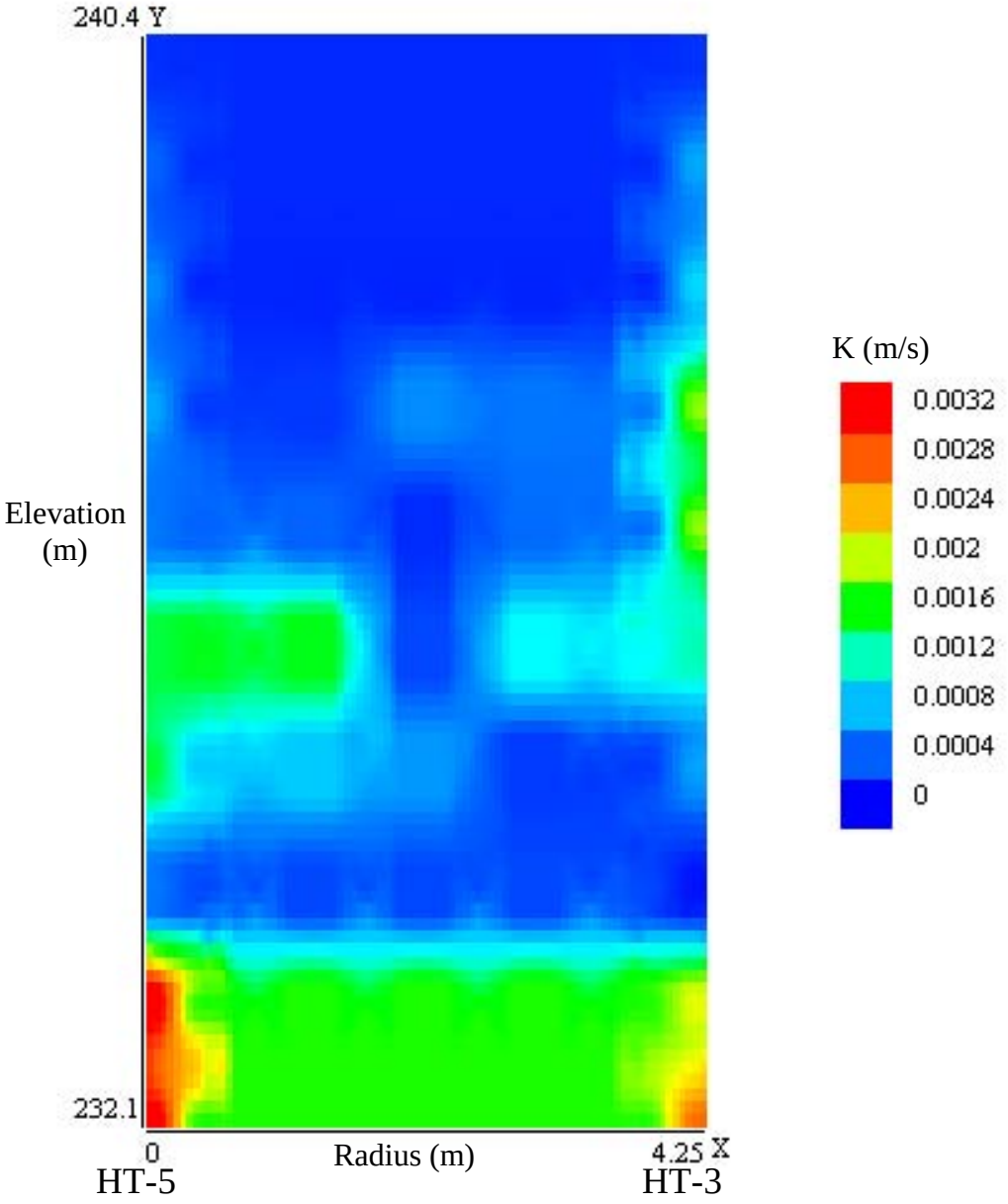

Figure 43: Interwell K values from constrained SVD analysis with HT-5 as the source well and HT-3 as the receiver well ($S_s = 10^{-5}$).

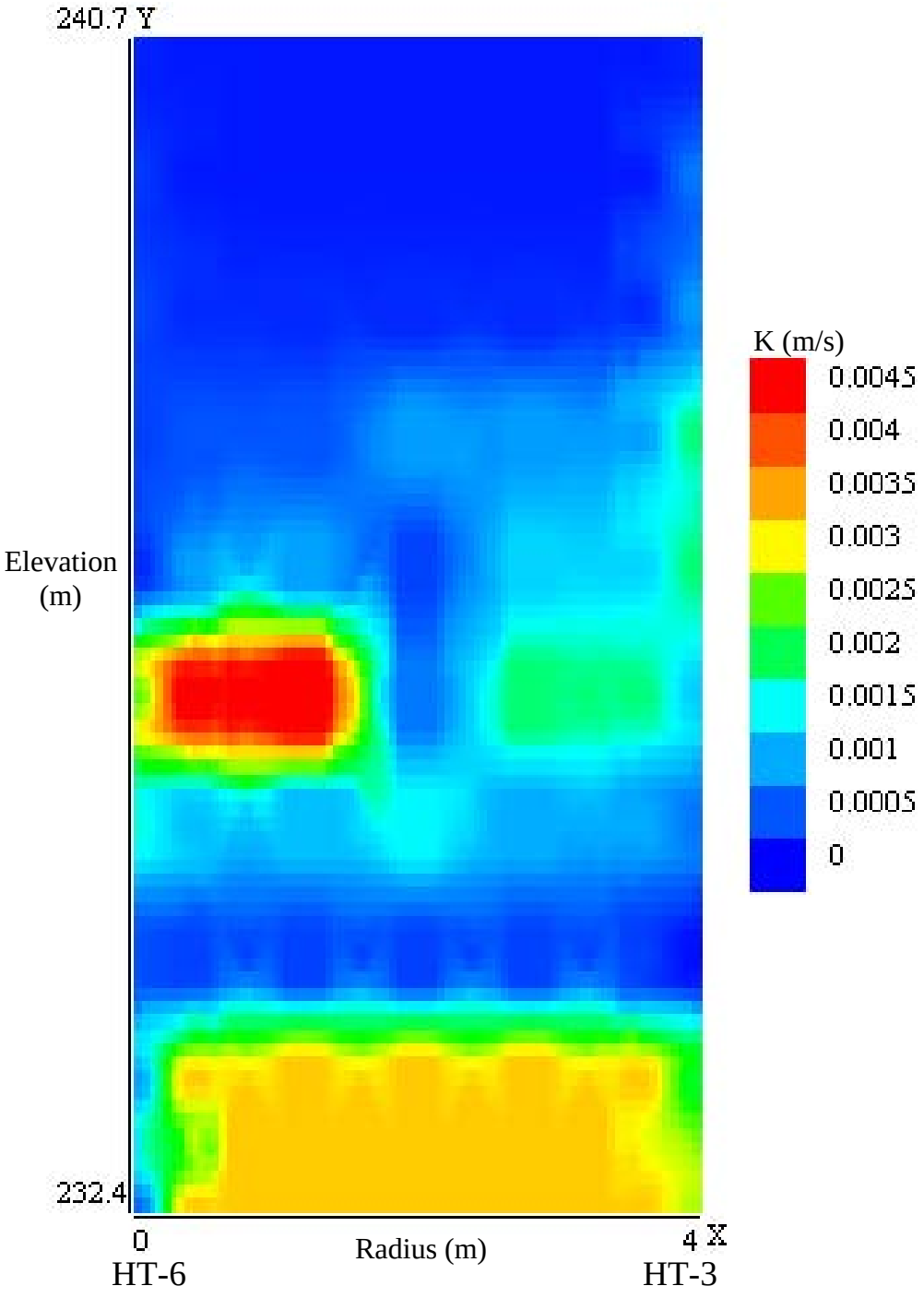

Figure 44: Interwell K values from constrained SVD analysis with HT-6 as the source well and HT-3 as the receiver well ($S_s = 10^{-5}$).

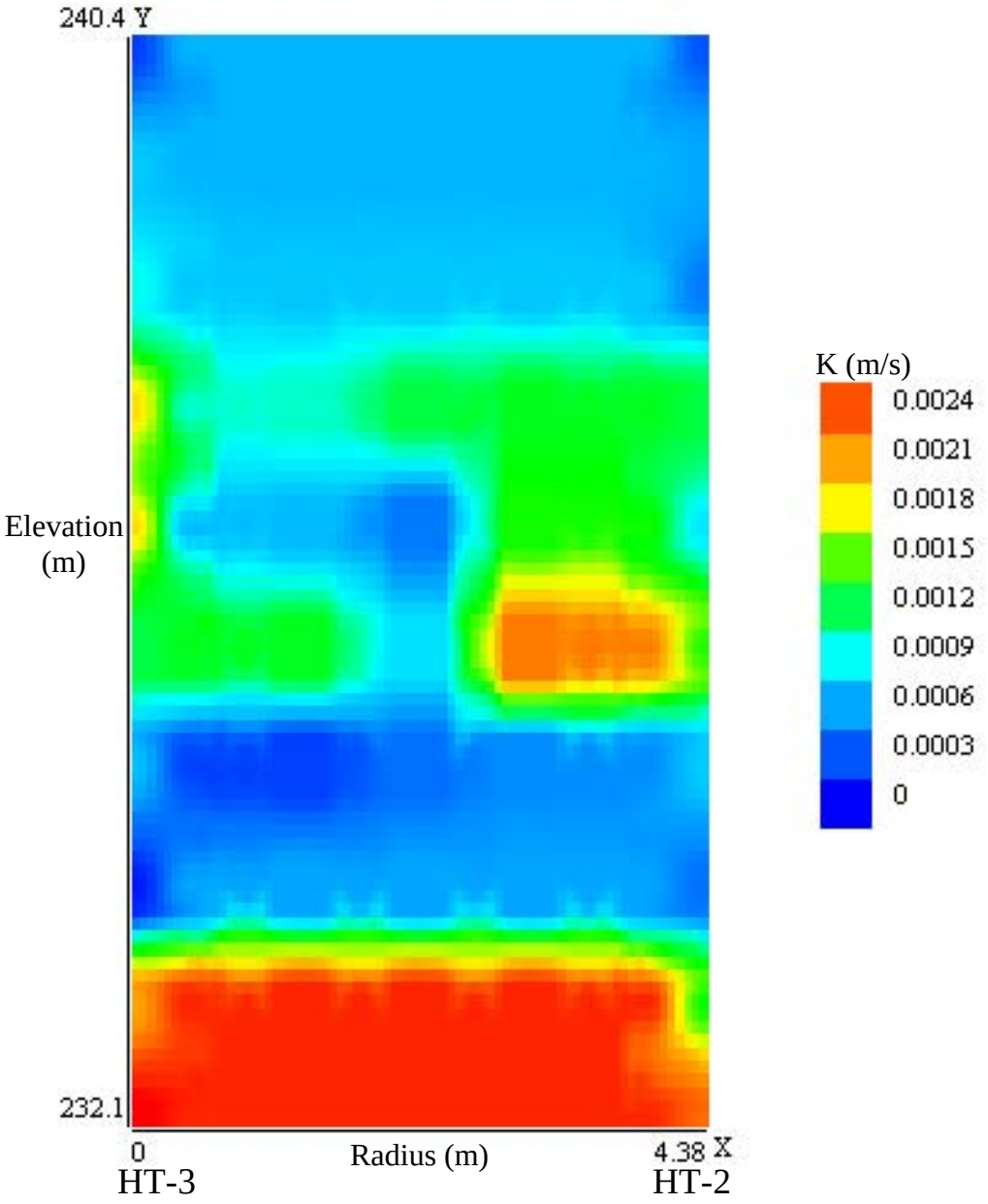

Figure 45: Interwell K values from constrained SVD analysis with HT-3 as the source well and HT-2 as the receiver well (750 rays, $S_s = 1.5 \times 10^{-5}$).

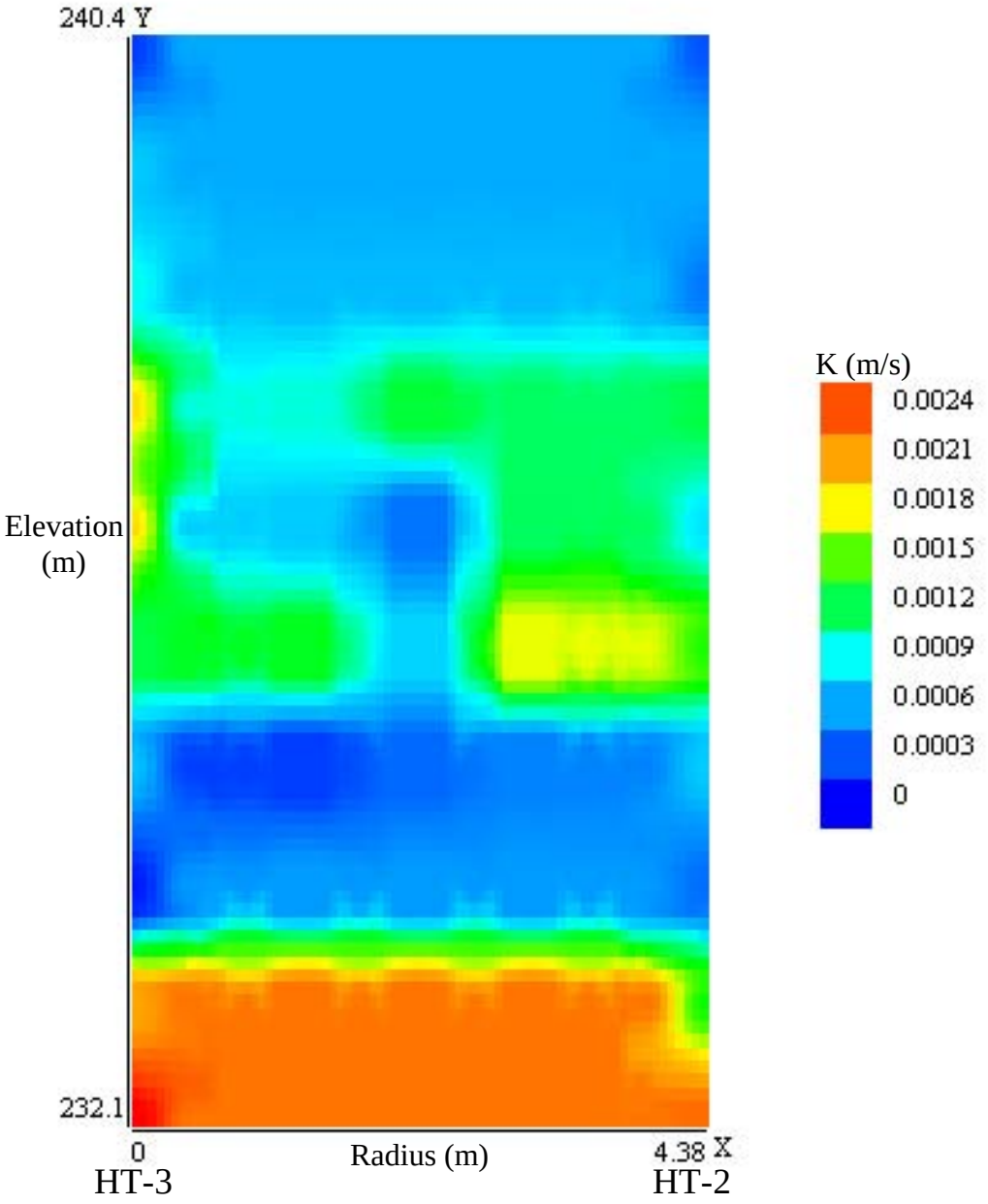

Figure 46: Interwell K values from constrained SVD analysis with HT-3 as the source well and HT-2 as the receiver well (270 rays, $S_s = 1.5 \times 10^{-5}$).

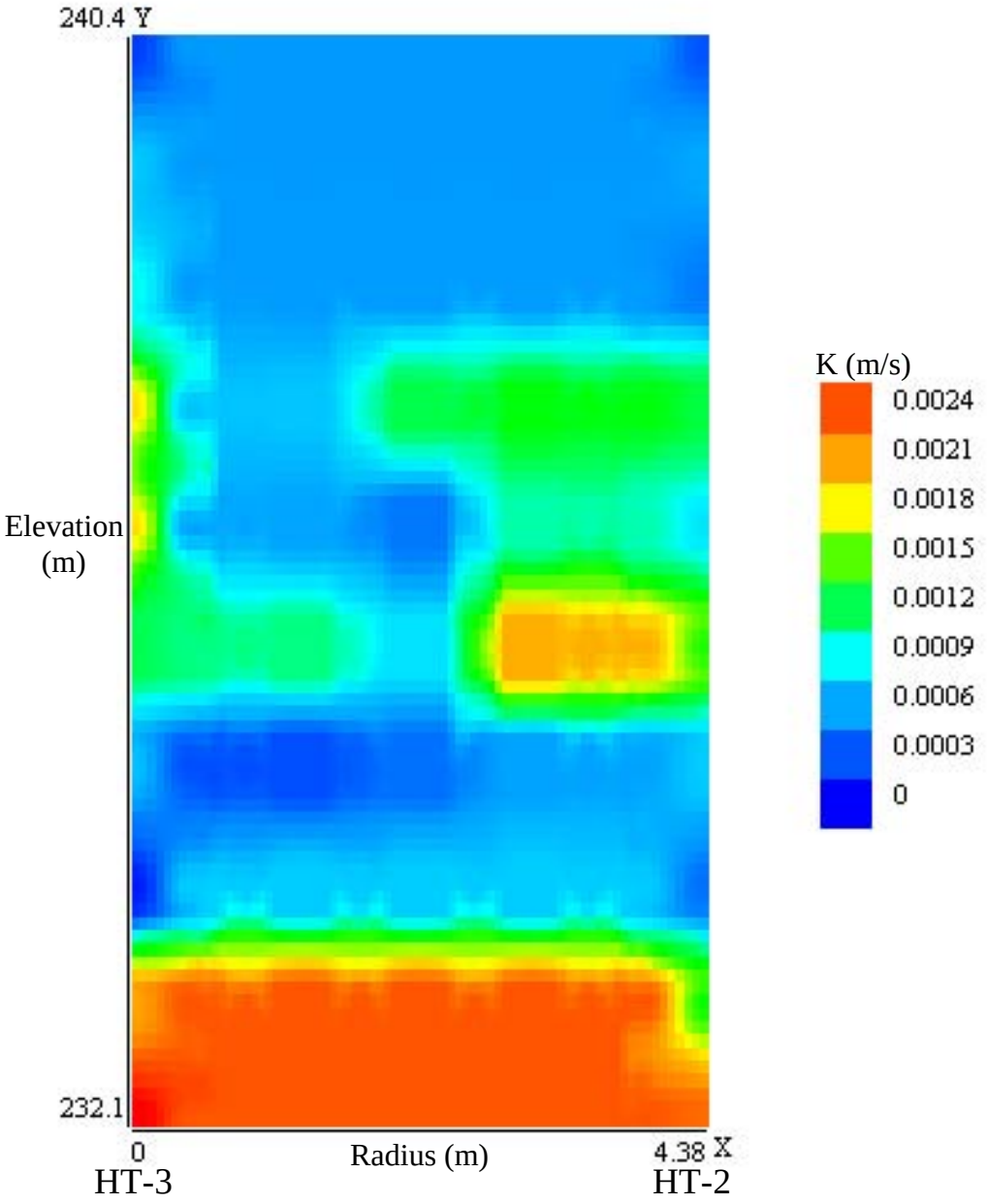

Figure 47: Interwell K values from constrained SVD analysis with HT-3 as the source well and HT-2 as the receiver well (170 rays, $S_s = 1.5 \times 10^{-5}$).

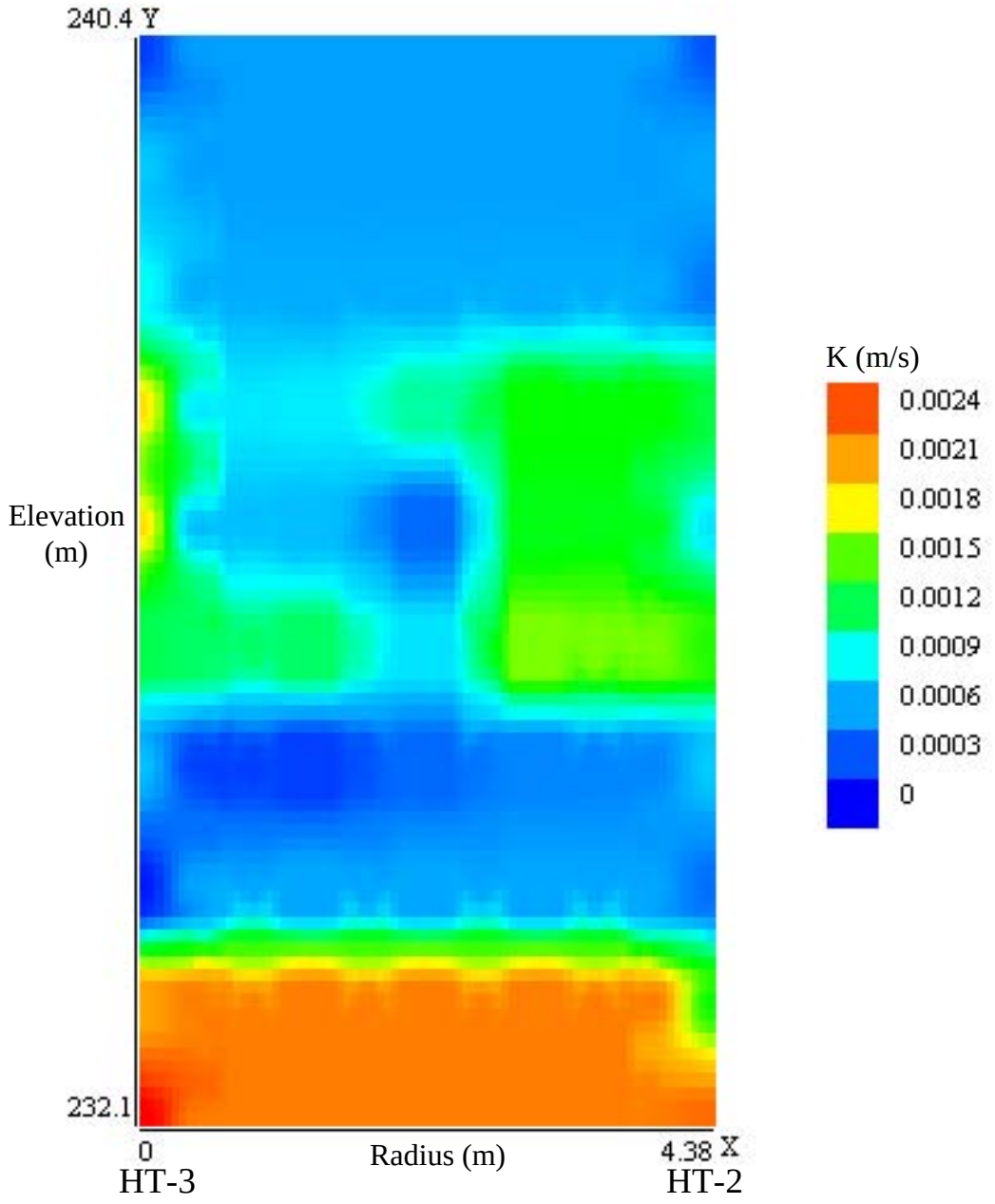

Figure 48: Interwell K values from constrained SVD analysis with HT-3 as the source well and HT-2 as the receiver well (90 rays, $S_s = 1.5 \times 10^{-5}$).

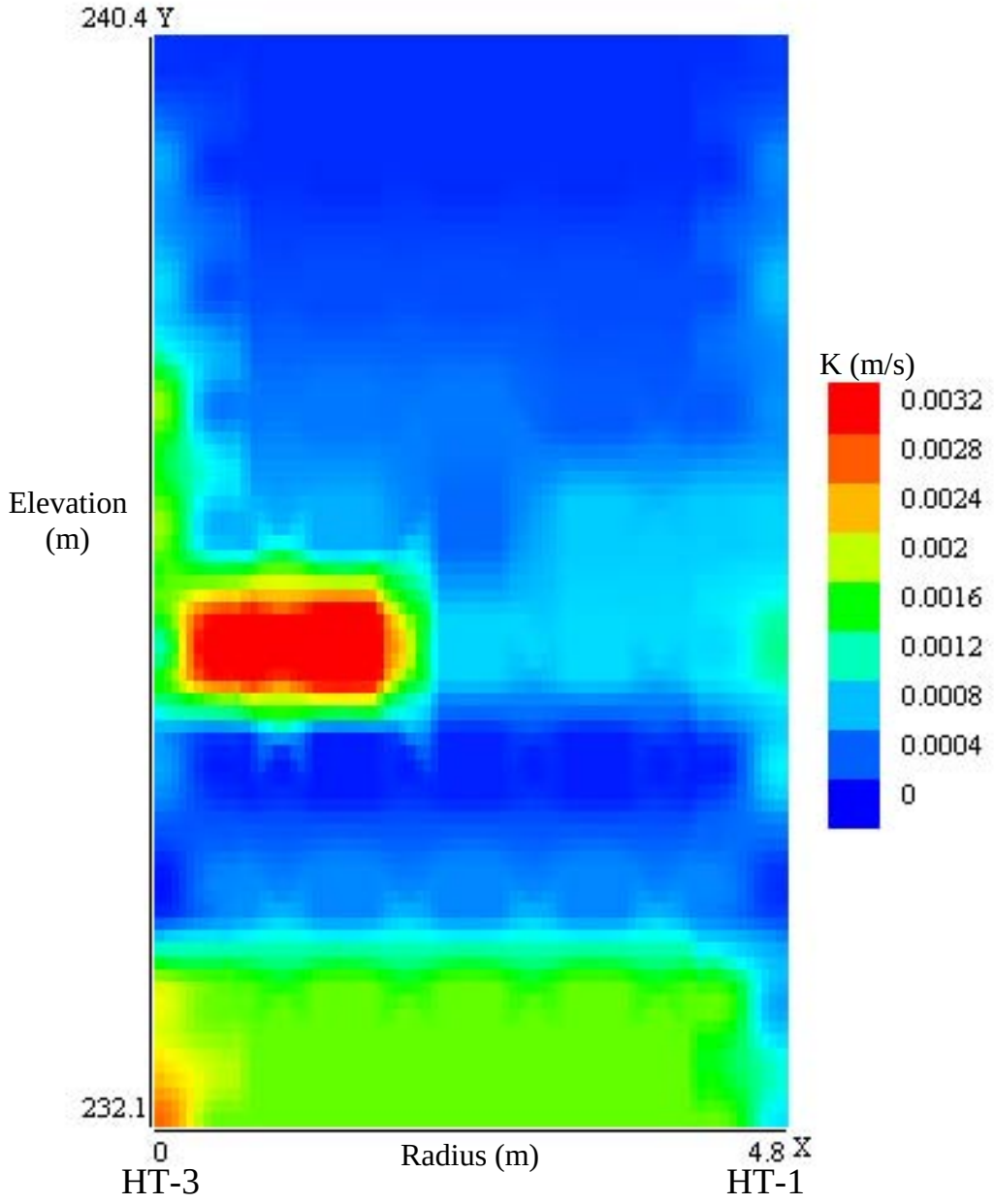

Figure 49: Interwell K values from constrained SVD analysis with HT-3 as the source well and HT-1 as the receiver well ($S_s = 1.5 \times 10^{-5}$).

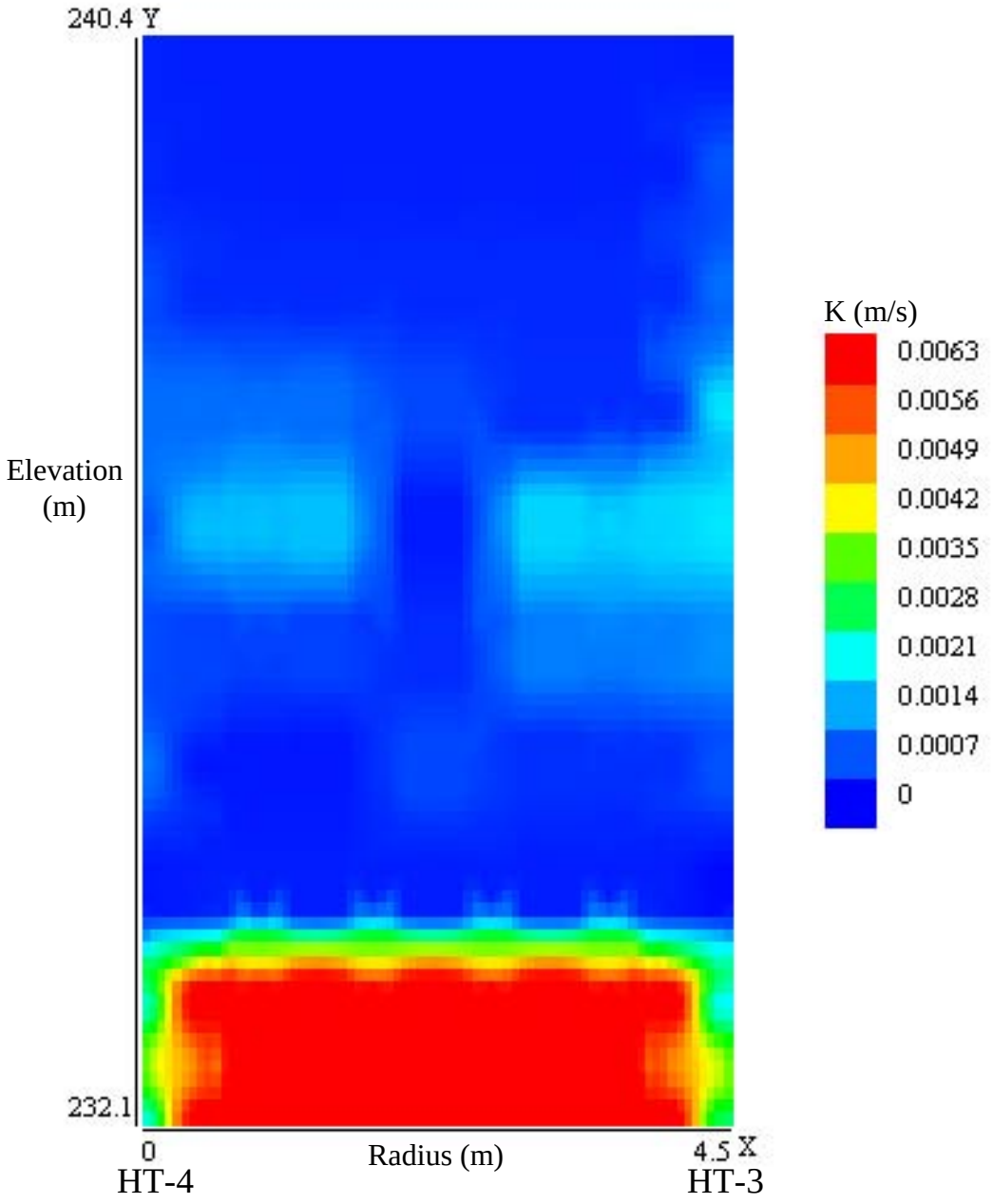

Figure 50: Interwell K values from constrained SVD analysis with HT-4 as the source well and HT-3 as the receiver well ($S_s = 1.5 \times 10^{-5}$).

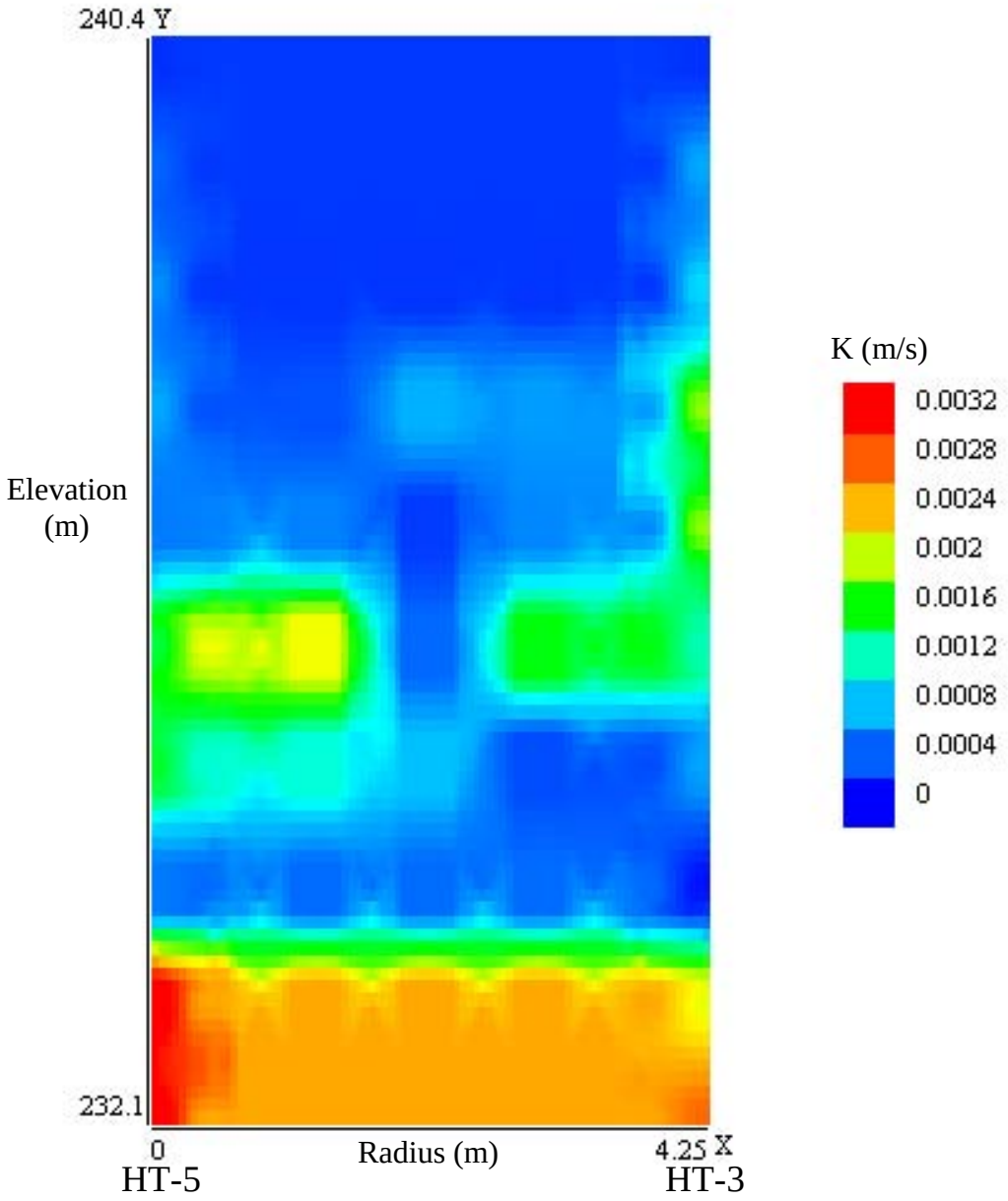

Figure 51: Interwell K values from constrained SVD analysis with HT-5 as the source well and HT-3 as the receiver well ($S_s = 1.5 \times 10^{-5}$).

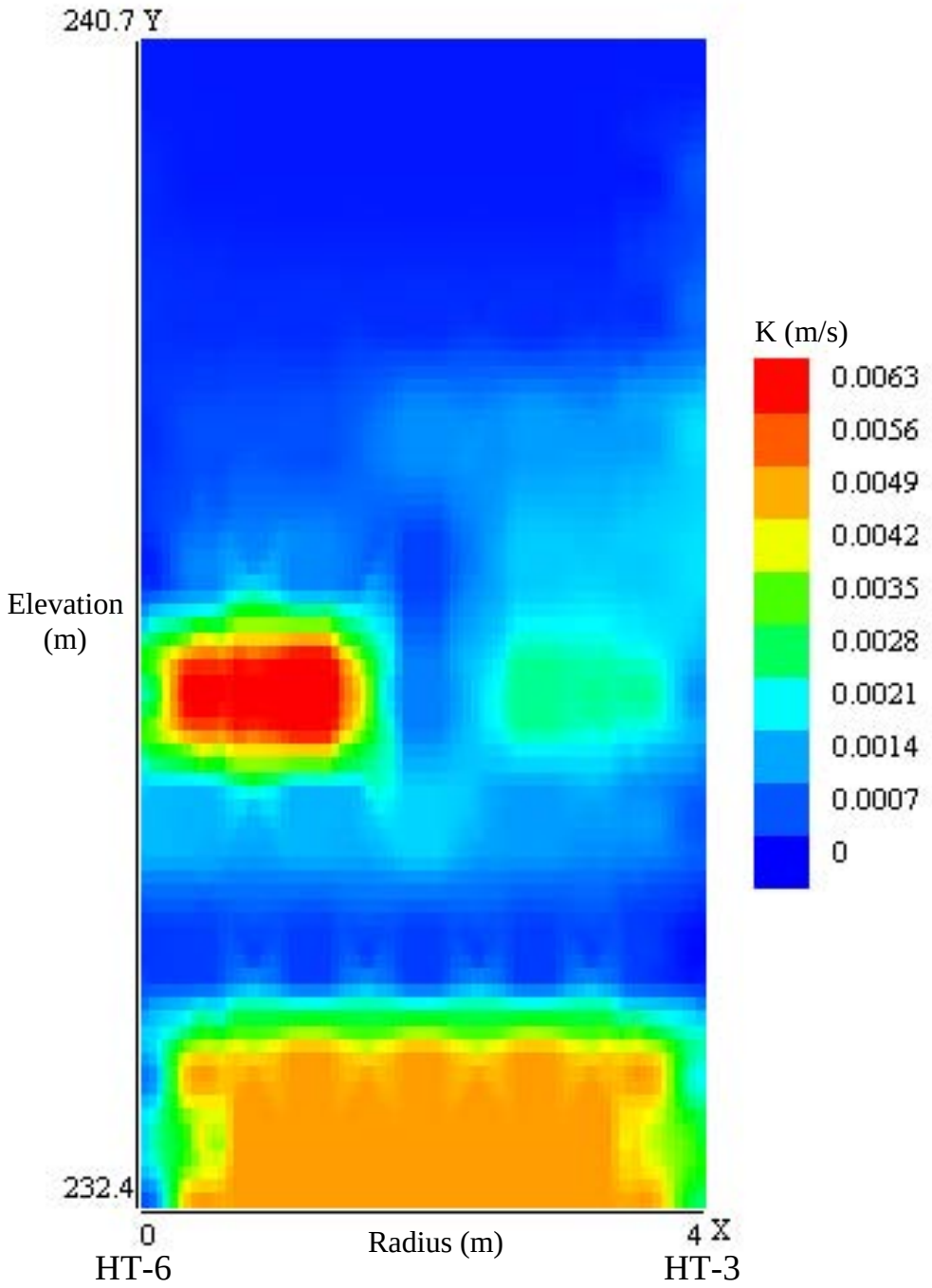

Figure 52: Interwell K values from constrained SVD analysis with HT-6 as the source well and HT-3 as the receiver well ($S_s = 1.5 \times 10^{-5}$).

Diagonal Ray Paths –30 Sec. Mechanical Pumping and 3 Sec. Pneumatic Geoprobe Source MOG Data

Introduction

The last phase of this project was to collect data with the mechanical pumping system and to see if the sinusoidal source could be operated from the end of a direct push system such as Geoprobe. Data were collected using the same set of hydraulic tomography (HT) wells as used for the pneumatic data collection. For the location of the Geoprobe source well we picked a location that keeps HT-3 as the center and fills in a vacant area, as shown in Figure 8. The pumping system was constrained to a period of 30 seconds because that was the minimum limit of our computer controlled servo-valve. It would be desirable to design and build a servo-valve that could bridge the gap between the 30 second data generated here and the 3 second data of the pneumatic system. As discussed earlier the wavelength of the driving signal is proportional to the period and the averaging volume is proportional to the wavelength.

Field Methods

The pumping system uses a reservoir on the surface, a pressurized water system, and a computer controlled servo-valve to supply the sinusoidally varying signal (the setup is shown in Figure 5c). We chose to use the pneumatic system and 3 second period data for the geoprobe source because of logistics and time critical scheduling of the geoprobe unit. However, it seems clear that the pumping system could have been adapted equally well. Using two vertical multi-level receiver arrays we collected data simultaneously in wells HT-2 and HT-3 while using the Geoprobe as source. The field setup of the Geoprobe unit is shown below in Figure 53a. The pneumatic source assembly for the

Geoprobe unit is shown in Figure 53b and consisted of a PVC screened one foot interval, blank PVC casing, a wafer packer, and an inflation packer. The purpose of the inflation packer and the wafer packer was to isolate the Geoprobe drill string from the source signal. Unfortunately, the wafer packer burst early in the data collection so only the wafer packer was available for isolation.

Figure 53a. Geoprobe unit on site for pneumatic 3 second data collection.

Figure 53b. Pneumatic source assembly consisting of a PVC screen interval, PVC blank, wafer packer, and inflation packer.

Data Processing

Data processing steps for these data were performed with the usual series of Visual Basic computer programs FitAmpPhase, HydraulicTomAnal, and LeastSquaresSVD discussed and used earlier. In general, analysis for this study used higher quality ZOP data to estimate K at relatively discrete locations and to develop a layered model grid to represent the aquifer between the well pairs. Then the full MOG data sets were used to evaluate aquifer heterogeneity. Linear tomographic inversion estimates K, which is derived from the diffusivity ratio and an estimate of S_s. S_s is difficult to measure and, typically, representative values are usually just assumed from literature references (Fetter, 2001). A corrected S_s estimated from baseline HRST K and the experimental phase data were used during the modeling and inversion process to best represent the aquifer storage characteristics at GEMS. Some records exhibited very poor signal to noise ratio due either to pressure transducer failure or attenuation by low K layers. In these cases the field data were replaced with synthetic data or surrogate phase which was calculated from the HRST results for K. Various data processing techniques were used to improve the fit of phase data to the layered heterogeneous models, such as

anisotropic ratios and linear constraint. For more details on data processing see Lyle (2011).

Aquifer heterogeneity for this research was simulated with successive model runs using ZOP and MOG data sets. In general, each of the well pairs had three modeling and corresponding inversion steps involving horizontal ZOP data to develop a reduced zone model to represent the aquifer, MOG data to evaluate aquifer anisotropy, and MOG data to evaluate aquifer lateral heterogeneity. First, ZOP data were modeled on a mesh grid spacing that corresponded to the 0.305 m (1 ft) spacing of the source-receiver, zero-offset profile locations within the well pair. Depending on the number of source intervals in a well pair, either a 27 or 28 Zone model was used with the higher quality ZOP data to calculate an initial K for each source-receiver location. The vertical profile of this horizontal K data was used to develop a reduced 7 or 8 Zone model grid which better represents the expected resolution of the tomographic method. ZOP ray path estimation through the 7 or 8 Zone model and corresponding phase inversion determined another vertical distribution of K values which were subsequently used to define the MOG model runs. Next, the reduced 7 or 8 Zone model along with ZOP calculated K was used with the MOG data to simulate isotropic and anisotropic conditions.

At the completion of the successive model runs, the final, constrained, least squares fit K values were contoured against elevation and radial distance between source and receiver using a public domain program called QuickGrid. The program contours between points written in an x,y,z format, which corresponds to radius, elevation, and K values determined by the SVD analysis from this research. In all of the contour plots of K, the source well is on the left side and receiver well is on the right. Using the HT-6 to

HT-3 well pair as an example because it seemed to be the best initial data set, the modeling, inversion, statistical K determination, anisotropy evaluation and constraint factors are further discussed below. For a more complete discussion of the data processing for all well pairs see Lyle (2011).

ZOP Modeling and Inversion

To obtain the expected, optimal 1 m (3.28 ft) grid resolution, ZOP data were initially modeled on a finer 0.3048 m (1 ft) vertical spacing in a 27 or 28 zone model (Fig. 54). This zone spacing corresponds to the experimental source and receiver locations in a well and the number of zones reflect the total number of source locations in CPT. ZOP data are expected to have the best quality within a MOG data set because it has the shortest ray path distance between the source and receiver. Consequently, ZOP data were used to develop a coarser model grid to represent the aquifer and better match the expected tomographic resolution. In the HT-6 to HT-3 ZOP model below (Fig. 54), source locations are on 0.3048 m (1ft) centers over the approximate well screen interval of 232.0 to 240.2 m msl (761 to 788 ft msl) and correspond to the odd numbered nodes, 3 – 57, within the model grid. Receiver locations are directly across from the source and correspond to the even number nodes, 4 – 58. Using K, S_s and ZOP data, HydraulicTomAnal modeled the 28 horizontal ray paths, each through their respective zone, to generate the model geometry and theoretical model phase for this grid. Either HRST K values or an average HRST K value (0.003 ft/sec) were input as reasonable initial constant K nodes to generate the model matrix and phase.

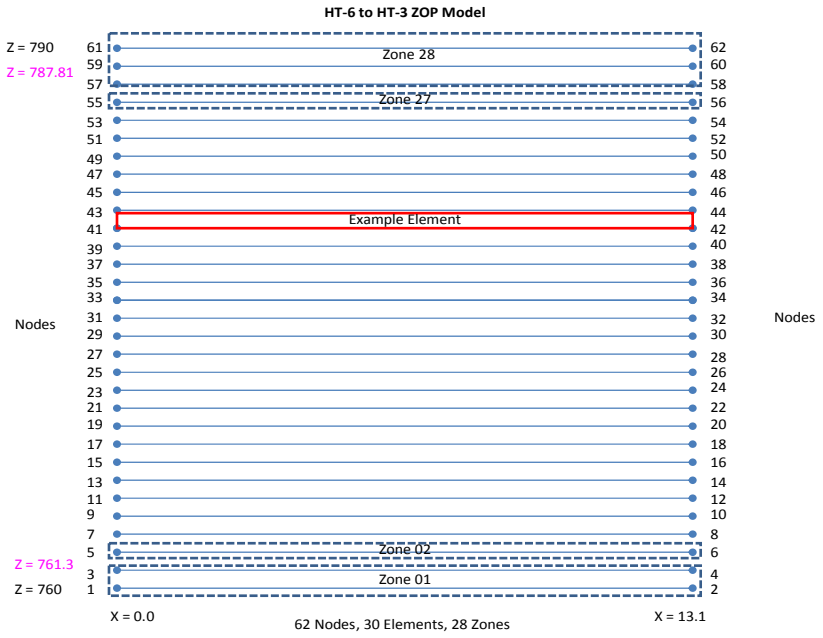

Figure 54 – Conceptual 28 zone finite difference model grid for HydraulicTomAnal.

As a representative data set, SVD analysis of the HT-6 to HT-3 is used to evaluate the deterministic K calculated from the ZOP data through the 28 zone model (Fig. 54). The K values correspond to the 28 zero-offset source and receiver locations in the ZOP data set (Fig. 55). The profile of the experimental test intervals was interpreted into a reduced zone model with thicker vertical zones that is more representative of the expected tomographic resolution. Typically, interpretation of the ZOP deterministic K between the different well pairs resulted in an either 7 or 8 reduced-zone model (Fig. 56).

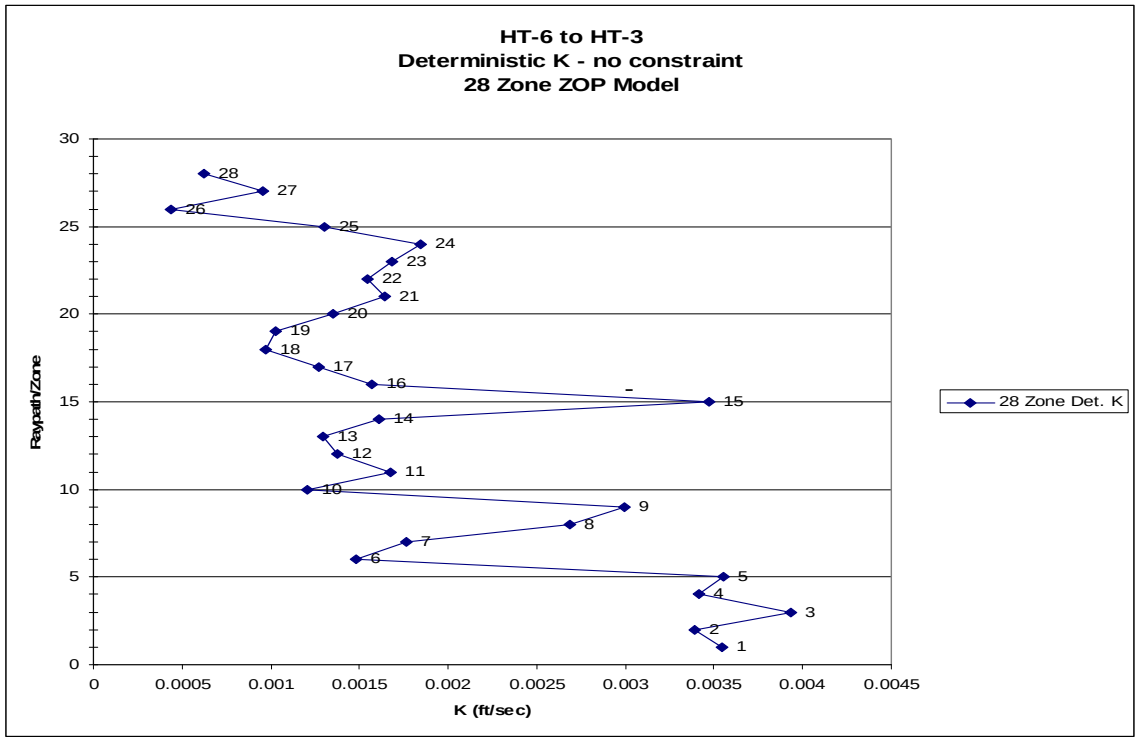

Figure 55 – HT-6 to HT-3 Deterministic calculated K from ZOP data set.

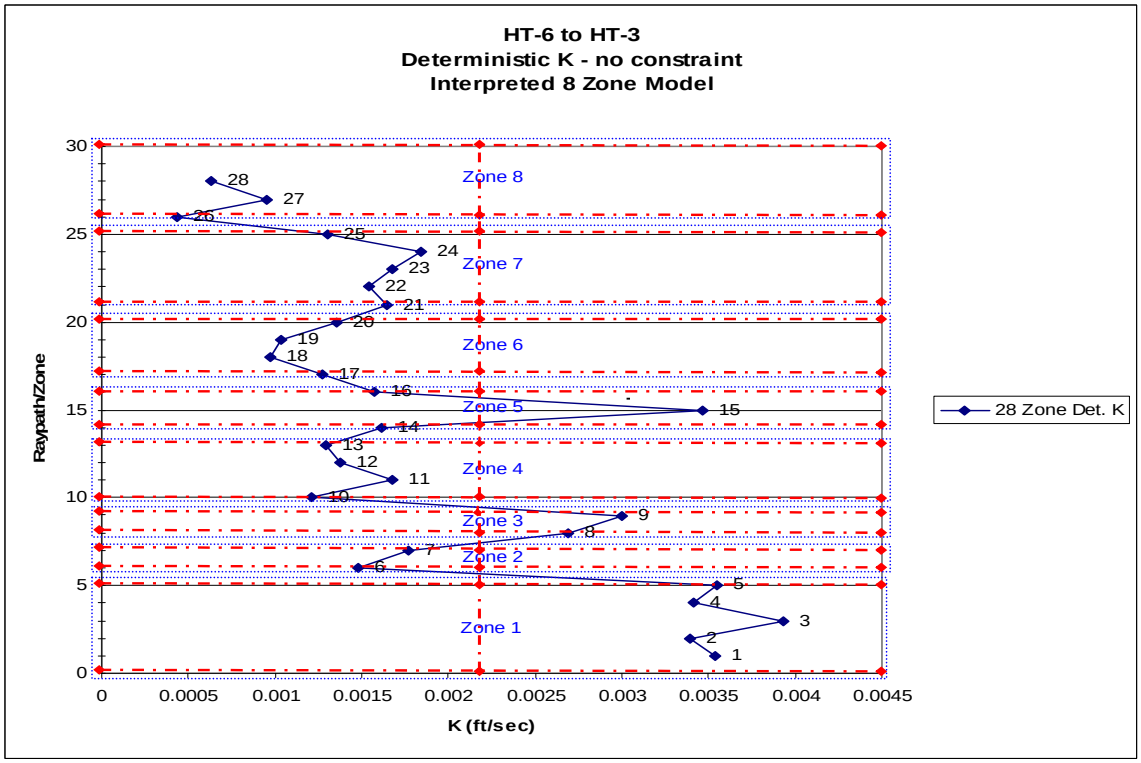

Figure 56. HT-6 to HT-3 interpretation of ZOP deterministic K.

The thicker vertical elements of the interpreted 8 Zone model (Fig. 56) more closely fall within the expected 1 m (3.28 ft) resolution of the tomographic method. The K value for each zone is an average of the deterministic K values in the model zone. The HT-6 to HT-3 example model has eight zones, 30 elements, and 48 nodes over the approximate 232.0 to 240.2 m msl (761 to 788 ft msl) well screen interval (Fig. 57). Each zone is composed of either two elements or six nodes (Fig. 57). The center nodes in the model grid define two lateral elements; these extra nodes correspond to the midpoint between the source and receiver location. These center nodes will be useful later when we consider lateral heterogeneity.

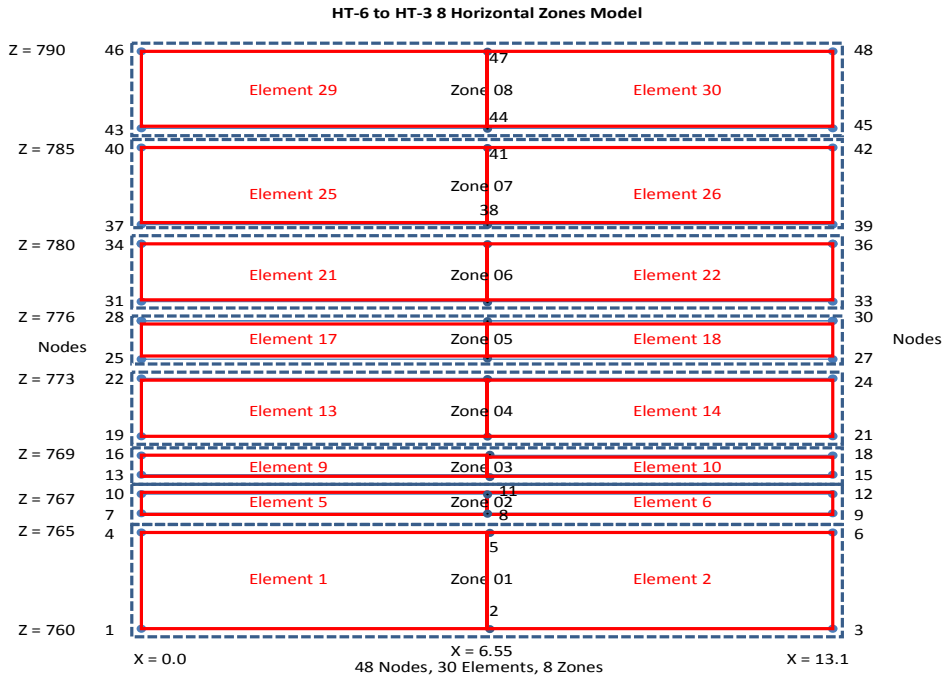

Figure 57. Conceptual 8 zone model grid with 8 zones (blue) and 30 elements (red).

To check if the 7 or 8 zone model adequately represents the larger ZOP data set, the modeled reduced zone model phase was plotted against the ZOP experimental phase

(Fig. 58). At HT-6 to HT-3, the smoother curve of the 8 zone model phase reflects the average value of the deterministic K assigned to the thicker layers of the model. The sharper curve of the experimental phase reflects the experimental phase at each of the initial layers used in the 28 zone model.

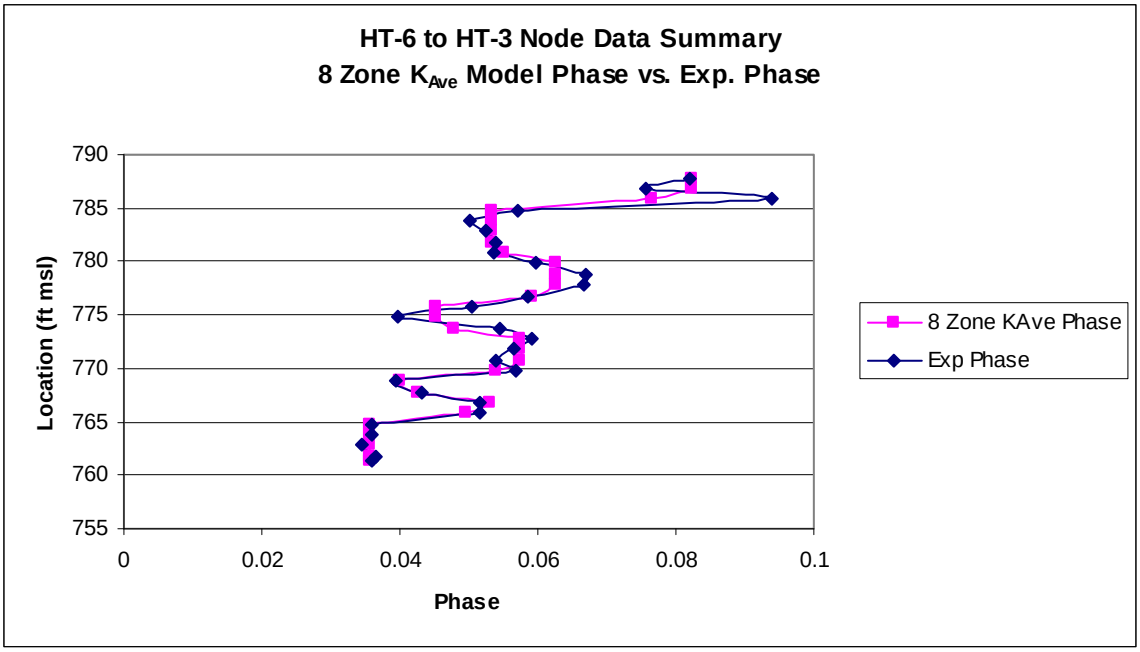

Figure 58. Experimental ZOP phase shift plotted against ZOP 8 zone model phase shift.

SVD analysis of the reduced zone model with the ratio of zones to rays no longer 1:1 generates a least squares fit of K. The reduced zone calculated K is an average value of the deterministic K in each zone (Fig. 59). Up to this point SVD analysis and modeling used an S_s estimate of 0.00001 to derive K from diffusivity. The initial 1E-05 value is considered to be representative of the aquifer storage characteristic at GEMS based on literature references and previous work by Wachter (2008) and others. The S_s

value and K from this inversion was further corrected to more closely match the baseline HRST K data and the phase shift data before further modeling with the MOG data sets.

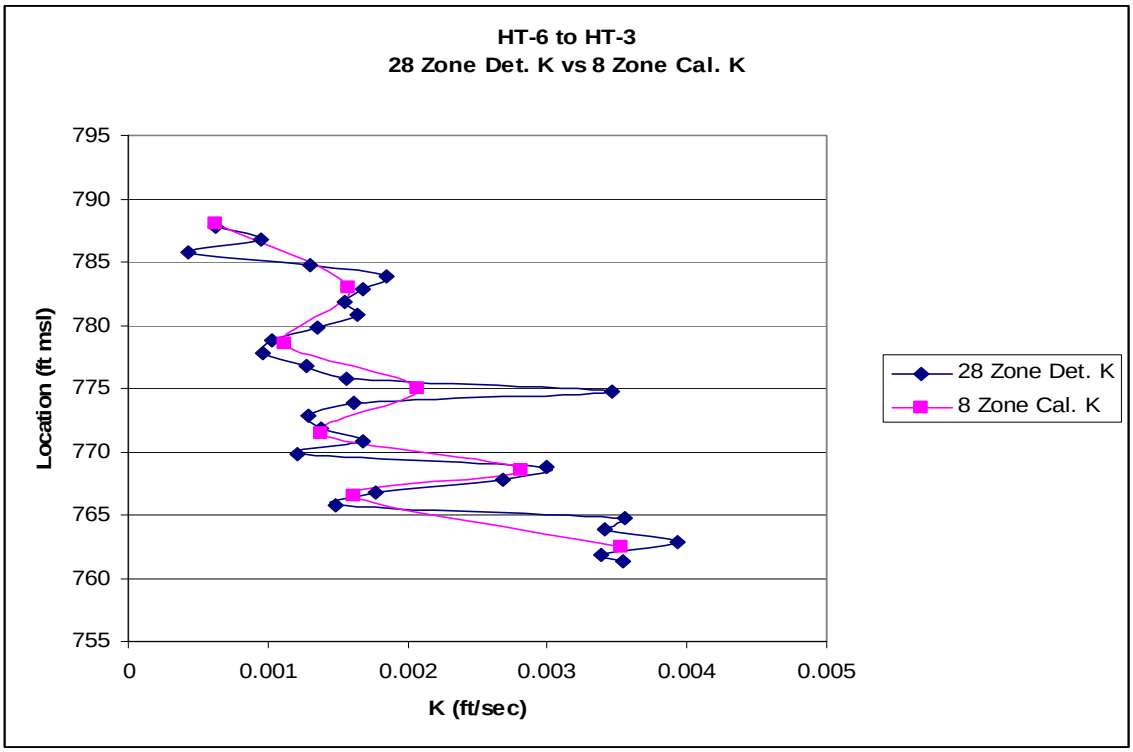

Figure 59. 28 Zone deterministic K plotted against 8 Zone calculated K.

Ss and K were corrected to match GEMS site conditions. Because phase should vary linearly with $\sqrt{S_s/K}$, the corrected S_s value, S_{sCorr}, was calculated from the average HSRT K values, K_{HRST_Ave}, and the average deterministic K values from the 28 zone ZOP model, $K_{Det\_ZOP\_Ave}$. Based on the theory, all analyses were simply adjusted to the new S_{sCorr} value with a correction factor derived from a ratio of the average slug test and model deterministic K values:

(12) $$\frac{K_{HRST\_Ave}}{K_{Det\_ZOP\_Ave}} = \text{Correction Factor}$$

When phase shift is constant, the relationship between S_s and K in the basic phase shift equation is linear, so changes to K or S_s will vary in proportion to each other. Accordingly, the deterministic and least squares calculated K values were multiplied by the correction factor to reflect the corrected Ss. The corrected HT-6 to HT-3 deterministic K values from the reduced zone model are presented below (Fig. 60).

HT-6 to HT-3 Corrected Ss and K

HRST Well	HRST K_{Ave}	28 Zone ZOP Model	28 Zone Det. K (ft/sec)	Corr. Factor	28 Zone Det. K (ft/sec)	8 Zone ZOP Model	8 Zone Cal. K (ft/sec)	Corr. Factor	8 Zone Cal. K (ft/sec)
		Ss_{Est} 1.00E-05		1.6265	Ss_{Corr} 1.63E-05	Ss_{Est} 1.00E-05		1.6924	Ss_{Corr} 1.69E-05
HT-6	0.0025	1	0.0035		0.0058	1	0.0035		0.0060
HT-3	0.0038	2	0.0034		0.0055	2	0.0016		0.0027
		3	0.0039		0.0064	3	0.0028		0.0048
		4	0.0034		0.0056	4	0.0014		0.0023
		5	0.0036		0.0058	5	0.0021	x 1.6924 =	0.0035
		6	0.0015		0.0024	6	0.0011		0.0019
		7	0.0018		0.0029	7	0.0016		0.0027
		8	0.0027		0.0044	8	0.0006		0.0011
		9	0.0030		0.0049				
		10	0.0012		0.0020				
		11	0.0017		0.0027				
		12	0.0014		0.0022				
		13	0.0013		0.0021				
		14	0.0016	x 1.6265 =	0.0026				
		15	0.0035		0.0056				
		16	0.0016		0.0026				
		17	0.0013		0.0021				
		18	0.0010		0.0016				
		19	0.0010		0.0017				
		20	0.0014		0.0022				
		21	0.0016		0.0027				
		22	0.0015		0.0025				
		23	0.0017		0.0027				
		24	0.0018		0.0030				
		25	0.0013		0.0021				
		26	0.0004		0.0007				
		27	0.0010		0.0016				
		28	0.0006		0.0010				
	Ave K_{HRST_Ave}		Ave K_{Det_Est}		Ave K_{Det_Corr}		Ave 8 Zone K_{ZOP_Est}		Ave 8 Zone K_{ZOP_Corr}
	0.0031		0.0019		0.0031		0.0018		0.0031

Figure 60. HT-6 to HT-3 correction for Ss and K.

A comparison of the corrected vertical K profile, which best represents the storage characteristic of the aquifer, to the uncorrected values is presented in Figure 61.

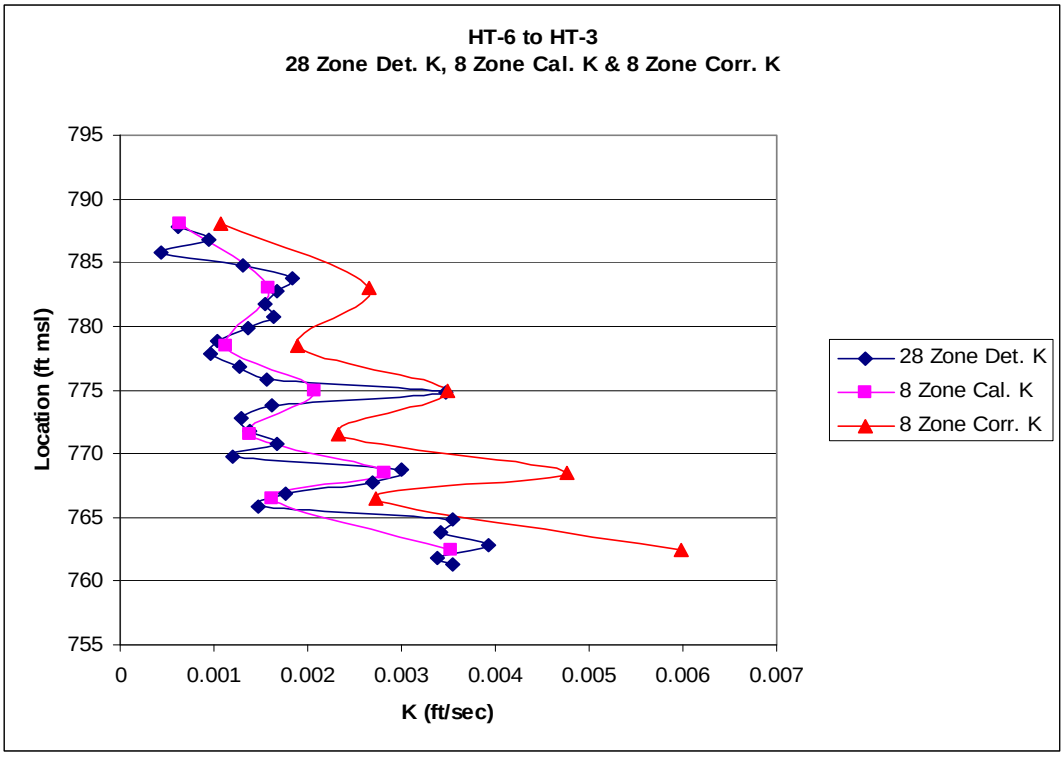

Figure 61. HT-6 to HT-3 vertical K profile adjusted for the calculated S_s that represents site-specific aquifer storage characteristics.

MOG Modeling, Inversion, and Anisotropy

After the 7 or 8 reduced-zone model geometry was developed and verified, and the S_s and calculated K were corrected to site-specific conditions, modeling with MOG data sets was initiated with the reduced-zone model to determine a representative ratio of anisotropy for data processing. In an idealized system, isotropic conditions are often assumed where $K_H = K_V$. In a natural system anisotropy prevails and typically $K_H >>> K_V$ (Domenico and Schwartz, 1998). The anisotropic ratios applied to the model simulate a more realistic flow regime to better imitate the directional dependency exhibited by alluvial sediments oriented by grain size and direction. In this case, an anisotropic ratio of 10 is $K_H = 10K_V$ and an anisotropic ratio of 2 is $K_H = 2K_V$. Anisotropic evaluation was completed for both the pumped hydraulic CPT data (30-sec period) and the

pneumatic CPT data (3-sec period). Different anisotropic ratios were evaluated with HydraulicTomAnalV21Aniso which functions the same as HydraulicTomAnalV21, but generates anisotropic effects across an element or zone. Anisotropic ratios can be applied in multiple combinations over different layers to simulate greater or lesser anisotropy. A typical, complete CPT well pair may have 28 MOG data sets with 784 rays instead of just the 28 ZOP rays initially used to develop the reduced-zone model of the aquifer for heterogeneity evaluation. With the same K inputs between the anisotropic and isotropic models, varying anisotropy can be statistically evaluated after model inversion. The offset MOG rays should measure the anisotropic variation in the aquifer, so an anisotropic correction should theoretically improve the data fit to the model.

Considerable experimentation with anisotropy ratios was carried out (Lyle, 2011). It was anticipated that a single best anisotropic ratio could be found and applied to all well pairs. However, a significant statistical deviation occurred when processing the 3-sec data sets, so additional anisotropic evaluation was completed for the pneumatic 3-sec data. Evaluation results suggested that different anisotropic ratios and data constraints are needed to adequately model CPT data with different oscillating periods. So, after the initial assessment, different anisotropy ratios were applied to the 30 and 3-sec data sets, but all the model layers used a single, best case anisotropy ratio (e.g., 2 or 10).

Inversion and least squares fitting to the reduced zone model was evaluated under different constraints (weights on initial estimates of K), as well as isotropic and anisotropic ratios of 2 and 10 for the two CPT sources. Chi squared and standard deviation values from the least squares fit for the hydraulic 30-sec data indicate that an anisotropic ratio of 10 produced a poorer data fit (representative data for HT-1 to HT-3

shown in Fig. 62). Both the isotropic and the anisotropic 2 models were relatively good, although the anisotropic model provided a slightly better data fit. Most of the K values solved from the anisotropic 2 model were near or less than 10% standard deviation.

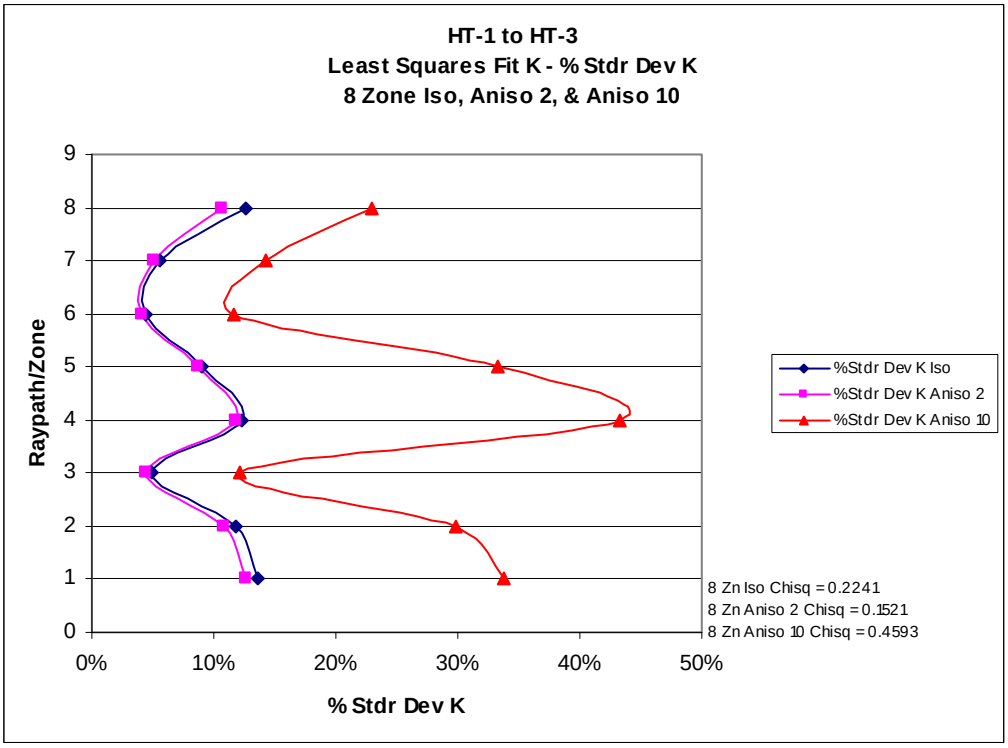

Figure 62. HT-1 to HT-3 least squares fit K under isotropic, anisotropic-2, and anisotropic-10 conditions.

The overlap of field data and the calculated phase values (e.g., isotropic, anisotropic 2, anisotropic 10, etc.) should indicate the relative goodness of fit between the experimental data and the straight ray approximation. As an example, MOG data from the first CPT source location at HT-1 to HT-3 for the isotropic, anisotropic 2, and anisotropic 10 scenarios are presented below (Fig. 63 to 65). In this example, the CPT source location is near the bottom of HT-3 on the left and the 28 receiver locations in HT-1 are on the right. The ray path of the CPT must travel farther to reach the receivers located in the higher parts of the well screen, so the phase shift will increase with

distance and form a half parabola at this location. The curves most closely match with an anisotropy ratio of 2 (Fig. 64), which correlates with the data fit indicated by the percent standard deviation results displayed in Figure 62. Additional experiments were run testing different anisotropy ratios for high K and low K zones, but no significant improvement was noted. So, an anisotropic ratio of 2 was chosen to evaluate all the MOG data sets for the 30-sec CPT data (i.e., the pumped hydraulic source).

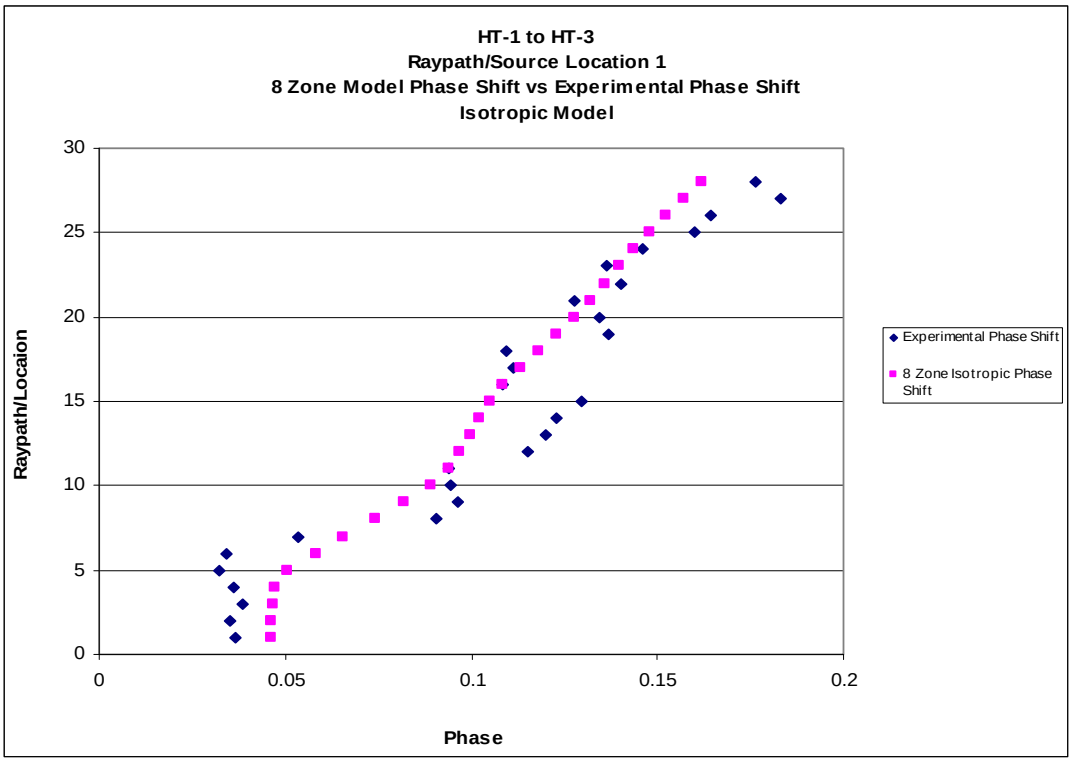

Figure 63. HT-1 to HT-3 experimental phase shift and SVD calculated phase shift under isotropic conditions.

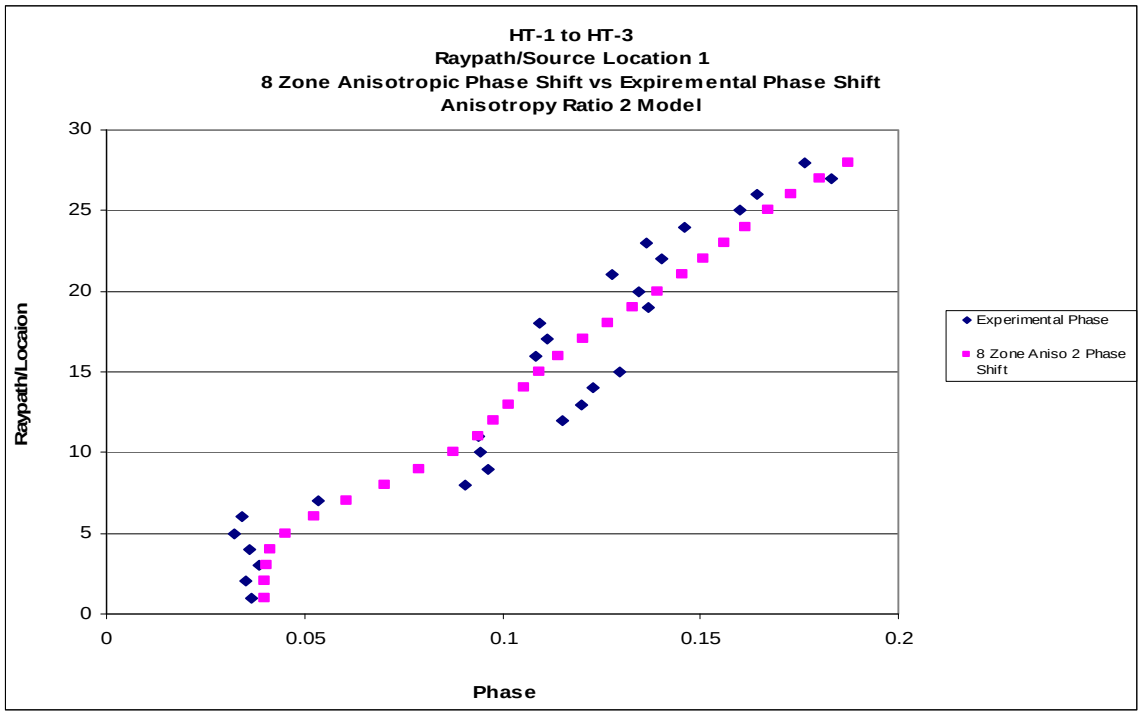

Figure 64. HT-1 to HT-3 experimental phase shift and SVD calculated phase shift with an anisotropic ratio 2.

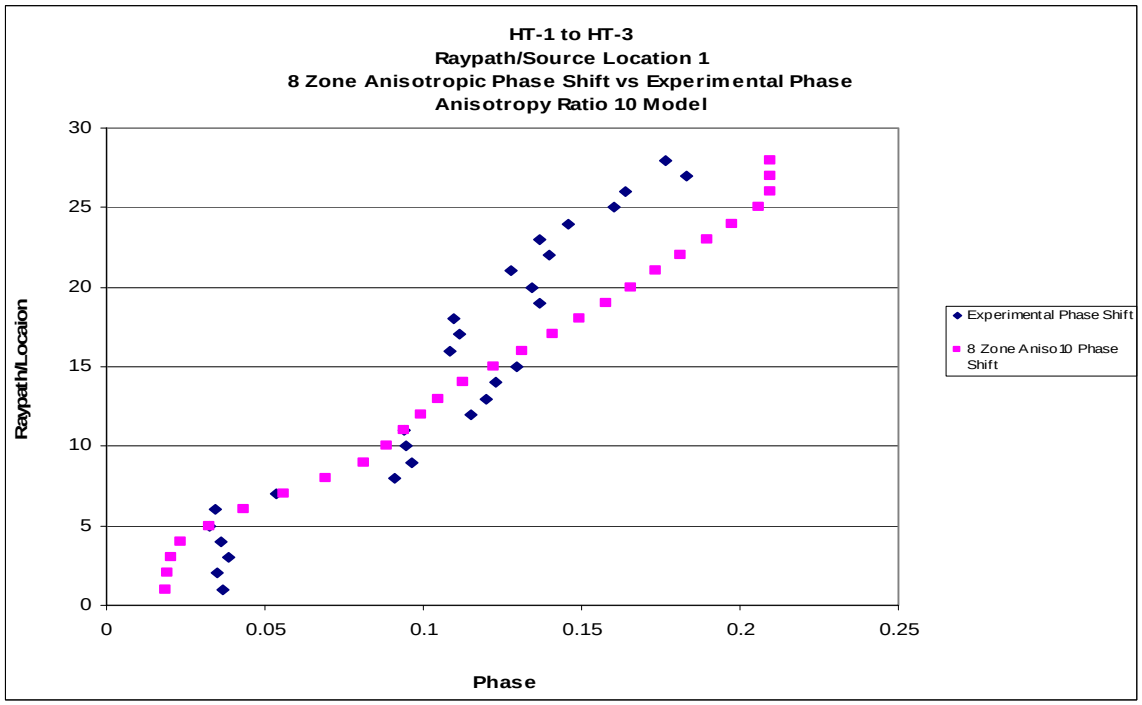

Figure 65. HT-1 to HT-3 experimental phase shift and SVD calculated phase shift with an anisotropic ratio 10.

Conversely, modeling for the 3-sec pneumatic data from HT-GP to HT-2 using an anisotropic ratio of 2 did not result in the best data fit. Large chi squared and standard deviation values resulted from the inversion of this anisotropic scenario (Fig. 66). In addition, some of the fitted K values were out of the expected range, suggesting some constraint may be needed. Inverse problems are sometimes constrained by other sources of data or by mathematical methods if the results prove to be unrealistic. In some of the earlier tomographic research on this project, Wachter (2008) found that some of the calculated K values were an order of magnitude higher than the rest of the data set and a weighting factor within LeastSquaresSVD program was used to constrain the inversion closer to site-specific HRST K values. Up to this point in the data processing, all the ZOP and anisotropy model inversions were completed with a constraint factor (CLS) of 0, which is unconstrained. Increasing constraint values gives more weight to input K values and therefore restrict deviations of the inversion results from the input model K values.

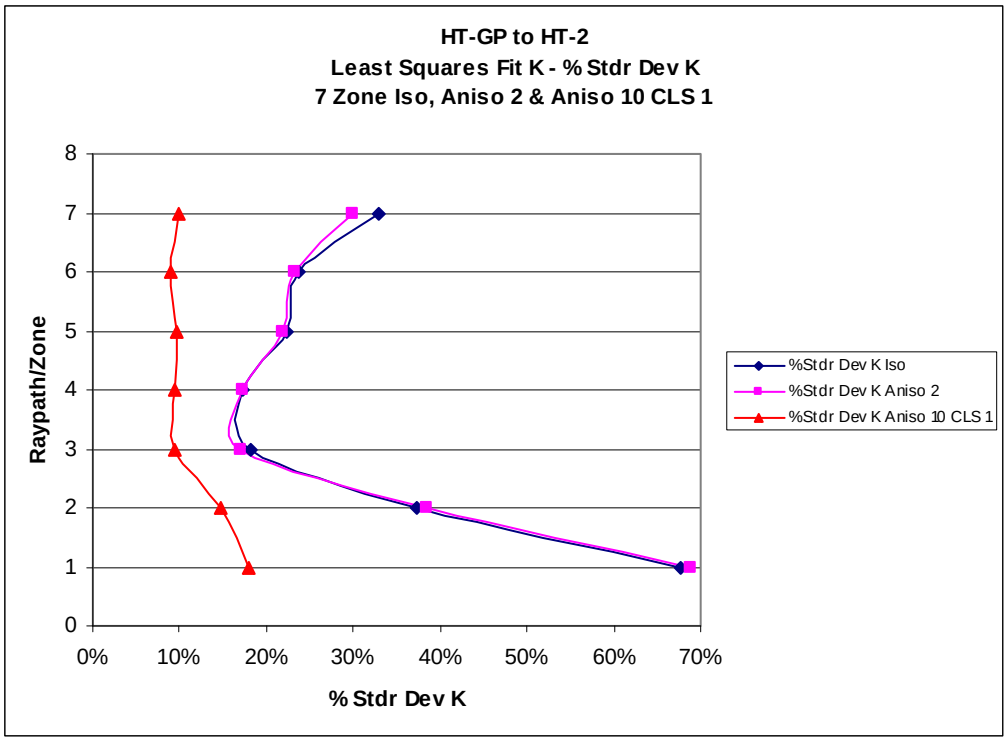

Figure 66. HT-GP to HT-2 least squares fit K under isotropic, anisotropic-2, and anisotropic-10 CLS 1 conditions.

The 3-sec data from the pneumatic HT-GP to HT-2 well pair were remodeled with isotropic, anisotropic 2, and anisotropic 10 models to determine a better aquifer model and inversion for the pneumatic data. A constraint factor of 1 on the anisotropic 10 model was chosen for SVD analysis, which still lends equal weight to both the input K of the model and the inverted results to help avoid an artificial data fit to the model. The data fit was much improved; the constraint factor of 1 kept the K values in the expected range.

Interestingly, the larger anisotropy ratio improved the overall data fit of the offset diagonal rays in the MOG pneumatic data. Initial inversion of the anisotropic 2 model resulted in a relatively good fit between the experimental phase shift data and the model

generated phase shift for many of the MOGs at HT-GP to HT-2, although the fit of the offset rays increasingly deteriorated with distance (Fig. 67). This was somewhat expected for the short period data sets since higher frequencies are more strongly attenuated. Attenuation of the signal is inversely proportional to K of the medium and the period, so the factor of 10 difference between the two CPT the periods and low K alluvium in the upper portion of the test interval will exacerbate the attenuation. It was unknown if the attenuation with distance through low K material would negate the greater resolution gained by the short period CPT source, but data analysis of MOG phase data at HT-GP to HT-2 suggests that a greater anisotropy ratio seems to help fit the low K data points (i.e., high phase) of the long offset rays. The calculated anisotropic 10 phase from the longest rays or uppermost receivers more closely fits the experimental data set than the calculated anisotropic 2 phase (Fig. 68 vs Fig. 67). The 30-sec period data sets were relatively insensitive to different anisotropy ratios greater than 2, so this suggests that the 3-sec CPT period data are more sensitive to aquifer anisotropy than the 30-sec CPT period data in spite of signal attenuation associated with increasing radial distance, decreasing K, and decreasing period.

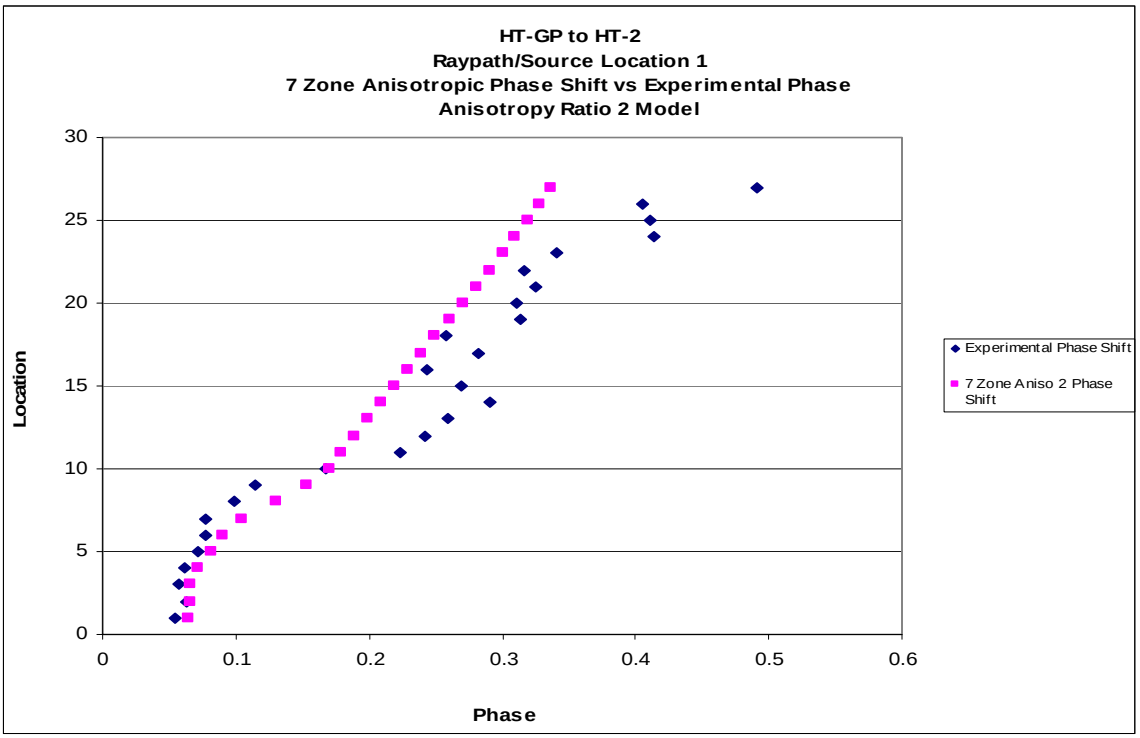

Figure 67. Experimental field phase shift and phase shift calculated using unconstrained SVD for the first MOG from HT-GP to HT-2.

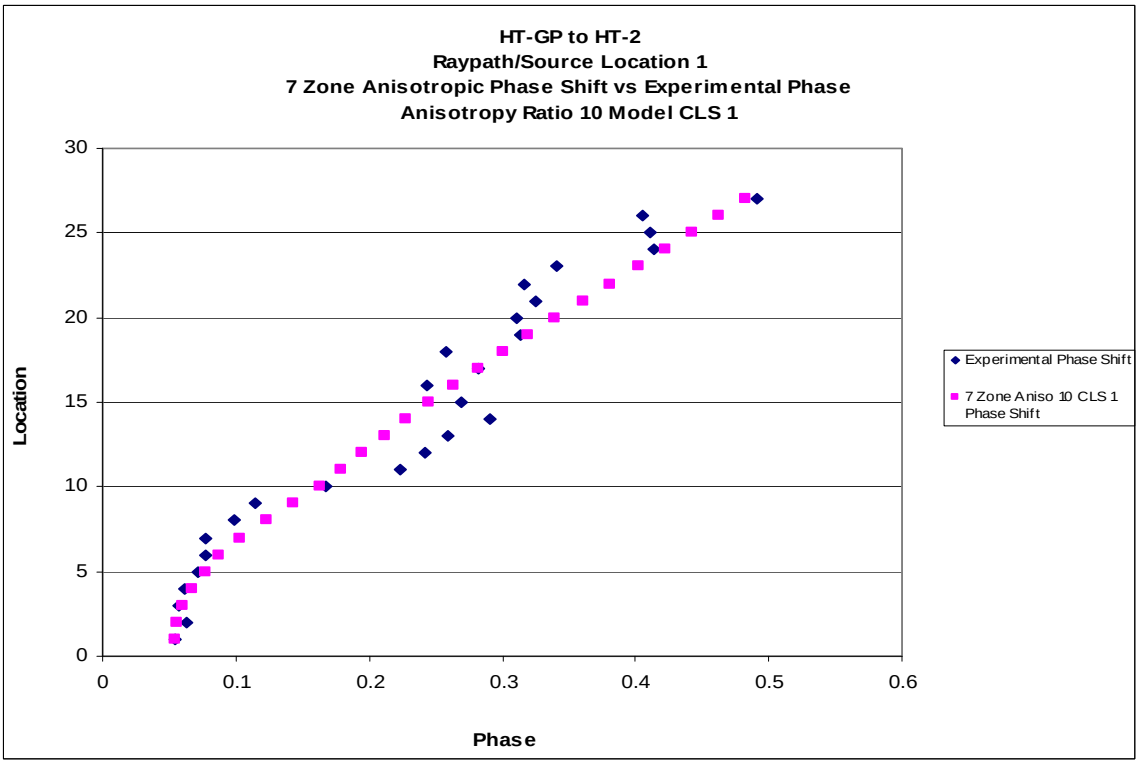

Figure 68. Experimental field phase shift and phase shift calculated using constrained SVD for the first MOG from HT-GP to HT-2.

Most of the zones from the constrained SVD analysis of the anisotropic 10 model at HT-GP to HT-2 had an approximately 10% standard deviation value, although two zones in the basal, higher K portion of the aquifer were somewhat higher, but still remained less than 20% (Fig. 66). Based on the statistical evaluation of the SVD inversion, an anisotropic ratio of 10 and constrained least squares factor of 1 was chosen to evaluate all the MOG data sets with a 3-sec oscillation period (i.e., pneumatic source) for lateral heterogeneity. Lateral heterogeneity modeling and inversion constraint are further discussed in the subsequent section.

MOG Modeling with Lateral Heterogeneity

Finally, the effect of lateral heterogeneity was evaluated with a 24 zone model (Fig. 69). Each of the horizontal zones that correspond to the interpreted hydrostratigraphic layers of the GEMS aquifer (Fig. 56) was subdivided to include three lateral zones. The HT-6 to HT-3 example model has 24 zones, 30 elements, and 48 nodes over the approximate 232.0 to 240.2 m msl (761 to 788 ft msl) well screen interval. The nodes at the source well (e.g., node 1 and 4) and the midpoint between the well pair (e.g., node 2 and 5) and receiver well (node 3 and 6) define the lateral zones. Instead of holding K constant across a single horizontal zone, the K value for each layer was allowed to vary laterally at these nodal points. HydraulicTomAnalV21Aniso linearly interpolates between the nodes to simulate the effects of lateral heterogeneity across the model (Fig. 69). As determined by the MOG anisotropy evaluation, phase data were simulated through the aquifer with an anisotropy ratio of 2 for the 30-sec data and an anisotropy ratio of 10 for the 3-sec data.

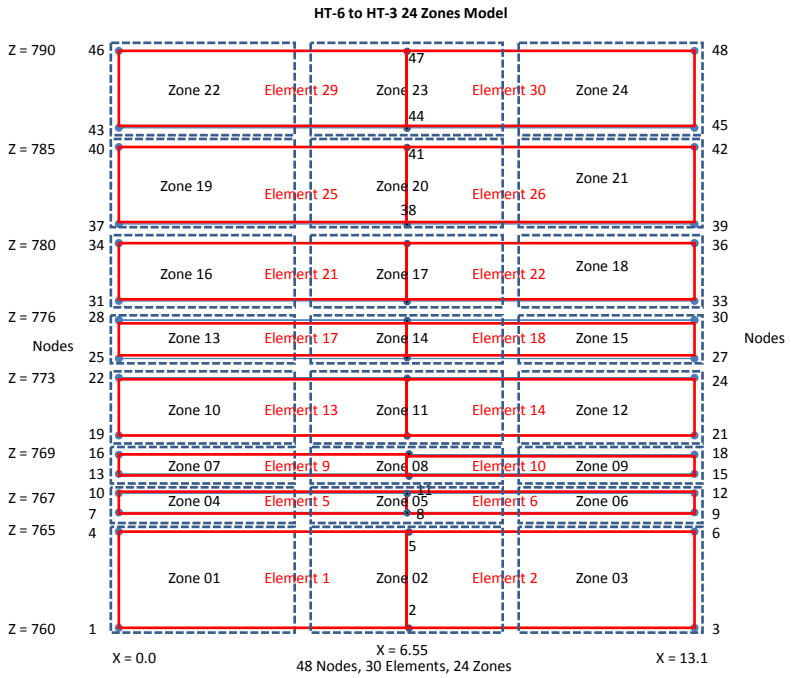

Figure 69. Conceptual 24 zone model grid for determining lateral heterogeneity.

The inversion and least squares fit to the lateral heterogeneity model for the 30-sec and 3-sec period CPT data was evaluated under different constraints. As discussed in the previous section, MOG ray path estimation was generated through the lateral heterogeneity model for the 30 and 3-sec data sets with anisotropy ratios of 2 and 10, respectively. The lateral subdivision of the reduced zone model adds more variables to the SVD inversion, possibly increasing the generation of non-unique results or uncertainty within the data fit. SVD constraint factor experiments for the 30 and 3-sec CPT data sets were performed.

Chi squared and standard deviation values for the calculated K from the 30-sec data indicate that a constraint factor of 1 is generally acceptable for the inversion of the pumped hydraulic CPT data (Fig. 44 and Fig. 45). Most of the standard deviation values are approximately 10%. However, the fit is less good in the basal, high K portions of the

aquifer although the percent standard deviation does remain below 20%. The calculated K values from the 30-sec MOGs are still within the range typically encountered at GEMS, so a constraint factor of 1 was chosen to evaluate lateral heterogeneity for the 30-sec CPT data.

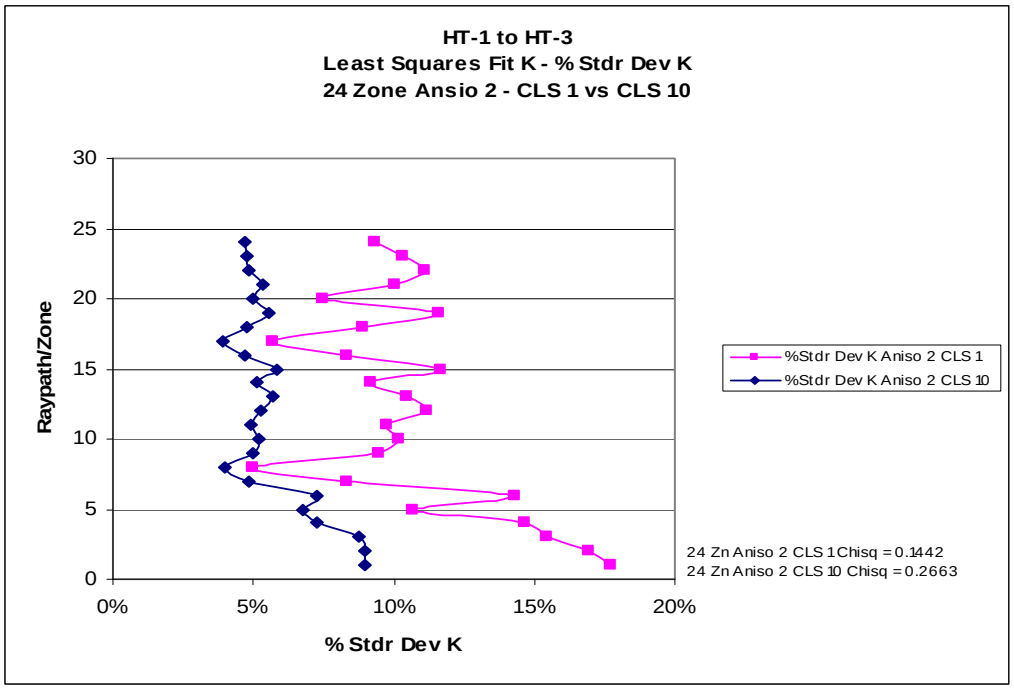

Figure 70. HT-1 to HT-3 least squares fit K under anisotropy-2 CLS 1 (Ave 10.73 %) and anisotropy-2 CLS 10 (Ave 5.72%) conditions.

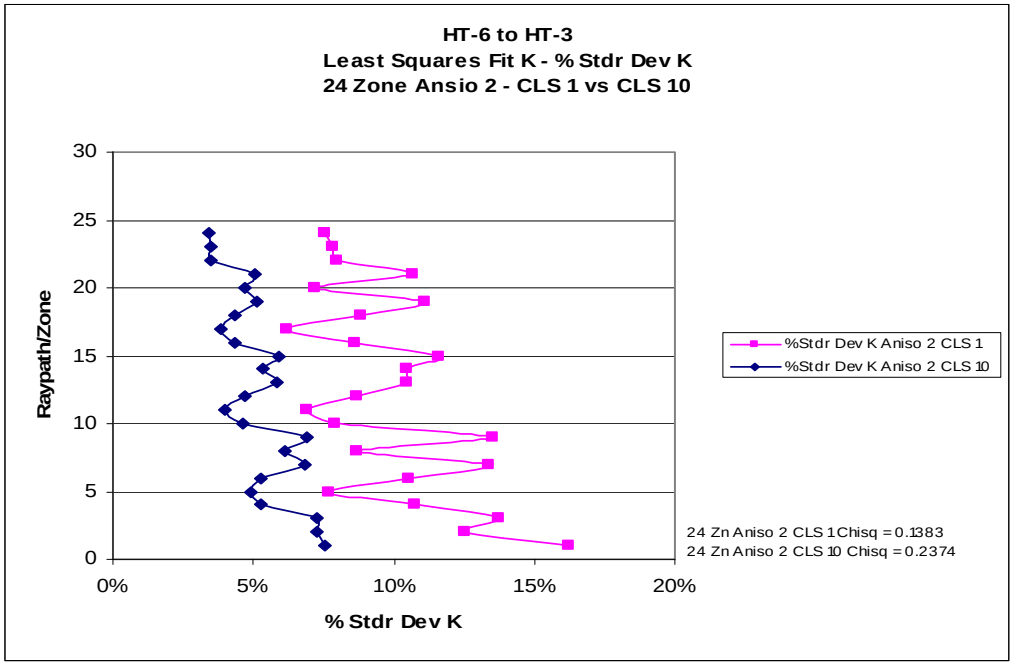

Figure 71. HT-6 to HT-3 least squares fit K under anisotropy-2 CLS 1 (Ave 9.95%) and anisotropy-2 CLS 10 (Ave 5.23%) conditions.

Initially, a constraint factor of 1 was used for the 3-sec CPT data inversion. However, once the HT-GP to HT-2 data were processed, the chi squared and percent standard deviation values of the calculated K from the SVD analysis increased markedly (33.6 % vs the approximate 10% average of the hydraulic data), and indicated that the pneumatic data were responding differently to the inversion and fit to the lateral heterogeneity model (Fig. 2). An additional SVD inversion with a constraint factor of 10 was completed to evaluate the pneumatic data at HT-GP to HT-2. Some error was removed with the additional constraint and the average percent standard deviation was reduced to about 12%, although a plot of the percent standard deviation has little variability, so the data fit appears somewhat artificially constrained. The calculated K values with a least squares constraint of 1 are still within the expected range of reported

K values at GEMS so this constraint factor was still assumed for this CPT well pair. Again, generally, the fit is less good in the basal portion of the aquifer.

In contrast to the other hydraulic and pneumatic CPT well pairs, the remaining pneumatic location, HT-GP to HT-3, required a constraint factor of 10 to generate K values within the expected range at GEMS (Fig. 73). Although a constraint factor of 1 still resulted in a slightly better data fit than the other pneumatic well pair, (29.2% vs 33.6% average standard deviation) the K values deviated from the expected range and, in particular, one K value from Zone 19 (0.0624 ft/sec) was an order of magnitude greater than the rest of the data set with a percent standard deviation error of 243% (Fig. 73). A constraint factor of 10 resulted in reasonable K values and percent standard deviation (16.9%); therefore, it was used for lateral heterogeneity evaluation at HT-GP to HT-3.

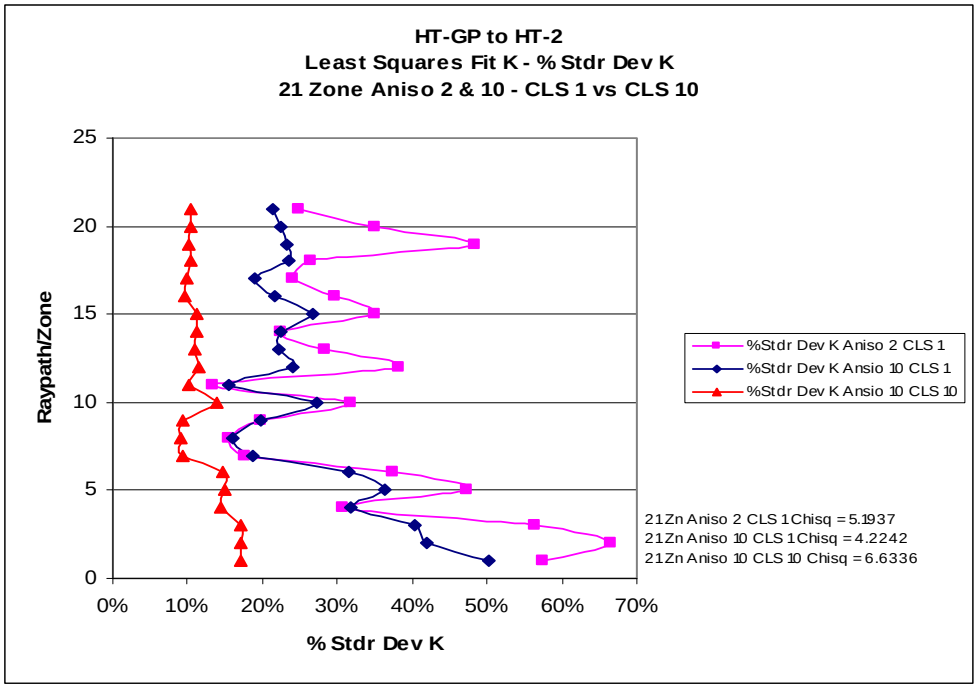

Figure 72. HT-GP to HT-2 least squares fit K under anisotropic-2 CLS 1 (Ave 33.6%), anisotropic-10 CLS 1 (Ave 26.5%), anisotropic-10 CLS 10 (Ave 12.1%) conditions.

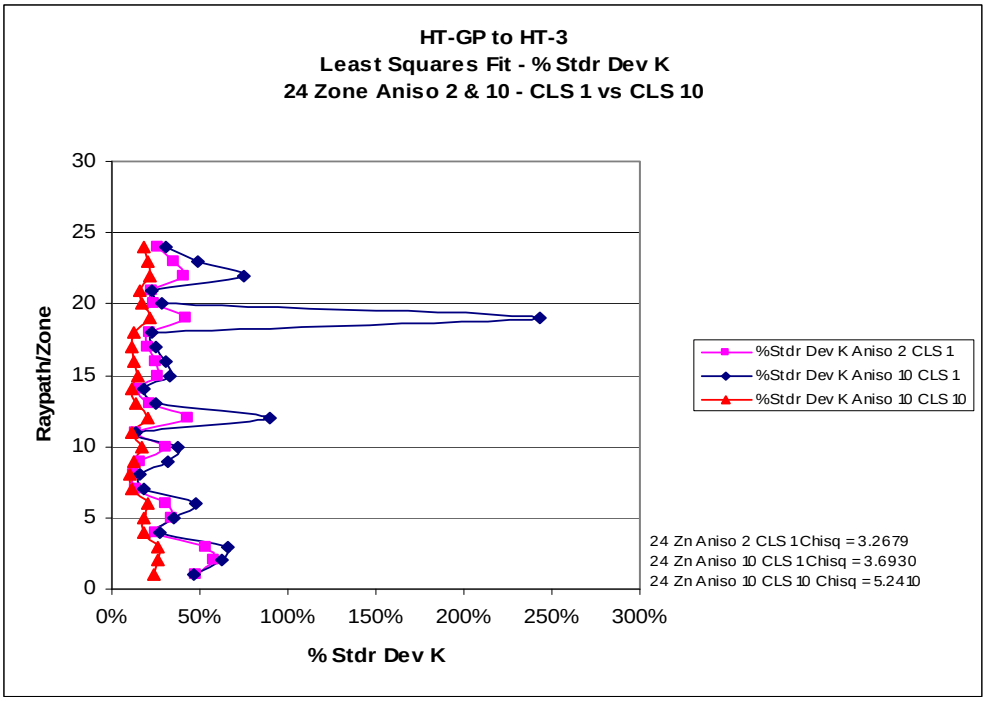

Figure 73. HT-GP to HT-3 least squares fit K under anisotropic-2 CLS 1 (Ave 45.5%), anisotropic-10 CLS 1 (Ave 29.2%), anisotropic-10 CLS 10 (Ave 16.9%) conditions.

Hydraulic Conductivity Distributions – Pumped Hydraulic CPT Source

After the data processing outlined above was completed for all well pairs, contour plots were made of K values plotted against elevation and the radial distance between a well pair using the graphing program, QuickGrid. The program contours between points written in an x,y,z format, which corresponds to the radius, elevation, and constrained K value determined from SVD analysis. Five pumped hydraulic CPT well pairs were plotted with the receiver well on the left (HT-3) and the source wells on the right (HT-1, HT-2, HT-4, HT-5 and HT-6). The K values from this radial array were obtained with the pumped hydraulic CPT source which had a 30-sec oscillating period. A best case anisotropic ratio and inversion constraint factor for the lateral model grid and SVD

inversion, respectively, were chosen based on the evaluation of different anisotropic scenarios of the reduced zone MOG model at HT-3 to HT-6 and HT-3 to HT-1, as well as, the expected range of K values at GEMS (0.0003 to 0.003 m/sec [0.001 to 0.01 ft/sec]). In particular, the well pair at HT-3 to HT-6 was thought to have the best overall data quality and was used as a benchmark reference for the other data sets. K evaluation by individual well pair is further discussed below. Tables of K values are available in Lyle (2011).

The K values for the CPT well pair HT-3 to HT-6 are presented in Fig. 74 and are within the range expected at GEMS (0.0003 to 0.0018 m/sec [0.0010 to 0.0058 ft/sec]). The contour trend follows the expected results for the GEMS lithology and HRST results, with high K values in the coarser, basal portion of the aquifer and low K values in the finer, upper portion of the aquifer. The HT-3 to HT-6 data set did not have any poor quality data and the data fit (9.95% average standard deviation K) was relatively good. Some of the larger percent standard deviation occurred in the high K portions of the test interval.

The K values presented in Figure 75 for the well pair HT-3 to HT-1 (0.0002 to 0.0017 m/sec [0.0008 to 0.0056 ft/sec]) are generally within the range expected at GEMS, although the low range K value is slightly lower than what has been reported in the past for the fine grained portion of the GEMS aquifer. However, the slight deviation is not considered significant and the overall contour trend of the plot still follows the expected GEMS lithology and HRST results. The HT-3 to HT-1 data set did not have any HRST replacement data used and the data fit (10.7% average standard deviation K)

was relatively good. As usual, some of the larger percent standard deviation occurred in the high K portions of the test interval.

The data set presented in Figure 76 from HT-3 to HT-2 has a range of K values (0.0002 to 0.0016 m/sec [0.0005 to 0.0051 ft/sec]) that is generally within the expected range at GEMS and the contour plot depicts the expected K distribution. The well pair did not have any HRST replacement data but the data set was not quite as good as the benchmark well pairs. The amount of error between calculated and observed phases (14.6% average standard deviation K) was greater than the benchmark well pairs at HT-6 to HT-3 and HT-1 to HT-3. Some of the error could likely be removed from the data set with greater constraint during SVD analysis, but because the K trends remain reasonable, additional constraint was deemed unnecessary.

The CPT data presented in Figure 77 from HT-3 to HT-4 include some HRST replacement data in the middle of the test section (see Lyle, 2011 for details). The ranges of K values (0.0002 to 0.0019 m/sec [0.0006 to 0.0061 ft/sec]) are within the expected range and the contour plot depicts a reasonable K distribution, although some of the heterogeneity graduation seen between the lower and upper zones in the benchmark well pairs seems to be suppressed or absent in the zones with replacement data. The K values are still within the range of other K data and the amount of error between calculated and observed phases is relatively good (9.43% average standard deviation), so the plot appears to be a representative depiction of the aquifer heterogeneity expected at GEMS. Comparison of this plot to Wachter's (2008) interpretation of the well pair would tend to confirm this lack of heterogeneity in this portion of the aquifer. The upper and middle zones are largely low K alluvium with the high K alluvium limited to just the basal

portion of the aquifer, although the K values in the basal portion from this research are somewhat lower in magnitude and not as consistently extensive across the section.

The CPT data shown in Figure 78 from HT-3 to HT-5 include replacement HRST data for over half of the upper test interval (see Lyle, 2011 for details), due to pressure transducer failures**.** The ranges of K values (0.0002 to 0.0024 m/sec [0.0005 to 0.0079 ft/sec]) are within the expected range at GEMS. Compared to the other hydraulic CPT well pair with HRST replacement data (HT-4 to HT-3), the data fit is not as good (11.6% vs 9.43% average standard deviation). However, the amount of error between calculated and observed phases at this well pair (11.6% average standard deviation K) is still consistent with HT-1 to HT-3 (10.7% average standard deviation K), which is one of the benchmark well pairs. The greatest standard deviation again appears in the lower high K zone. The heterogeneity trends are consistent with the other well pairs, but a higher K zone in the upper portion of the aquifer near the source well (HT-3) seems somewhat more pronounced and probably reflects the direct measurement of the HRST K point source data used to replace the bad data for the CPT well pair.

The pumped hydraulic CPT data (30-sec period) collected from the radial well area replicate the aquifer interval that Wachter (2008) tested with a pneumatic CPT source (3-4 second period). The summary results of that earlier research were evaluated and compared to the present research to evaluate the difference between the two different CPT source methods. Wachter, to identify the best model to evaluate heterogeneity as well as inversion constraint, used a number of different model configurations, ray paths and different S_s values (1E-05 and 1.5E-05). The phase depends on a ratio between S_s and K, so changes in S_s will also result in changes in K. This introduces a potential

source of error, due to the difficulty of measuring S_s in situ. In this research, an attempt to limit this error was implemented by correcting S_s using the measured phase and HRST or ZOP K. The corrected S_s was used for modeling and inversion. Wachter determined that a S_s value of 1.5E-05 and about 750 rays produced the best results. The corrected S_s values (about 1.1E-05 to 1.69E-05) and MOG rays (756 to 784) used for this research were comparable to Watcher's earlier tomographic work. Wachter's model configurations were slightly different, which used elements instead of nodes for straight ray approximation through the model grid, and his model generally had fewer total zones (e.g., 16 vs 24). The different model configuration for the present research was developed from the use of the relatively unattenuated ZOP data to create a representative aquifer model. It was expected that utilizing a node model grid along with more vertical and lateral zones and initial use of ZOP phase data could improve the resolution of the method.

The range of K values derived by Wachter (2008) with the 4-second CPT period are relatively consistent with the ones in this research and follow the expected trends based on the aquifer lithology and range of reported K values at GEMS. However, in general, there was some difference in heterogeneity resolution between the two CPT sources. Wachter, with the exception of the HT-4 to HT-3 well pair, was able to resolve a somewhat higher K zone (e.g., 0.0015 – 0.0045 m/sec [0.0049 – 0.0148 ft/sec]) in the middle of the aquifer. In contrast, the K values derived with the pumped hydraulic CPT were mostly lower in the intermediate zone (e.g., 0.0006 to 0.001 m/sec [0.0020 to 0.0033 ft/sec]). Although, as an exception, the HT-5 to HT-3 well pair did have somewhat higher K values (e.g., 0.0015 m/sec [0.0049 ft/sec]) through this zone.

This heterogeneity difference through the middle zone could reflect the way the data plots were constrained during contouring or a difference between the periods of the two CPT sources. Wachter's contour plots used SVD-determined K values which were constrained by HRST K data along the source and receiver well locations. The contour plots for this research were not constrained by HRST K. The HT-5 to HT-3 contour (Fig. 58) may reflect this constraint difference. This well pair had a significant portion of the field data replaced with surrogate phase data which are estimated from HRST K, so the SVD analysis there may be replicating some of the HRST K constraint within the 3-4 second CPT period data sets. Also, in consideration of the period differences, results from the numerical modeling of the heterogeneity extension indicate that the 30-second CPT period does not have as much resolution as the 3-4 second CPT period, so some of this heterogeneity loss is possibly due to the different CPT source periods.

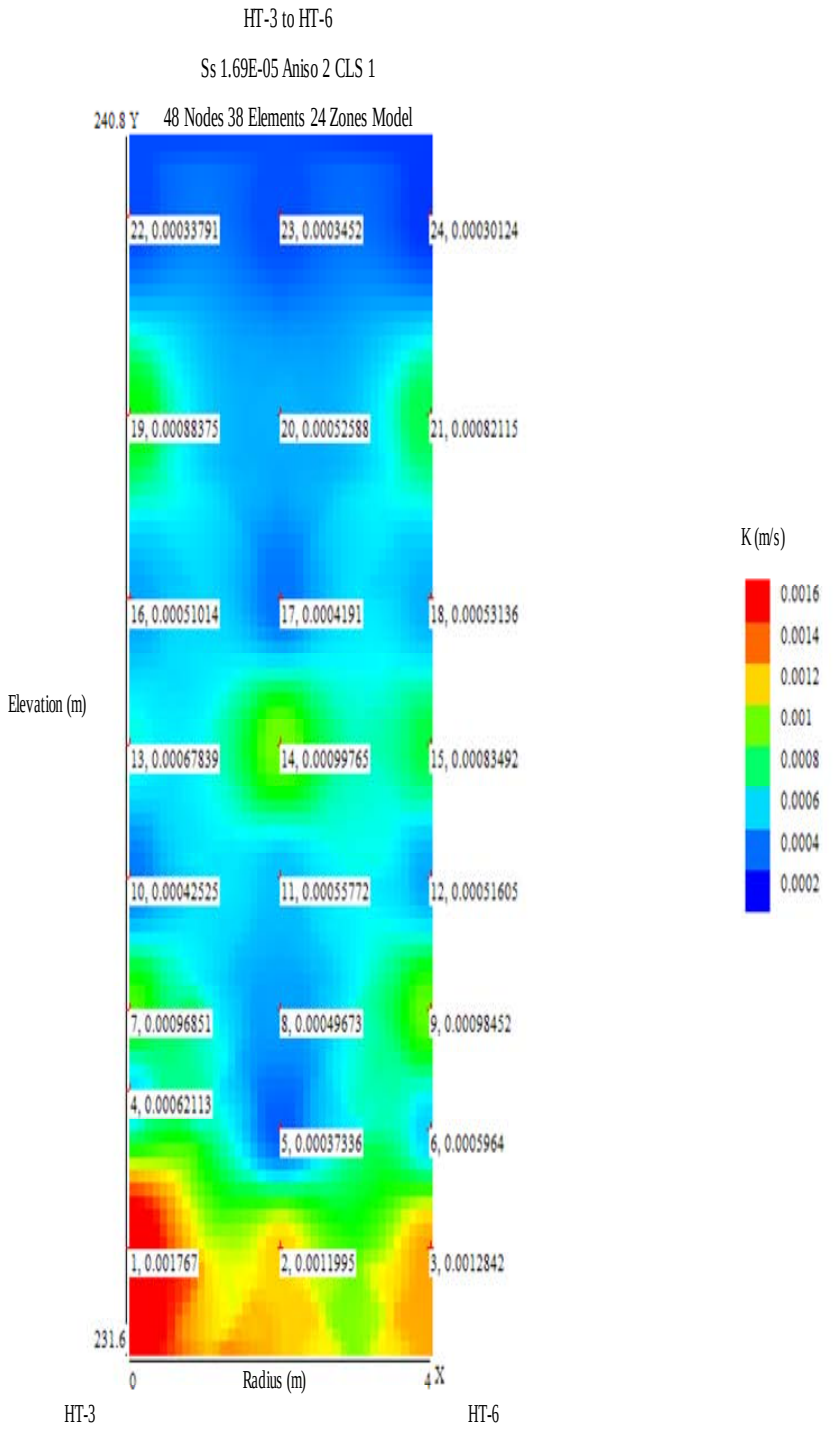

Figure 74. K values from constrained SVD analysis of 784 rays at HT-3 (receiver) to HT-6 (source). K values range from 0.0003 to 0.0018 m/sec (0.0010 to 0.0058 ft/sec).

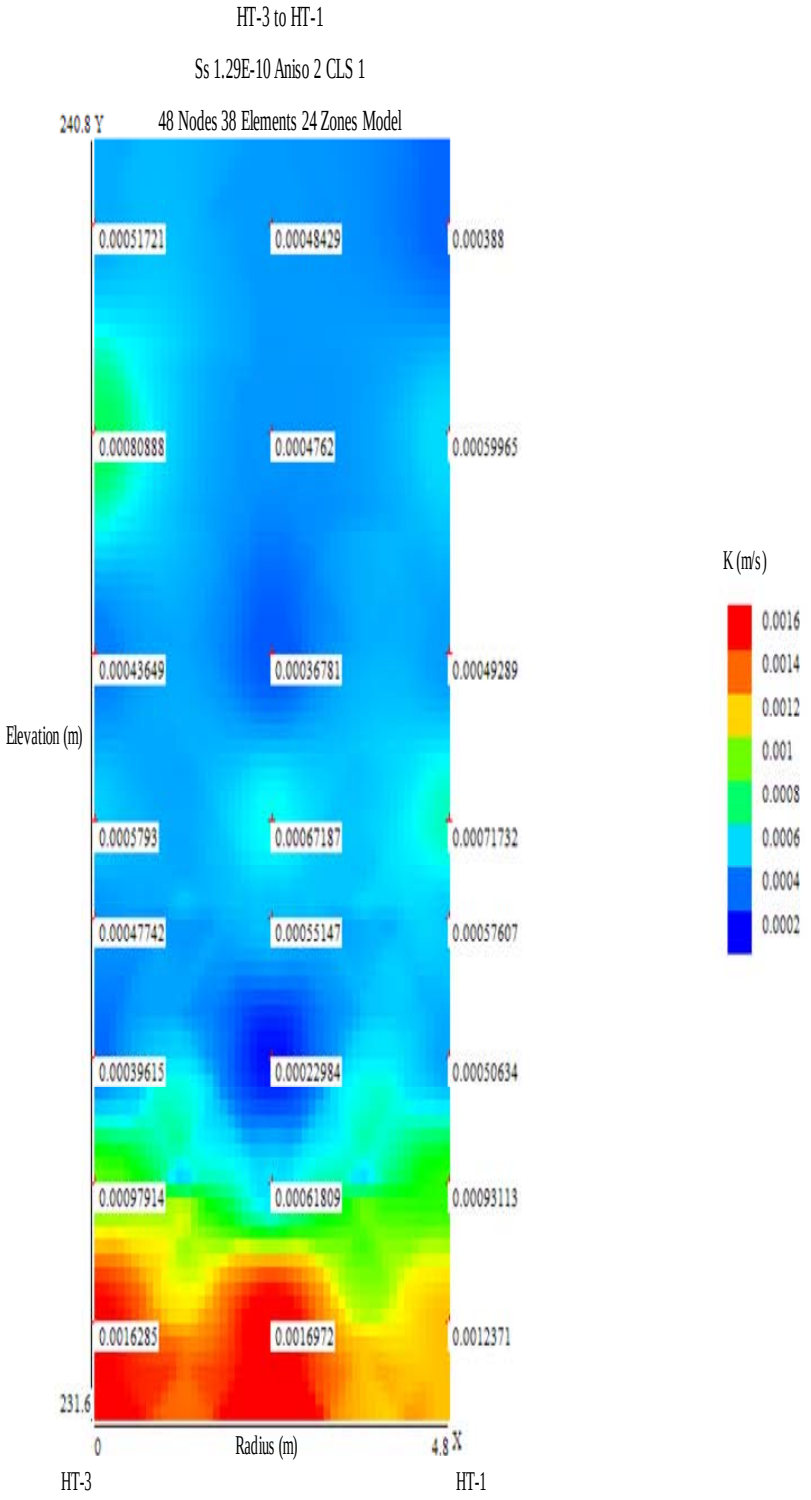

Figure 75. K values from constrained SVD analysis of 756 rays at HT-3 (receiver) to HT-1 (source). K values range from 0.0002 to 0.0016 m/sec (0.0005 to 0.0051 ft/sec).

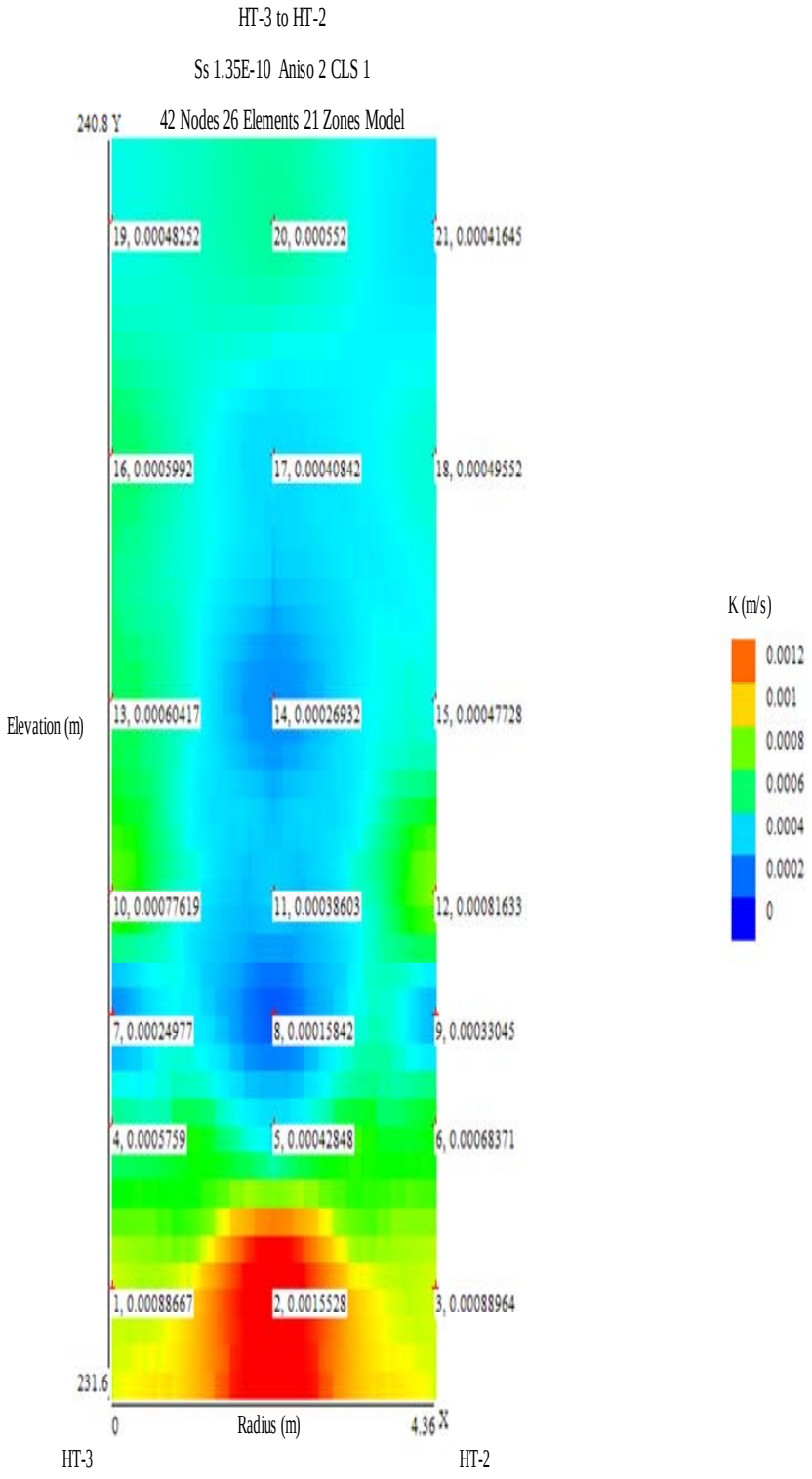

Figure 76. K values from constrained SVD analysis of 756 rays at HT-3 (receiver) to HT-2 (source). K values range from 0.0002 to 0.0016 m/sec (0.0005 to 0.0051 ft/sec).

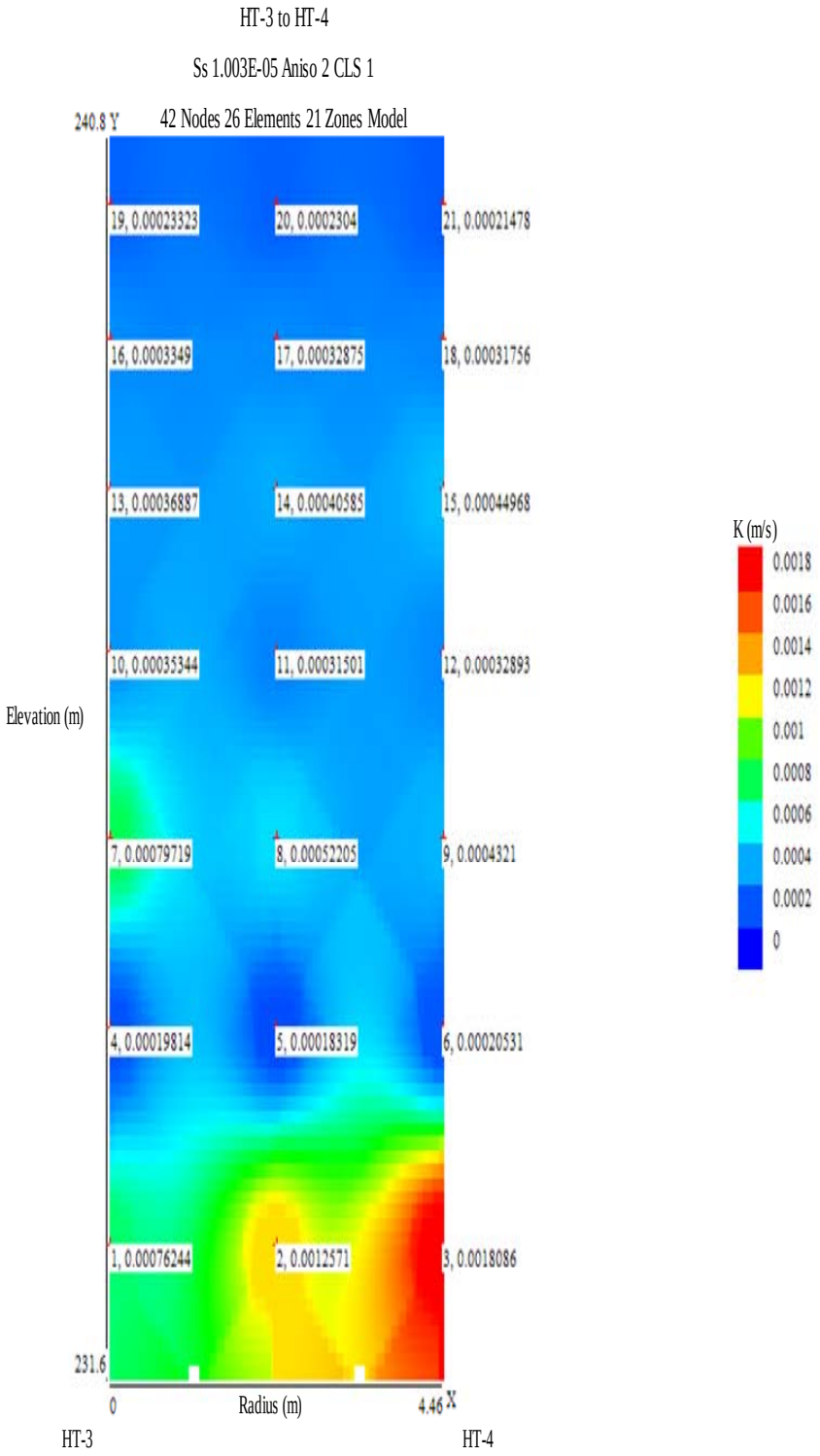

Figure 77. K values from constrained SVD analysis of 784 rays at HT-3 (receiver) to HT-4 (source). K values range from 0.0002 to 0.0019 m/sec (0.0006 to 0.0061 ft/sec).

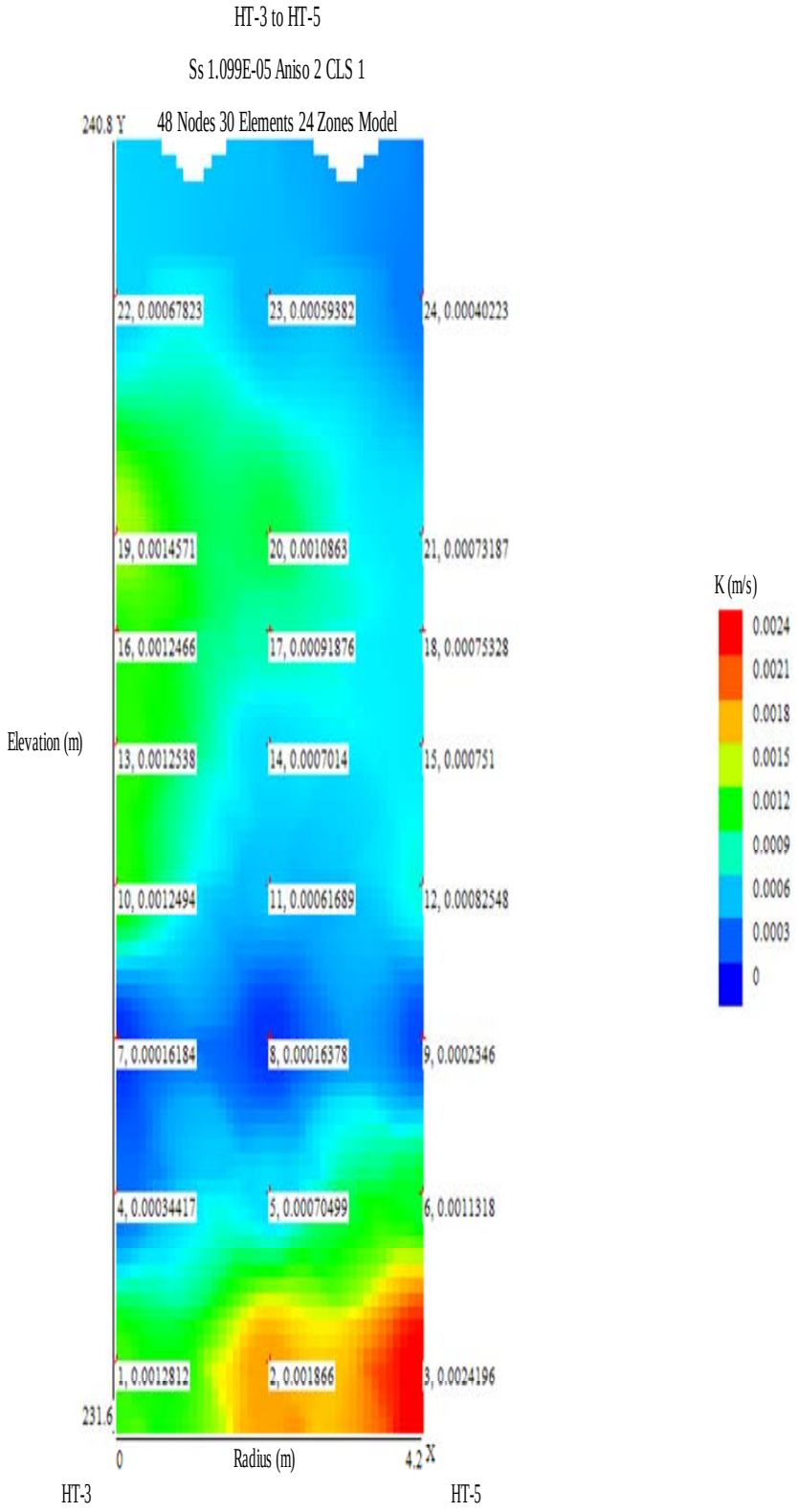

Figure 78. K values from constrained SVD analysis of 784 rays at HT-3 (receiver) to HT-5 (source). K values range from 0.000 to 0.00 m/sec (0.000 to 0.00 ft/sec).

Hydraulic Conductivity Distributions – Pneumatic CPT Geoprobe Source

Contour plots were made of K values plotted against elevation and the radial distance between the Geoprobe source location and two receiver wells using the graphing program, QuickGrid. Two pairs of results for K were plotted with the source location (HT-GP) on the left and receiver wells on the right (i.e., HT-2 or HT-3). The K values from this triangular array were obtained with the pneumatic CPT method at the source and a 3-sec oscillating period. A best case anisotropic ratio and inversion constraint factor for the lateral model grid and SVD inversion, respectively, were chosen based on the anisotropic evaluation of the reduced-zone MOG model and the lateral heterogeneity model at HT-GP to HT-2. Data fit to these models was significantly improved with a constraint factor of 1 (which better fit the replacement data) and, by increasing the anisotropic ratio from 2 to 10 (which better fit the farthest offset rays of the MOG). This improved fit due to the application of a larger anisotropic ratio was not apparent in the 30-sec CPT data sets and suggests that the 3-sec data sets were more sensitive to anisotropy. However, as discussed previously, additional inversion constraint was needed for the HT-GP to HT-3 well pair to suppress a K data point that was an order of magnitude greater than the rest of the K values in the lateral model. These constraints, anisotropy, and the expected range of K values at GEMS (0.0003 to 0.003 m/sec [0.001 to 0.0098 ft/sec]) were used to evaluate the lateral heterogeneity. K evaluation by individual well pair is further discussed and presented below.

The K values presented in Figure 79 from HT-GP to HT-2 involve some replacement data in the middle and upper portion of the test section, replacing some unusable field data (see Lyle, 2011 for details). The ranges of K values (0.0003 to 0.002

m/sec [0.0009 to 0.0067ft/sec]) are within the expected range at GEMS. Different anisotropic ratios and constraint factors were considered for this data set, and larger anisotropic ratios showed some good improvement of the data fit to the reduced zone model, indicating that the low period data are more sensitive to the anisotropy of the aquifer. But when considering the lateral heterogeneity, compared to the pumped hydraulic CPT locations with surrogate data (26.47% vs 11.6% average standard deviation), the fit between the model and measured data is not as good. However, most of the error in the lateral heterogeneity model occurs around the six nodes in the basal high K portion of the aquifer (Fig. 79). Fewer multiple intersecting rays through the basal zones may exacerbate this; diagonal rays are needed for good lateral resolution. If these zones are not considered, the average percent standard deviation is lowered to about 22%, which is improved and more comparable to the error in the other pneumatic data set.

The K values presented in Figure 80 from HT-GP to HT-3 involve some replacement data in the middle and upper portion of the test section, replacing some unusable field data (see Lyle, 2011 for details). The ranges of K values (0.0002 to 0.001 m/sec [0.0006 to 0.0037ft/sec]) are within the expected range at GEMS. Inversion of the experimental phase shift with an anisotropy ratio of 10 produced K values that exceeded the expected range and several orders of magnitude greater than the data set. A larger constraint factor of 10 produced reasonable K values with an average percent standard deviation of about 17%; but, the data fit tends to be more biased towards the initial K estimates than the full experimental data set would suggest. In contrast to the other CPT

data sets, the data fit in the high K portion of the aquifer is comparable to the fit in the rest of the aquifer.

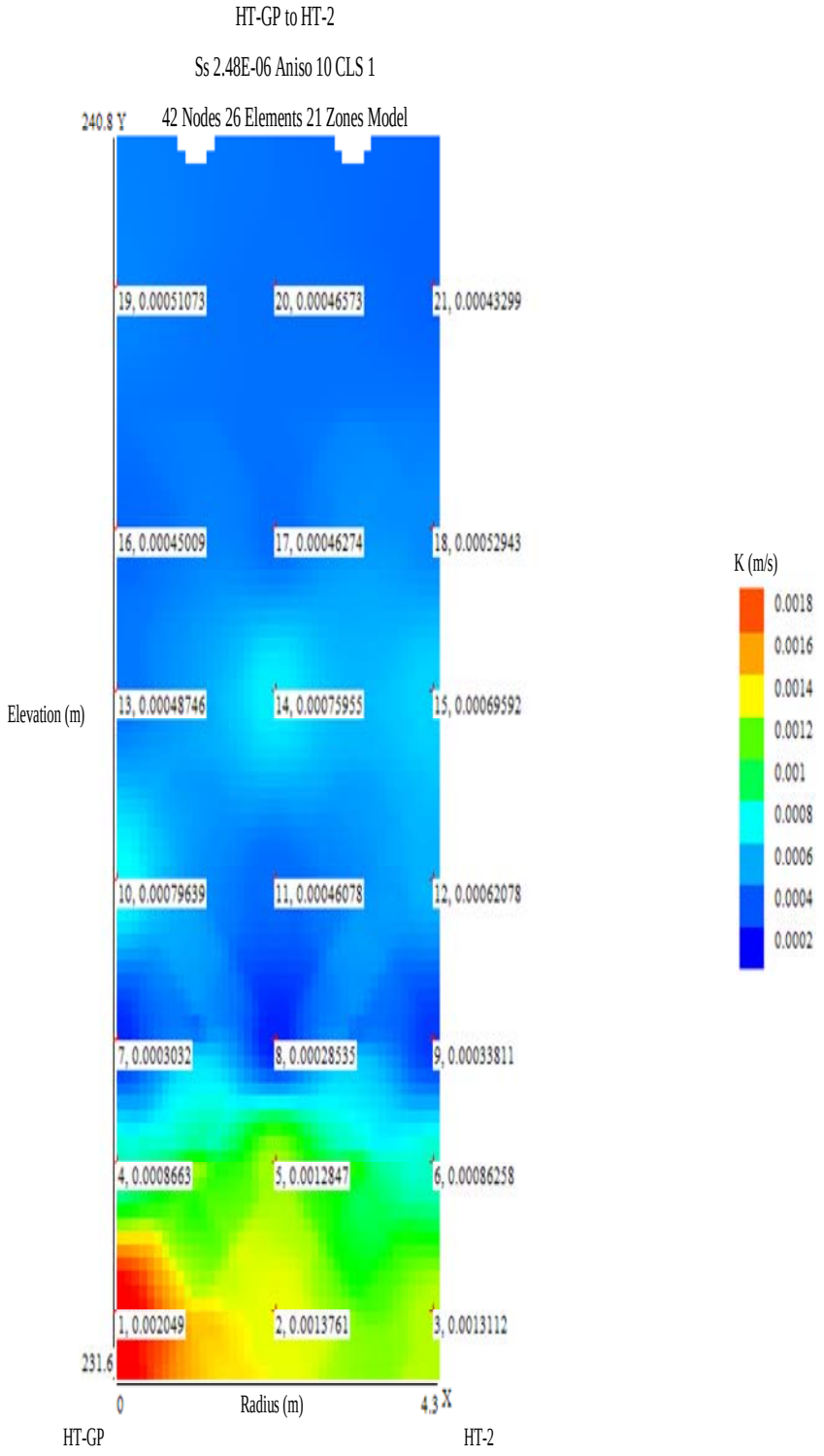

Figure 79. K values from constrained SVD analysis of 729 rays at HT-GP (source) to HT-2 (receiver). K values range from 0.0003 to 0.002 m/sec (0.0009 to 0.0067 ft/sec).

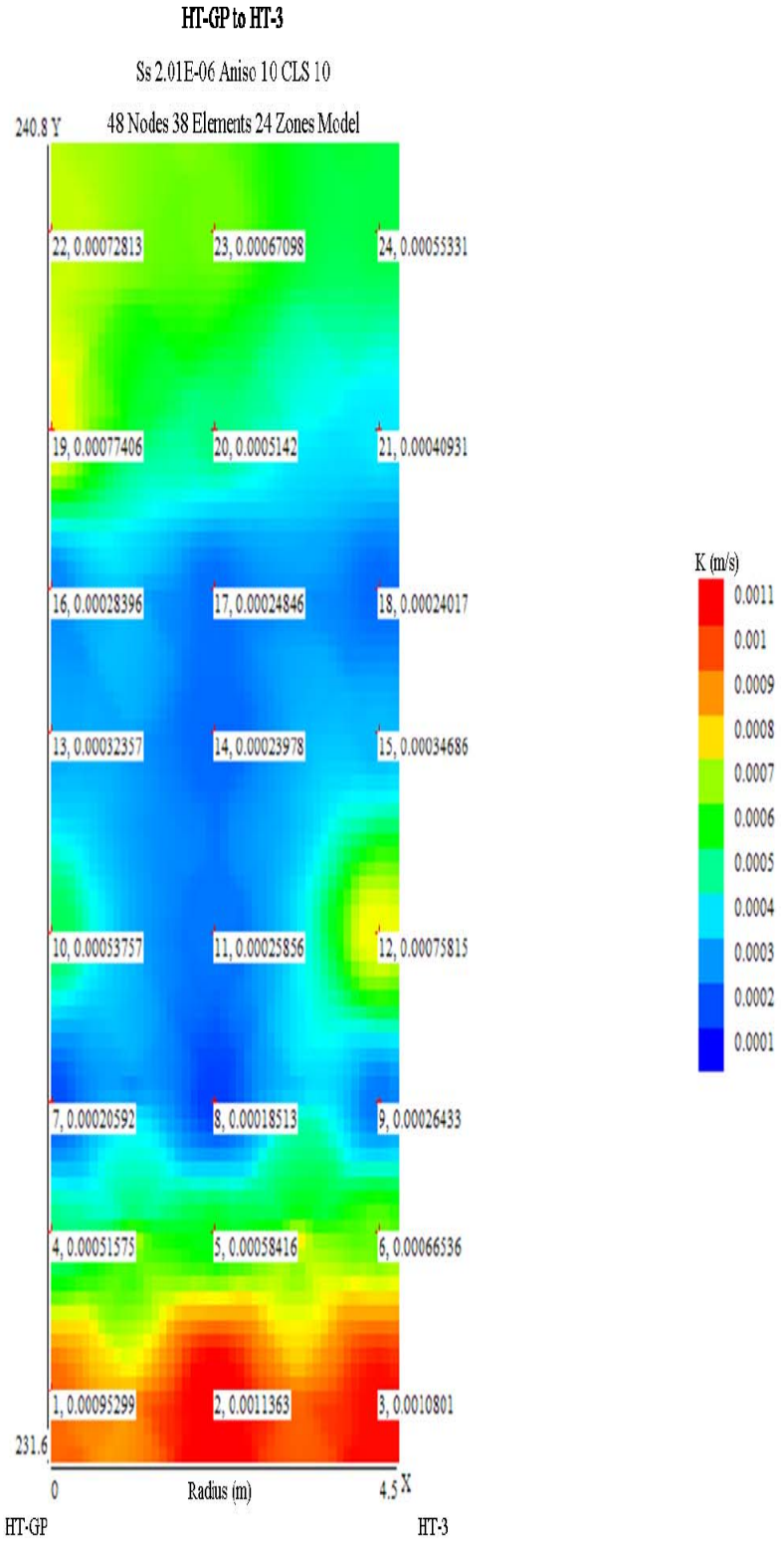

Figure 80. K values from constrained SVD analysis of 784 rays at HT-GP (source) to HT-3 (receiver). K values range from 0.0002 to 0.0011 m/sec (0.0006 to 0.0037 ft/sec).

Summary and Conclusions

Since spatial changes in hydraulic conductivity are a major factor governing the transport and fate of a pollutant as it moves through an aquifer, we have focused on the development of new innovative methods to delineate these spatial changes. The objective of the research presented here was to build on our previous work to develop and improve field techniques for better definition of the three-dimensional spatial distribution of hydraulic conductivity by using hydraulic tomography coupled with high-resolution slug testing. Hydraulic tomography has received a lot of attention in the literature in recent years, but little field work has been done on the small scale presented here using a sinusoidally varying signal The first thing that we did was to lay out the basic theory of groundwater flow that would govern the experiments. The basic theory of tidal influences on inland wells has been known and used for many years. The basic idea is that the amplitude and phase of the received signal depend on the aquifer properties traversed. The same theory is applicable to the research presented here except the geometry and time scales are different. Instead of the ocean providing the signal over a long boundary with a period of about 24 hours, we are dealing with a small diameter well providing a signal over a relatively short wellbore interval and having a period of seconds. We developed some approximate homogeneous solutions with radial geometry and suggested that these solutions could be applied to the heterogeneous case by using a straight ray spatially weighted approximation. The advantage to this approach is that the tomographic inversion can be done without the need for an iterative non-linear regression using a numerical model. The traditional approach to the tomographic inversion is very computational intensive and requires considerable computer resources and time.

In order to process the data a number of new programs had to be written. One of the authors (Carl McElwee) has been programming in Visual Basic for a number of years and this was the programming platform chosen. Using Visual Basic has the additional advantage of being closely interfaced with the Excel spreadsheet program which is widely used and understood. Three new programs were written and improved continually (denoted by version numbers) during the course of this research. The first program was FitAmpPhase, which in the end could input the field data, take off a level trend, filter the data, and finally fit a sine wave to the data giving the amplitude and phase of the signal at the receiver. The basic theory states that the amplitude and phase of the received signal depends on the diffusivity of the material through which the signal passed. The diffusivity is the ratio of hydraulic conductivity to specific storage. After determining the amplitude and phase it was necessary to extract the diffusivity by an inversion process. The first step in the inversion process was to create a program which would implement the straight ray spatially weighted approximation. This program would calculate the ray path lengths in each zone of differing K and calculate the theoretical phase resulting from that path. The output of this program (HydraulicTomAnal) would be a set of matrix equations, with a matrix of path lengths multiplying a vector of diffusivities resulting in the theoretical phase. An option for the HydraulicTomAnal program is to specify the anisotropy ratio for each layer The next step in the inversion process was to develop a program that would use the matrix of ray path lengths and either theoretical phase or experimental phase to calculate the diffusivities in each zone. That inverse program (LeastSquaresSVD) used singular value decomposition to perform a least squares fit and estimate zonal diffusivities. We usually assumed a value of specific

storage and then calculated hydraulic conductivity from the diffusivity. The inverse program could perform inverses for a single data set or it could add random error and perform inverses for a large suite of data sets to generate a Monte Carlo analysis. Another option for the inverse program was to perform a constrained inverse, where the initial input estimates of K were given some additional weight.

Since analytical solutions do not exist for the heterogeneous case, numerical modeling was performed to check the spatially weighted straight ray approximation. Synthetic data were generated with a numerical Finite Difference model and modeling studies were performed to demonstrate that data could be inverted with reasonable amounts of error. Zones could be resolved using the LeastSquaresSVD program to dimensions of about 1 m (3 ft). Comparison of the 4 and 30-sec CPT modeling studies indicate that the 30-sec period CPT does have more inherent error than the 3-sec CPT, but error associated with the inversion of field data is comparable between the two sources. Theoretically, it is expected that the 4-sec data would be better than the 30-sec data due to averaging over volumes comparable to the wavelength. The modeling estimate is that the 30-sec CPT has about 27-29% total error and the 4-sec CPT has about 16-19% total error associated with the straight ray method, ambient noise, and the inversion of field data.

It is well known in the inverse literature that the stability and uniqueness can be affected by the model structure, experimental design, and data quality. In our case this means that the number and placement of the zones of constant K, the number and distribution of ray paths in our data sets, and the ambient noise can have a dramatic effect on the K results produced by the inverse program. We have performed a number of

experimental designs to arrive at model structures that can produce a reasonable degree of resolution in the presence of expected levels of noise. In the end, we believe that the 3-30 sec period sinusoidal tomographic method applied to situations like the GEMS site is capable of resolving zones of K on the order of 1 m (3ft) square in regions having adequate ray path coverage.

The application of the theory to the field was an evolving process; as the source and receiver equipment was refined, the field procedures needed to be reassessed. The HRST procedures and equipment used by other researchers at the GEMS location guided the transition to sinusoidal CPT and made it relatively easier. Many of the equipment items used in CPT were initially borrowed or adapted from previously existing HRST equipment. To make this type of testing readily available to future researchers, the majority of the equipment was put together from "off the shelf" sources. After an experiment was conducted, the equipment could be revamped to suit the particular stratagem of future experiments. It was important to us to design equipment that could be used in standard 2 inch monitoring wells, so compact design was important. The single source location was isolated by a straddle packer inflated with nitrogen. Receiver location varied from one to five for a given record, depending on whether we were doing a ZOP or MOG well survey. In any case, each receiver location was also isolated by straddle packers. Early research results showed the importance of packing off the measurement interval to obtain the best quality data. In the course of this research several designs for multilevel receivers and types of pressure transducers were evaluated, with several resulting failures. In the end, we developed two multilevel receivers each containing five pressure transducers that yielded good data. The source and receiver

locations were established in absolute elevation by the use of steel tapes attached to the riser pipes measuring the distance below top of casing, and then surveying in all the well tops with respect to a benchmark at the site. Two mechanisms were used to obtain oscillatory source inputs. The first used air pressure from a compressor to depress and oscillate the water column in the source well. It was necessary to stay close to the natural frequency of the well to obtain a good sinusoidal signal, so a period in the 3-4 sec range was used. The second source used mechanical pumping with a computer controlled servo-valve to inject water into the aquifer to create a sinusoidal pressure signal. We were limited by available equipment to a 30 sec period for this source. Additionally, an in-situ pneumatic source with a computer controlled 3-sec period was developed and deployed by a Geoprobe rig to evaluate the feasibility of tomographic application by direct-push technology. The two multi-level receivers were used in separate wells so data acquisition was very efficient while using the Geoprobe source.

Six new wells were installed at GEMS for this project. The wells were installed with direct push technology (Geoprobe), which causes less aquifer disturbance than many other methods. Electrical conductance profiles (ECPs) were obtained at the first three well locations and we were able to discern the boundaries between the Tonganoxie Sandstone member, the unconsolidated sands and gravels, and the confining silts and clays. The locations were chosen to give an area of study with some lateral extent. Basically there is a center well and five surrounding wells allowing for five cross sections connecting the center well and surrounding ones. The 22 m (70 ft) deep wells were fitted with .05 m (2 in) PVC casing and with 11 m (35 ft) of screen at the bottom. These wells were extensively developed to prepare them for data collection. Three of the existing

wells at GEMS were also used for early ZOP work. High resolution slug testing (HRST) was performed on each of the wells used in this research at .30 m (1 foot) intervals. The HRST vertical profiles of K values at each well were invaluable for delineating high and low K zones and constraining the tomographic inverses.

Early data collection on the wells consisted of ZOP surveys looking only at horizontal ray paths; but later work consisted of MOG surveys with many diagonal ray paths. In the beginning two types of source geometries were used: the whole well line source (entire open screen water column oscillated) and the isolated point source (oscillation was only in contact with a small packed off interval of the screen). The line source introduces a greater amount of energy, and therefore has a greater propagation distance than the point source. On the other hand, the point source geometry allows for a better vertical resolution of the aquifer characteristics. For the ZOP work seven pneumatic line source CPT profiles and six point source CPT profiles were completed at GEMS. MOG surveys were completed between all five well pairs each involving the center well, both using pneumatic 3 to 4-sec data and mechanical pumping 30-sec data. In addition, we adapted the pneumatic 3-sec source method to be used with a Geoprobe unit. We collected MOG data in two receiver wells simultaneously while the Geoprobe unit pulled the source up in one foot increments from the bottom of the aquifer. The range of radial distances between tested well pairs was 1.5 to 11.5 m.

The horizontal ray (ZOP) data that were collected show that the CPT K profiles mimic the general trends in the HRST K profiles measured at the respective wells. Overall, the CPT data appear to average the K profiles of the well pair in question. However, there are important differences. The heterogeneities of the aquifer between the

well pair are probably the cause of this difference, and the difference can not be fully explained without collecting diagonal ray path data, using more advanced models, and using tomographic methods. We made an elementary attempt at calculating "anomalous K values" between well pairs. According to simple theory, the CPT data should be an average of the HRST measurements and should fall somewhere within the HRST limits. If not, then the differences may represent heterogeneities between the well pair. Both the line source data and the point source data appear to distinguish variations in K that are not present in the HRST data. However, the point source data appear to have the best resolution of the data presented here. The line source method is very difficult to interpret and was not used in later experiments. Experiments indicate that the data are reproducible at different times and with the source and receiver wells reversed, within experimental accuracy. Initially, both amplitude and phase data were used to estimate CPT K values; however, amplitude data are less reliable than the phase data because of the exacting experimental measurements that are necessary. Therefore, relative amplitude data were only used as a diagnostic tool and not used for determining K in later work. The ZOP CPT method can not estimate lateral heterogeneity, but it can be of practical use for discerning changing horizontal flow units.

Five well pairs were analyzed using pneumatic CPT MOG data with a period of 3 to 4-sec. The MOG data sets allowed the full use of tomographic methods to determine the K distribution. All had reasonable interwell K distributions after using a constrained inversion, as compared to the general range seen with HRST. K values at the site are known from HRST to range from about 0.000305 m/s to 0.00305 m/s, and follow the general trend of a higher K zone at the base of the aquifer, a low K zone above, a

moderately high K zone still higher up in the profile, and a low K zone at the top. The success or failure of the inversion was evaluated by comparing the resulting K values to the range of K values seen from HRST as well as the general trends of high or low K zones seen from HRST. The success of the inversion seems to be correlated with the number of ray paths between the source and receiver wells. Varying source and receiver intervals for each well pair offered the opportunity to examine how much data needed to be collected. Initial data were collected at a fine scale (0.305 m) given the resolution capabilities of the model. Editing the number of ray paths used in the inversion process allowed comparisons. Of the variations tested in this study, the geometry used for GEMS was most efficiently and accurately characterized with about 300 ray paths, but 750 ray paths will provide some additional accuracy if time is available for their collection. Some small problems with some well pairs can be explained by equipment problems in one case and by too few ray paths in another two cases. The results of this research show that hydraulic tomography combined with appropriate inversion programs can estimate interwell K distributions with resolutions down to about one square meter in the most sensitive regions.

Pumped hydraulic CPT MOG data with a 30-sec period were collected from a radial well array with a central source well (HT-3) and five receiver wells (HT-1, HT-2, HT-4, HT-5 and HT-6). In addition, the pneumatic method with a period of 3-sec was used with the Geoprobe as source to collect MOG data in wells HT-2 and HT-3. This generated a large tomography data set which was used to evaluate the variation of K across the area. In some instances, poor data were collected due to equipment failure or poor signal to noise ratio. To address that data loss, a method was devised to replace the

bad data with data based on the HRST K point source data, so that the larger data sets of multiple MOGs in a well pair could be preserved and tomographically analyzed as a whole. Various models of isotropy, anisotropy, and lateral heterogeneity were used to evaluate the goodness of the fit coming from the inversion process. Different degrees of constraint were evaluated to determine the best data fit by SVD analysis. Data analysis indicated that the 3-sec period data were more sensitive to vertical anisotropy than had been expected. Modeling with a greater degree of anisotropy allowed a better fit for K values using the 3-sec data when considering fine-grained material and long-offset rays, while the 30-sec CPT period data seemed somewhat insensitive to different degrees of anisotropy. In general the 3-sec data needed more constraint to produce a stable inverse. The ranges of calculated K values were compared to the lithology of the aquifer and HRST K values from the well array to evaluate the success of the inversion. Tomographic analysis from this research generated K values that fell within these guidelines, indicating good performance of the CPT equipment and data processing techniques. The hydraulic pumping 30-sec CPT data were compared to previous research completed with a pneumatic 3-4 sec CPT period. Data trends and K values were similar and within the general range seen with HRST, although the 30-sec data did not have some of the resolution obtained with the shorter period CPT source used for earlier research data and the direct push data.

This project has provided support for three students to finish the Masters Degree and some support for four others during their undergraduate or graduate degrees. This work has shown that the use of an oscillatory source together with tomographic techniques and supporting high resolution slug testing is a promising hydrogeological

tool to determine interwell hydraulic conductivity distributions. The data sets obtained in the course of this project have provided hydraulic conductivity estimation in a 360-degree radial array over an extended area at GEMS. We have shown that, at least at GEMS, a resolution of about one meter square can be achieved in areas with adequate ray path coverage. We have designed equipment that allows this work to be done in standard 2 inch monitoring wells with long screens. We have also shown that the work can be done using a direct push unit (Geoprobe) to deploy the source. We were constrained to using signals with periods of about 3-sec and 30-sec due to equipment limitations. We know that the resolution is dependent upon period, so further research needs to be done using a pumping source that can bridge the gap between 3 and 30 seconds. This research was supported in part by the U.S. Department of Defense, through the Strategic Environmental Research and Development Program (SERDP).

References

Aster, R.C., Borchers, B., and Thurber, C.H., 2005. Parameter Estimation and Inverse Problems, Elsevier Academic Press, Burlington, MA.

Barker, J.A., 1988. A generalized radial flow model for hydraulic tests in fractured rock. *Water Resources Research* 24. No. 10:1796-1804.

Black, J.H., and Kipp, K.L.,1981. Determination of hydrogeological parameters using sinusoidal pressure tests: A theoretical appraisal. *Water Resources Research* 17. No. 3:686-692.

Bohling, G.C., 1999. Evaluation of an induced gradient tracer test in an alluvial aquifer, Ph.D. Dissertation, University of Kansas, 224 p. Also Kansas Geological Survey Open-file Report # 1999-6.

Bohling, G.C., Zhan, X., Butler Jr, J.J., and Zheng, L., 2002. Steady shape analysis of tomographic pumping tests for characterization of aquifer heterogeneities. *Water Resources Research* 38: 601-605.

Bohling, G.C., Zhan, X., Knoll, M.D., and Butler J.J. Jr., 2003. Hydraulic tomography and the impact of a priori information: An alluvial aquifer example. Kansas Geological Survey Open-file Report # 2003-71 .

Brauchler, R., Liedl, R., and Dietrich, P., 2001. A travel time based hydraulic tomographic approach. *Water Resources Research* 39. No. 12:1-12

Bredehoeft, J.D and Papadopulos, S.S., 1980. A method for determining the hydraulic properties of tight formations. *Water Resources Research* 16. No. 1:233-238

Butler, J.J. Jr., Garnett, E.J., and Healey, J.M., 2002a. Analysis of slug tests in formations of high hydraulic conductivity, *Ground Water* 41. No. 5:620-630.

Butler, J.J. Jr., Healey, J.M., McCall, G.W., Garnett, E.J. and Loheide II, S.P., 2002b. Hydraulic tests with direct-push equipment, *Ground Water* 40, No. 1:25-36.

Cooper, H.H., Bredehoeft, J.D., Papadopulos, I.S., and Bennett, R.R., 1965. The response of well-aquifer systems to seismic waves. *Journal of Geophysical Research* 70, No. 16:3915-3926

Deki, P., 2008, Comparing Slug Tests to Oscillatory Stress Tests, Senior Thesis, University of Kansas, 18 p.

Domenico, P., A., and Schwartz, F., W., 1998. Physical and Chemical Hydrogeology, John Wiley & Sons, New York, 506 p.

Engard, B., 2006, Estimating Aquifer Parameters From Horizontal Pulse Tests, Masters Thesis, University of Kansas, 107 p.

Engard, B., McElwee, C.D., Healey, J.M., and Devlin, J.F., 2005, Hydraulic tomography and high-resolution slug testing to determine hydraulic conductivity distributions – Year 1: Kansas Geological Survey Open File Report #2005-36, 81 p.

Engard, B.R., McElwee, C.D., Devlin, J.F., Wachter, B., and Ramaker, B., 2006, Hydraulic tomography and high-resolution slug testing to determine hydraulic conductivity distributions – Year 2: Kansas Geological Survey Open-File Report # 2007-5, 57 p.

Ferris, J.G., 1951. Cyclic fluctuations of the waterlevels as a basis for determining aquifer transmissivity, *IAHS Publ.*, 33, p. 148-155.

Fetter, C.W., 2001. Applied hydrogeology, Prentice-Hall, Upper Saddle River, NJ, 598 p.

Hantush, M.S., 1960. Lectures at New Mexico Institute of Mining and Technology. unpublished, compiled by Steve Papadopulos, 119 p.

Healey, J., McElwee, C., and Engard, B., 2004. Delineating hydraulic conductivity with direct-push electrical conductivity and high resolution slug testing. *Trans. Amer. Geophys. Union* 85, No.47: Fall Meet. Suppl., Abstract H23A-1118.

Huettl, T.J., 1992. An evaluation of a borehole induction single-well tracer test to characterize the distribution of hydraulic properties in an alluvial aquifer. Masters Thesis, The University of Kansas.

Jiang, X., 1991. Field and laboratory study of the scale dependence of hydraulic conductivity. Masters Thesis, The University of Kansas.

Jiao, J.J. and Tang, Z., 1999. An analytical solution of groundwater response to tidal fluctuation in a leaky confined aquifer. *Water Resources Research* 35. No. 3:747-751

Johnson, C.R., Greenkorn, R.A., and Woods, E.G., 1966. Pulse-Testing: A new method for describing reservoir flow properties between wells. *Journal of Petroleum Technology*. (Dec 1966) pp. 1599-1601.

Lee, J., 1982. Well Testing, Society of Petroleum Engineers of AIME, New York, 156 p.

Lyle, S.A., 2011. Tomographic Characterization of Aquifer Heterogeneity, MS Thesis, University of Kansas, 170p. Also Kansas Geological Survey Open-file Report # 2011-1.

McCall, W., Butler J.J. Jr., Healey, J.M., and Garnett, E.J., 2000. A dual-tube direct push method for vertical profiling of hydraulic conductivity in unconsolidated formations, *Environmental & Engineering Geoscience* Vol. VIII, no. 2:75-84.

McElwee, C.D., 2000, Implementation of a nonlinear model for analysis of slug tests, Kansas Geological Survey Computer Program Series 2000-01.

McElwee, C.D., 2001. Application of a nonlinear slug test model, *Ground Water* 39. No. 5:737-744.

McElwee, C.D., 2002. Improving the analysis of slug tests, *Journal of Hydrology* 269:122-133.

McElwee, C.D., and Butler, J.J. Jr., 1995. Characterization of heterogeneities controlling transport and fate of pollutants in unconsolidated sand and gravel aquifers: Final report, Kansas Geological Survey Open File Report # 95-16.

McElwee, C.D., Devlin, J.F., and Wachter, B.J., 2007. Hydraulic tomography and high-resolution slug testing to determine hydraulic conductivity distributions – Year 3, Kansas Geological Survey Open File Report #2008-1, 57 p.

McElwee, C.D., and Zenner, M.A., 1998. A nonlinear model for analysis of slug-test data. *Water Resources Research* 34, No. 1:55-66.

Novakowski, K.S., 1989. Analysis of pulse interference tests. *Water Resources Research* 25. No. 11:2377-2387

O'Conner, H.G., 1960, Geology and ground-water resources of Douglas County, Kansas, Kansas Geological Survey Bulletin 148, p. 200.

Pierce, A., 1977. Case history: Waterflood performance predicted by pulse testing. *Journal of Petroleum Technology.* (August 1977) 914-918.

Prosser, D.W., 1981, A method of performing response tests on highly permeable aquifers, *Ground Water*, v. 19, p. 588-592.

Ross, H.C., 2004. Utility of multi-level slug tests to define spatial variations of hydraulic conductivity in an alluvial aquifer, northeastern Kansas, Masters Thesis, The University of Kansas.

Ross, H.C. and McElwee, C.D., 2007. Multi-level slug tests to measure 3-D hydraulic conductivity distributions, *Natural Resources Research*, DOI: 10.1007/s11053-007-9034-9.

Schad, H., and Teutsch, G., 1994. Effects of scale on pumping test results in heterogeneous porous aquifers, *Journal of Hydrology* 159. pp. 61- 77.

Schulmeister, M., 2000. Hydrology and geochemistry of an alluvial aquifer near a flood plain margin, Ph.D. Dissertation, University of Kansas.

Sellwood, S., 2001. A direct-push method of hydrostratigraphic site characterization, Masters Thesis, The University of Kansas.

Van Der Kamp, G.,1976. Determining aquifer transmissivity by means of whole well respons tests: The underdamped case, *Water Resources Research* 12, no. 1:71-77.

Wachter, B.J., 2008. Characterizing Aquifer Heterogeneity Using Hydraulic Tomography, M.S. Dissertation, The University of Kansas, 150p.

Wachter, B.J., McElwee, C.D., and Devlin, J.F., 2008. Hydraulic tomography and high-resolution slug testing to determine hydraulic conductivity distributions – Year 4, Kansas Geological Survey Open File Report #2008-23, 74 p.

Yeh, T.C., and Liu, S., 2000. Hydraulic tomography: Development of a new aquifer test method, *Water Resource Research* 36, no. 8:2095-2105.

Zemansky, G.M., and McElwee, C.D., 2005. High-Resolution Slug Testing, *Ground Water* 43, no. 2: 222-230.

Zurbachen, B.R., Zlotnik, V.A., and Butler, J.J. Jr., 2002. Dynamic interpretation of slug tests in highly permeable aquifers, *Water Resources Research* 38. no. 3:1-17.

Appendix A. Technical Publications

Published Abstracts.

Healey, J. M., McElwee, C. D., and Engard, B., 2004, Delineating hydraulic conductivity with direct push electrical conductivity and high-resolution slug testing: *Eos, Trans. Amer. Geophys. Union*, v. 85, no 47, Fall Meet. Suppl., Abstract H23A-1118, p. F773.

Engard, B. and McElwee, C. D., 2005, Continuous pulse testing for estimating aquifer parameters: *Proceedings 50th Annual Midwest Ground Water Conference*, Nov. 1-3, Urbana, Illinois.

Engard, B. and McElwee, C. D., 2005, Estimating aquifer parameters from oscillatory well stresses: *Proceedings SERDP Partners in Environmental Technology Technical Symposium and Workshop*, Nov. 29-Dec. 1, Washington, D.C., p. G-26.

Engard, B. and McElwee, C. D., 2005, Estimating hydraulic conductivity: Hydraulic tomography and high-resolution slug tests: *Eos, Trans. Amer. Geophys. Union*, 86(52), Fall Meet. Suppl., Abstract H21C-1359.

McElwee, C. D. and Engard, B., 2006, Using Oscillatory Pressure Waves to Measure Hydraulic Conductivity Distributions: *Proceedings SERDP Partners in Environmental Technology Technical Symposium and Workshop*, Nov. 28-30, Washington, D.C.

McElwee, C. D. and Engard, B., 2006, Hydraulic Tomography Using Oscillatory Pressure Waves: *Eos, Trans. Amer. Geophys. Union*, 87(52), Fall Meet. Suppl., Abstract H41B-0382.

McElwee, C. D., 2007, Hydraulic Conductivity Distributions from Pulsed Signals: Mini-Symposium 45 – Tomographic Approaches to High-Resolution Aquifer Characterization – Lab and Field Experiments, SIAM Conference on Mathematical & Computational Issues in the Geosciences, March 19-22, Santa Fe, NM.

McElwee, C. D. and Wachter, B. J., 2007, A Modeling Study Using Oscillatory Pressure Waves for Hydraulic Tomography: *Eos, Trans. Amer. Geophys. Union*, 88(23), Joint Assembly Suppl., Abstract H51E-01.

McElwee, C. D. and Wachter, B. J., 2007, Oscillatory Pressure Waves as Energy Source for Hydraulic Tomography: *Proceedings SERDP Partners in Environmental Technology Technical Symposium and Workshop*, Dec. 4-6, Washington, D.C.

Wachter, B. J. and McElwee, C. D., 2007, Hydraulic Tomography Study Involving the Singular Value Decomposition Method: *Eos, Trans. Amer. Geophys. Union*, 88(52), Fall Meet. Suppl., Abstract H23G-1725.

McElwee, C. D. and Wachter, B. J., 2008, Characterizing Aquifer Heterogeneity Using Hydraulic Tomography with a Sinusoidal Signal: *Proceedings SERDP Partners in Environmental Technology Technical Symposium and Workshop*, Dec. 2-4, Washington, D.C.

McElwee, C. D. and Wachter, B. J., 2008, Hydraulic Tomography Using A Sinusoidal Signal To Characterize Aquifer Hydraulic Conductivity: *Eos, Trans. Amer. Geophys. Union*, 89(53), Fall Meet. Suppl., Abstract H41A-0827.

Annual Report

Engard, B., McElwee, C.D., Healey, J.M., and Devlin, J.F., 2005, Hydraulic tomography and high-resolution slug testing to determine hydraulic conductivity distributions – Year 1, Project Report to the Strategic Environmental Research and Development Program, U.S. DoD, EPA, and DOE, 81 pp., also Kansas Geological Survey Open File Report #2005-36.

Engard, B.R., McElwee, C.D., Devlin, J.F., Wachter, B., and Ramaker, B., 2006, Hydraulic tomography and high-resolution slug testing to determine hydraulic conductivity distributions – Year 2, Project Report to the Strategic Environmental Research and Development Program, U.S. DoD, EPA, and DOE, 57 pp., also Kansas Geological Survey Open-File Report # 2007-5.

McElwee, C.D., Devlin, J.F., and Wachter, B., 2007, Hydraulic tomography and high-resolution slug testing to determine hydraulic conductivity distributions – Year 3, Project Report to the Strategic Environmental Research and Development Program, U.S. DoD, EPA, and DOE, 57 pp., also Kansas Geological Survey Open-File Report # 2008-1.

Wachter, B.J., McElwee, C.D., and Devlin, J.F., 2008. Hydraulic tomography and high-resolution slug testing to determine hydraulic conductivity distributions – Year 4, Project Report to the Strategic Environmental Research and Development Program, U.S. DoD, EPA, and DOE, 74 pp., also Kansas Geological Survey Open File Report #2008-23.

Lyle, S.A., and McElwee, C.D., 2011, Hydraulic tomography and high-resolution slug testing to determine hydraulic conductivity distributions – Years 2010-11, Project Report to the Strategic Environmental Research and Development Program, U.S. DoD, EPA, and DOE, 170 pp., also Kansas Geological Survey Open-File Report # 2011-1.

Masters Thesis

Engard, B., 2006, Estimating Aquifer Parameters From Horizontal Pulse Tests, Masters Thesis, University of Kansas, 107 pp.

Wachter, B., 2008, Characterizing Aquifer Heterogeneity Using Hydraulic Tomography, Masters Thesis, University of Kansas, 150 pp.

Lyle, S.A., 2011, Tomographic Characterization of Aquifer Heterogeneity, Masters Thesis, University of Kansas, 170p.

Appendix B: HRST K Profiles

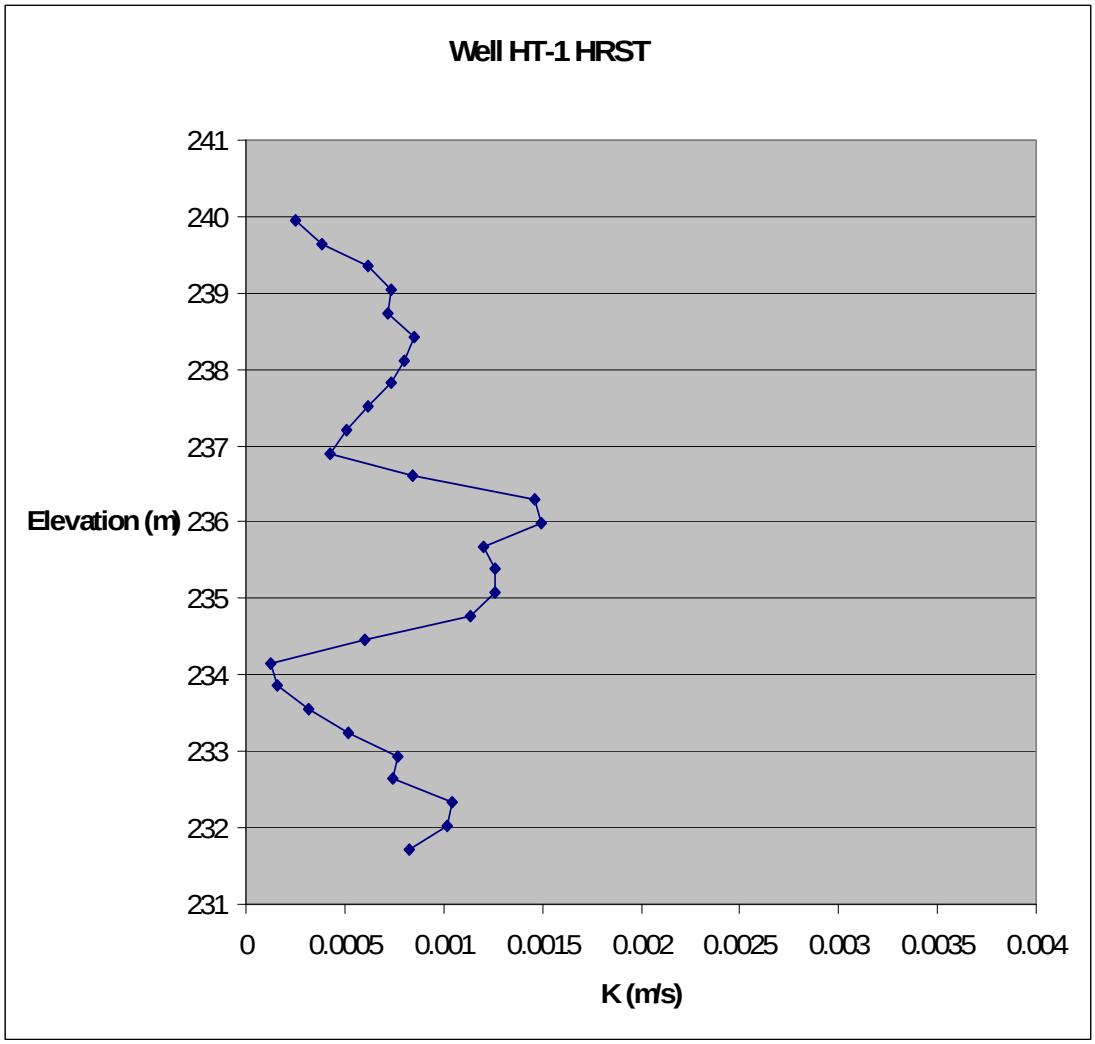

Figure B1: HRST results for well HT-1 (processed by Brett Engard).

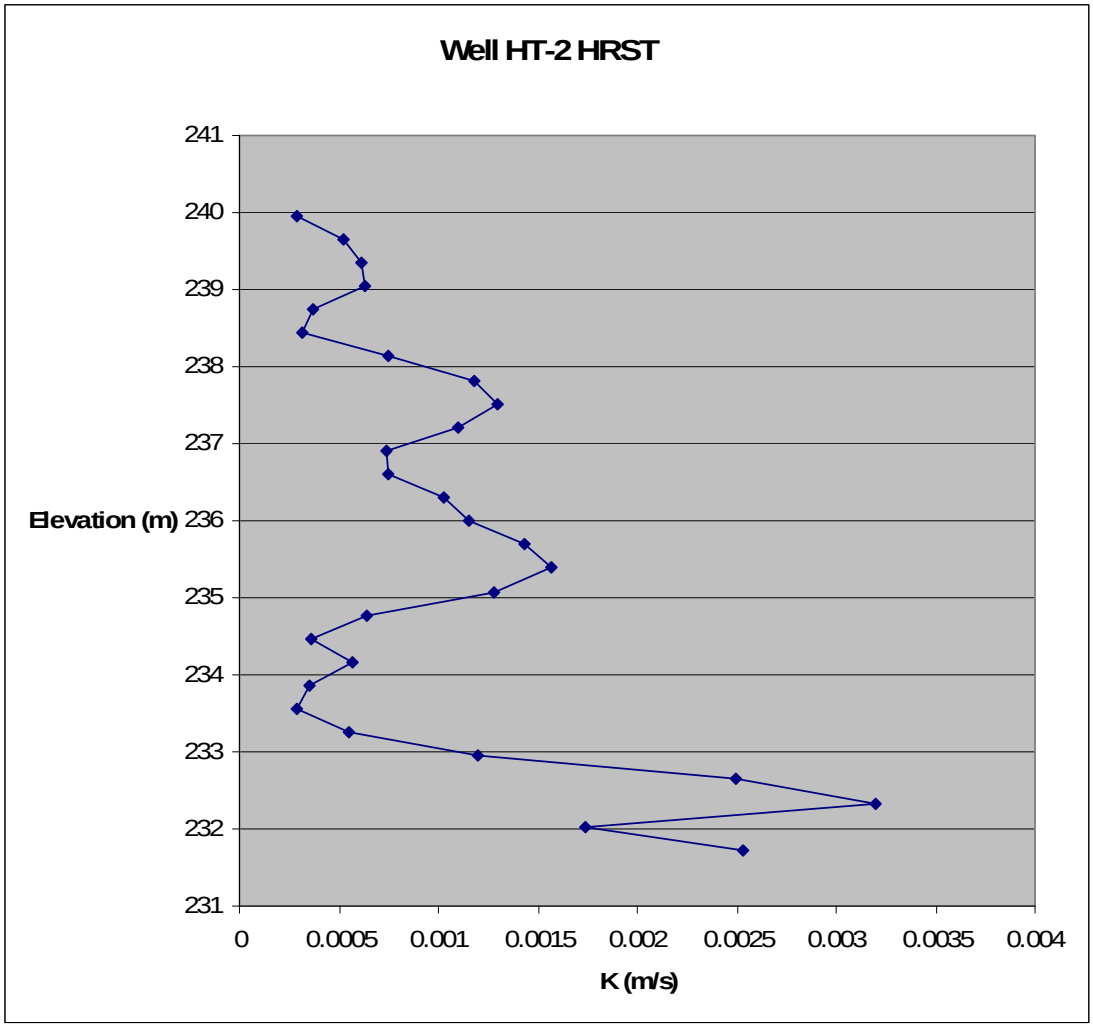

Figure B2: HRST results for well HT-2 (processed by Brett Engard).

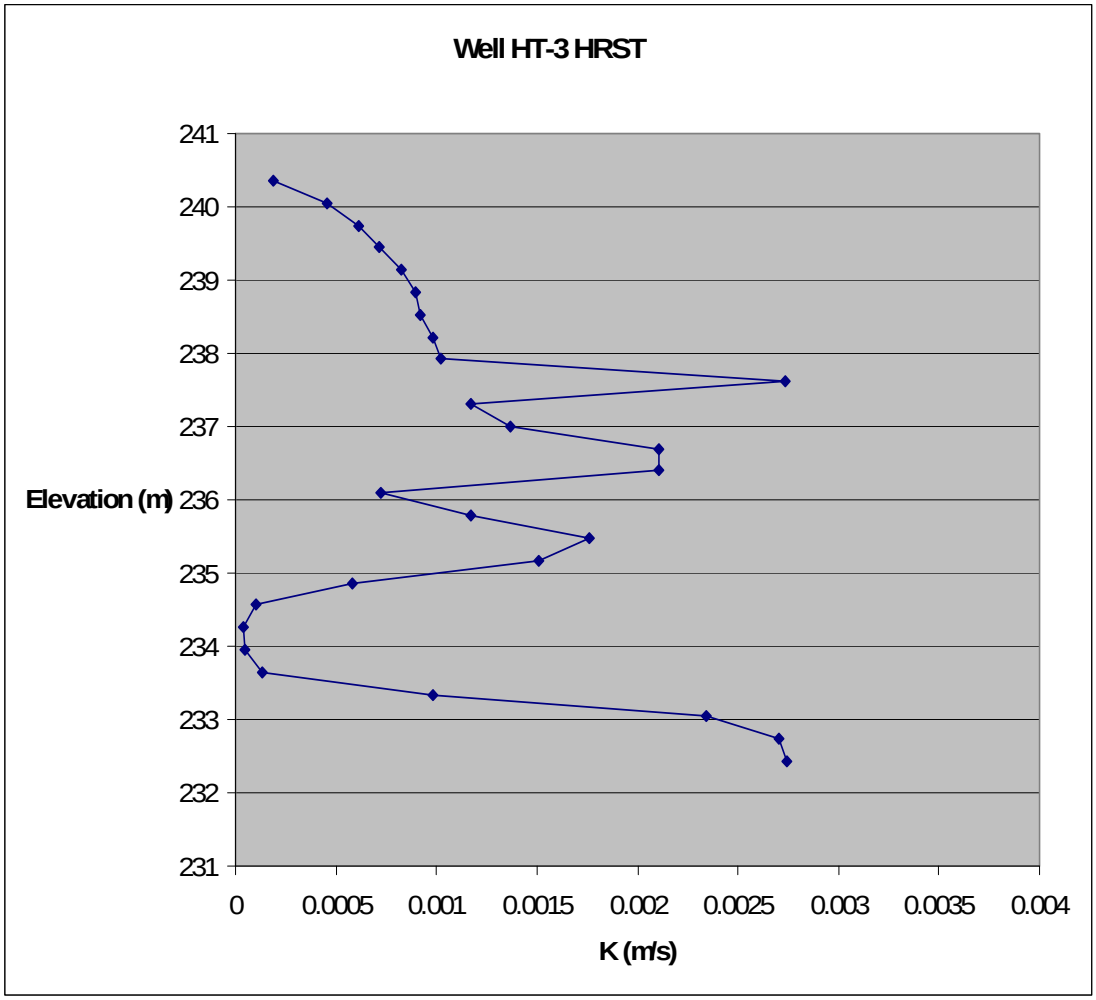

Figure B3: HRST results for well HT-3 (processed by Brett Engard).

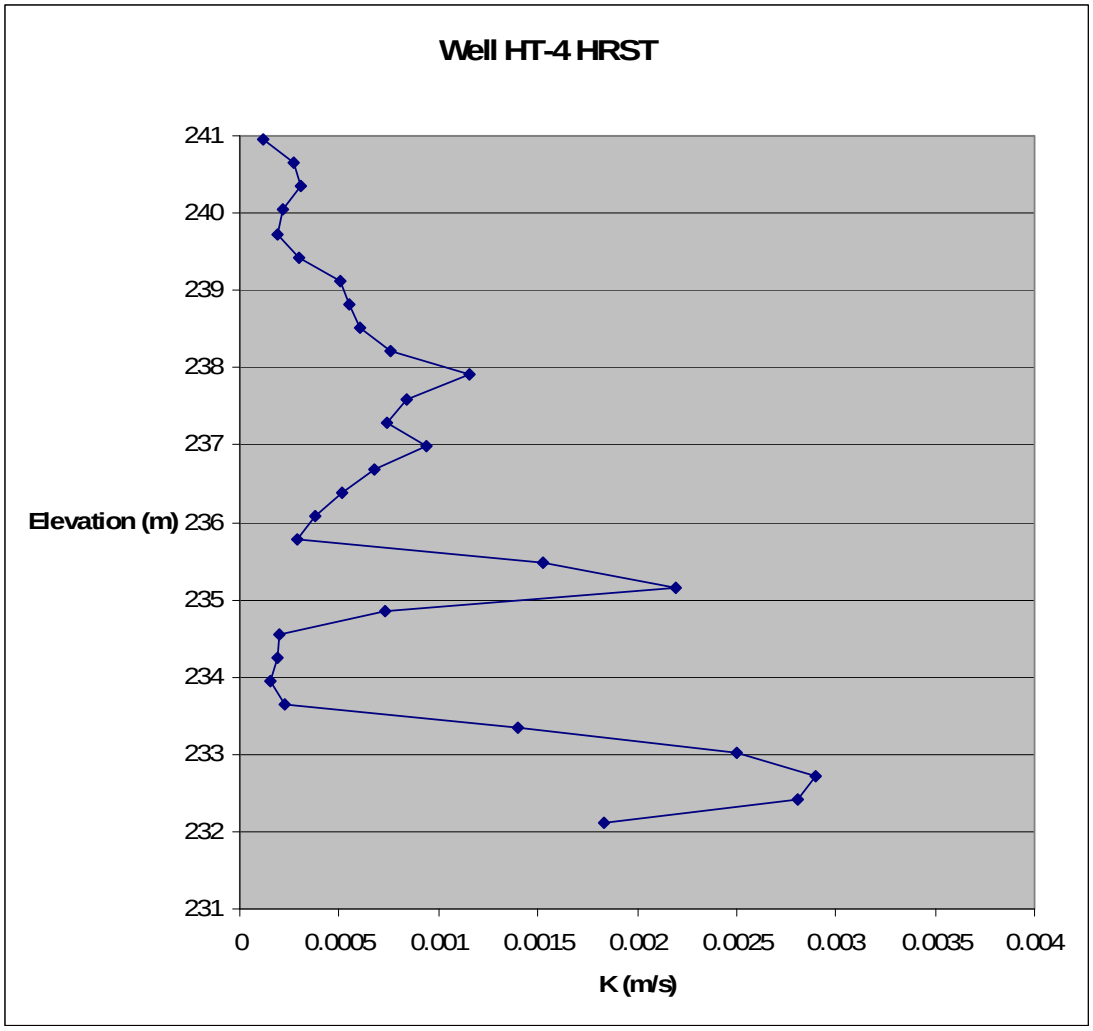

Figure B4: HRST results for well HT-4 (processed by Pema Deki).

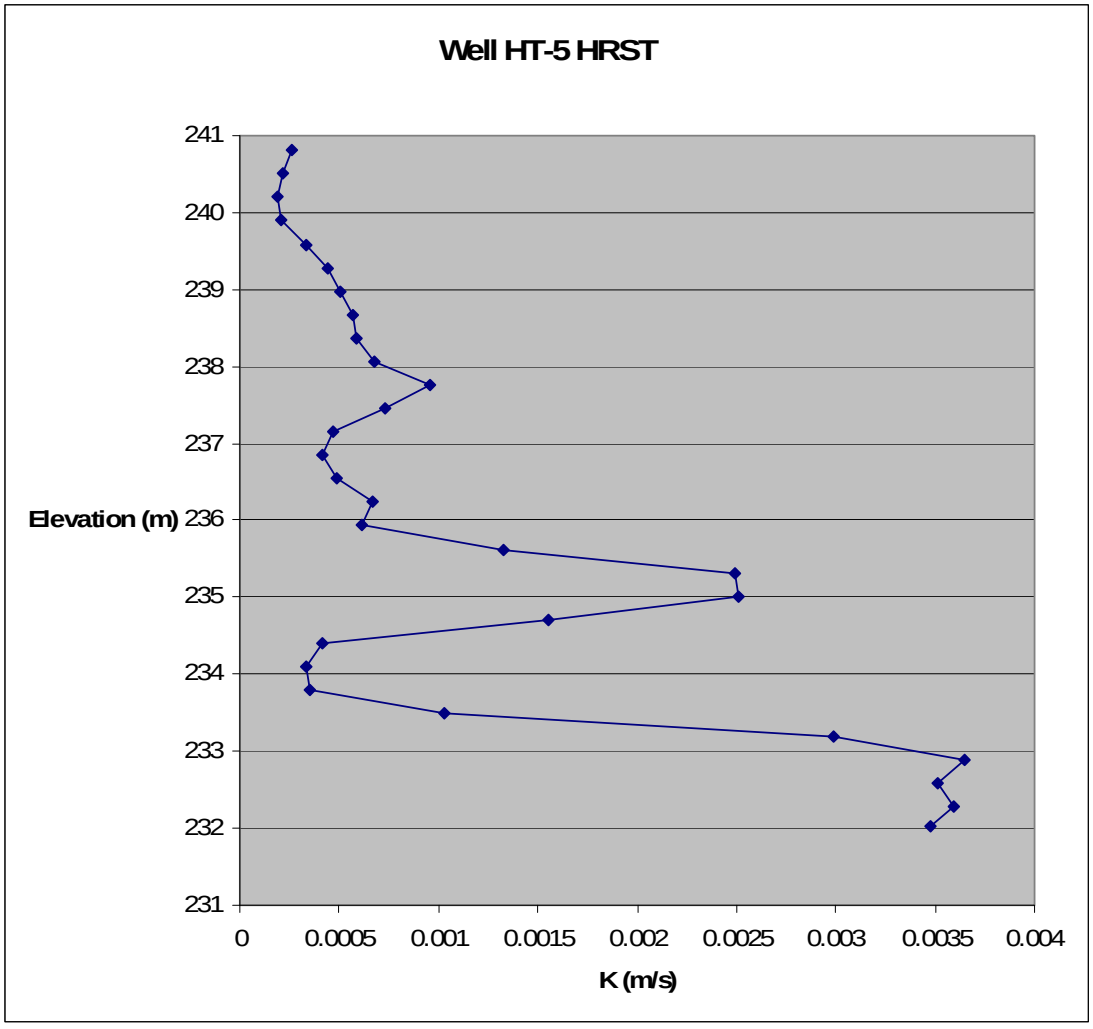

Figure B5: HRST results for well HT-5 (processed by Pema Deki).

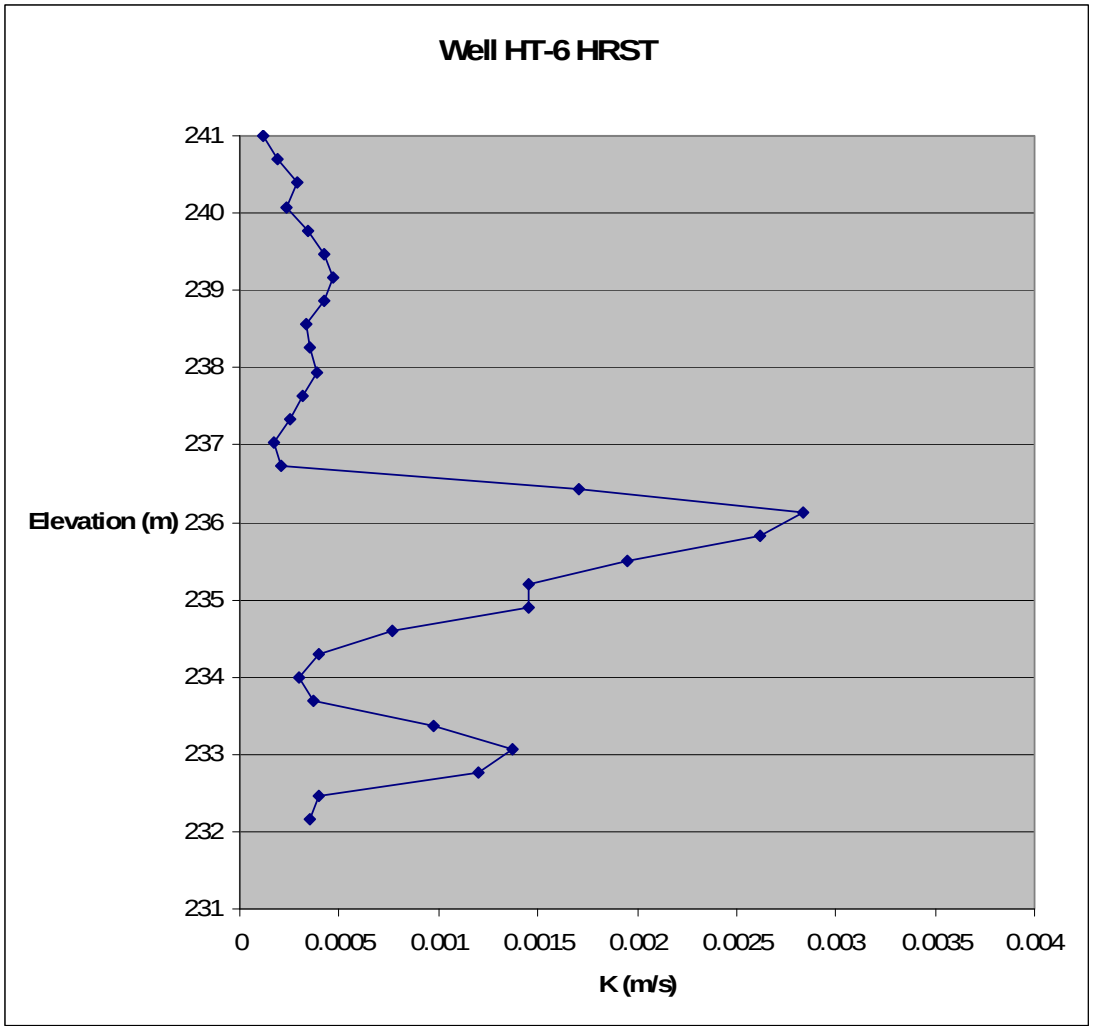

Figure B6: HRST results for well HT-6 (processed by Pema Deki).